WRDC-TR-90-2050

②

MAGNETIC DOMAIN STRAIN
SENSOR PROGRAM

BERNARD O'HALLORAN
HARVEY NISKA
STEVE MINA
DR. GORDON FISH
GARRETT ENGINE DIVISION
111 S. 34th STREET, P.O. BOX 5217
PHOENIX, ARIZONA 85010

AUGUST 1, 1990

FINAL REPORT FOR PERIOD SEPTEMBER 1986 TO MARCH 1990

AERO-PROPULSION AND POWER LABORATORY
WRIGHT RESEARCH AND DEVELOPMENT CENTER
AIR FORCE SYSTEMS COMMAND
WRIGHT-PATTERSON AIR FORCE BASE, OHIO 45433-6563

AD-A227 225

DTIC
ELECTE
OCT.0 2 1990
S B D

90 10 02 02

NOTICE

WHEN GOVERNMENT DRAWINGS, SPECIFICATIONS, OR OTHER DATA ARE USED FOR ANY PURPOSE OTHER THAN IN CONNECTION WITH A DEFINITELY GOVERNMENT-RELATED PROCUREMENT, THE UNITED STATES GOVERNMENT INCURS NO RESPONSIBILITY OR ANY OBLIGATION WHATSOEVER. THE FACT THAT THE GOVERNMENT MAY HAVE FORMULATED OR IN ANY WAY SUPPLIED THE SAID DRAWINGS, SPECIFICATIONS, OR OTHER DATA, IS NOT TO BE REGARDED BY IMPLICATION, OR OTHERWISE IN ANY MANNER CONSTRUED, AS LICENSING THE HOLDER, OR ANY OTHER PERSON OR CORPORATION; OR AS CONVEYING ANY RIGHTS OR PERMISSION TO MANUFACTURE, USE, OR SELL ANY PATENTED INVENTION THAT MAY IN ANY WAY BE RELATED THERETO.

THIS REPORT HAS BEEN REVIEWED BY THE OFFICE OF PUBLIC AFFAIRS (ASD/PA) AND IS RELEASABLE TO THE NATIONAL TECHNICAL INFORMATION SERVICE (NTIS). AT NTIS IT WILL BE AVAILABLE TO THE GENERAL PUBLIC INCLUDING FOREIGN NATIONS.

THIS TECHNICAL REPORT HAS BEEN REVIEWED AND IS APPROVED FOR PUBLICATION.

WILLIAM A. STANGE
PROJECT ENGINEER
AERO PROPULSION AND POWER
               Laboratory

GEOFFREY W. JUMPER, MAJ, USAF
CHIEF/WRDC/POTC
AERO PROPULSION AND POWER
  LABORATORY

FOR THE COMMANDER

ROBERT E. HENDERSON
Deputy for Technology
Turbine Engine Division
Aero Propulsion & Power Laboratory

IF YOUR ADDRESS HAS CHANGED, IF YOU WISH TO BE REMOVED FROM OUR MAILING LIST, OR IF THE ADDRESSEE IS NO LONGER EMPLOYED BY YOUR ORGANIZATION PLEASE NOTIFY   WRDC/POTC , WRIGHT-PATTERSON AFB, OH 45433- 6563 TO HELP MAINTAIN A CURRENT MAILING LIST.

COPIES OF THIS REPORT SHOULD NOT BE RETURNED UNLESS RETURN IS REQUIRED BY SECURITY CONSIDERATIONS, CONTRACTUAL OBLIGATIONS, OR NOTICE ON A SPECIFIC DOCUMENT.

REPORT DOCUMENTATION PAGE	Form Approved OMB No. 0704-0188

1a. REPORT SECURITY CLASSIFICATION Unclassified	1b. RESTRICTIVE MARKINGS

2a. SECURITY CLASSIFICATION AUTHORITY	3. DISTRIBUTION/AVAILABILITY OF REPORT Approved for public release; distribution is unlimited.
2b. DECLASSIFICATION/DOWNGRADING SCHEDULE	

4. PERFORMING ORGANIZATION REPORT NUMBER(S) 21-7574	5. MONITORING ORGANIZATION REPORT NUMBER(S) WRDC-TR-90-2050

6a. NAME OF PERFORMING ORGANIZATION Allied-Signal Aerospace Garrett Engine Division	6b. OFFICE SYMBOL (If applicable)	7a. NAME OF MONITORING ORGANIZATION Aero Propulsion and Power Lab(WRDC/POTC) Wright Research Development Center
6c. ADDRESS (City, State, and ZIP Code) 111 S. 34th St., P.O. Box 5217 Phoenix, AZ 85010		7b. ADDRESS (City, State, and ZIP Code) Wright-Patterson Air Force Base, Ohio 45433-6563

8a. NAME OF FUNDING/SPONSORING ORGANIZATION Wright Research and Development Center	8b. OFFICE SYMBOL (If applicable) WRDC/POTC	9. PROCUREMENT INSTRUMENT IDENTIFICATION NUMBER F33615-86-C-2646

8c. ADDRESS (City, State, and ZIP Code) Wright-Patterson Air Force Base, Ohio 45433-6563	10. SOURCE OF FUNDING NUMBERS			
	PROGRAM ELEMENT NO. 62203F	PROJECT NO. ILIR 3036	TASK NO. P6 12	WORK UNIT ACCESSION NO. 13 97

11. TITLE (Include Security Classification)

MAGNETIC DOMAIN STRAIN SENSOR PROGRAM

12. PERSONAL AUTHOR(S)
O'Halloran, Bernard; Niska, Harvey; Mina, Steve; Fish, Dr. Gordon

13a. TYPE OF REPORT Final	13b. TIME COVERED FROM 9/86 TO 3/90	14. DATE OF REPORT (Year, Month, Day) 90 August 1	15. PAGE COUNT 136

16. SUPPLEMENTARY NOTATION
This research was partially funded by the inhouse independent research fund.

17.	COSATI CODES		18. SUBJECT TERMS (Continue on reverse if necessary and identify by block number)
FIELD	GROUP	SUB-GROUP	

19. ABSTRACT (Continue on reverse if necessary and identify by block number)

The Magnetic Domain Strain Sensor Program began in September 1986 to demonstrate the feasibility of using the magnetostrictive properties of magnetic alloys in the design of a new type of strain gage. The Magnetic Domain Strain Sensor offered advantages over the resistive strain gage in the areas of: digital data acquisition; increased temperature capability; and potentially determining residual strain and fatigue.

Theory development bore out a modified Sixtus-Tonks model, measuring domain inversion time instead of magnetic, pulse propagation. The modified theory that developed led to improved gage measurement accuracy. Phase I testing of wire, and ribbon magnetic alloy sensors supported the theory development. Phase II developed the thin film technology for both the amorphous metallic glass sensor and the coils for eventual full gage fabrication in the program's Phase III portion.

Many obstacles had to be overcome in this program, especially in developing the thin film sputtering technology. The feasibility of the magnetic domain strain gage was demonstrated, but significant development still remains to be performed before the sensor can be considered a production test device. (JS)

20. DISTRIBUTION/AVAILABILITY OF ABSTRACT ☒ UNCLASSIFIED/UNLIMITED ☐ SAME AS RPT ☐ DTIC USERS	21. ABSTRACT SECURITY CLASSIFICATION UNCLASSIFIED
22a. NAME OF RESPONSIBLE INDIVIDUAL W. Strange	22b. TELEPHONE (Include Area Code) (513) 255-2081 22c. OFFICE SYMBOL WRDC/POTC

DD Form 1473, JUN 86   Previous editions are obsolete.

P-1138:0807

TABLE OF CONTENTS

LIST OF FIGURES

LIST OF FIGURES (Contd)

LIST OF FIGURES (Contd)

LIST OF FIGURES (Contd)

LIST OF FIGURES (Contd)

1.0 EXECUTIVE SUMMARY

Research and development by the Garrett Engine Division (GED) on the Magnetic Domain Strain Sensor began in September 1986. The goal of the program was to demonstrate the feasibility of using the magnetostrictive properties of magnetic alloys for a new type of static strain gage. The program was conducted for the United States Air Force under contract F33615-86-2646. The underlying theory of the Magnetic Domain Strain Sensor is based on the magnetostrictive phenomenon that the change in time for the inversion or switching of magnetic domains is directly related to the strain to which the gage is subjected. The gage offered the following advantages over conventional resistive strain gages:

o   Direct compatibility with digital data acquisition systems.

o   Higher temperature capability (800F-1000F)

o   The possibility of determining residual strain and fatigue.

The program was divided into three phases:

Phase I - Literature Search and Feasibility Study - which also included testing of wire and ribbon magnetic sensors to validate the theory development.

Phase II - Development and Testing of the thin film technologies (sensor and coil) needed for eventual full gage fabrication in Phase III.

Phase III - Fabrication and Testing of a full demonstrator gage.

The following presents a summary of the three major test/evaluation phases of the program.

Phase I

Phase I was highlighted by theory development and the use of round wire and metallic glass ribbon to demonstrate the input-output relationship for domain inversion.

Phase I testing concluded with the realization that follow-up phases needed to be restructured to better meet the project objectives and goals. Wire specimens were used to verify and develop the theory. Ribbon specimens were then tested to simulate a thin film system. After evaluation, the thin film fabrication techniques to demonstrate a prototype gage were formulated and a metallic glass was selected as the best candidate sensor material.

Phase II

Phase II required the development of the thin film techniques necessary for the eventual gage manufacture. This included the testing of thin film metallic glass sensor specimens to better quantify the response to strain. In addition, thin film coils were designed that would be integrated into the gage during Phase III. The testing of these parallel paths allowed for the greatest chance of success and demonstration of a viable strain gage in Phase III.

Vendors were contracted to provide coating services for the metallic glass and coil depositions. These depositions were then evaluated to determine thin film metallic glass response and coil current capacity and structural integrity.

Phase III

A working gage was produced in Phase III; however, it could only be demonstrated in a prototype bench test. Costly deposition runs and specimen deposition failures precluded further development efforts.

In Phase III, the metallic glass deposition technology and the coil photofabrication and deposition methods were integr..ced into a completed gage. Evaluation of the completed gage was hindered by several factors:

o   Insufficient samples
o   Grounding problems within the gage-coils
o   Low gage output
o   Film deposition problems
o   Metallic glass sensor oxidation
o   Coil design configuration

The focus of Phase III was to demonstrate a functioning magnetic strain gage. The demonstration gages consisted of 26 sputtered layers of materials forming a metallic glass sensing element enclosed by gold excitation and signal coils. The various elements are formed within the layers, along with insulation and diffusion barrier layers. All of the above was accomplished while keeping the overall thickness of the strain gage at 20 to 25 microns.

This program embarked on a totally different approach to measuring strain in modern gas turbine engines. The Magnetic Domain Strain Sensor offered significant advantages over the current resistive type gages, thereby providing the motivation to demonstrate the feasibility of the new gage. There were numerous obstacles to overcome during the development of the gage. The most significant hurdle was the development of the thin film techniques needed for gage fabrication. Thin film development is a costly process and con-

3

sidering the limited funds available for this effort, the successes achieved, though modest, were nonetheless impressive. GED had hoped to demonstrate the new gage alongside a resistive gage on an engine but schedule and resource constraints would not permit this desired conclusion to the program.

2.0 INTRODUCTION

2.1 Background

The propulsion industry has made intensive efforts to improve the stability and temperature range of the widely used resistive static strain gage. The use of magnetics to measure static strain is a new concept in measurement technology. This program addressed the current limitations in resistive strain gage application methods and demonstrated that a strain gage based on magnetics is feasible. The difference between static (steady-state) strain and dynamic (vibrating or variable) strain is illustrated in Figure 1. Fatigue life is evaluated from the dynamic strain levels while static strain is more critical to design within safety limitations.

The aerospace industry currently measures dynamic or vibratory strain by using foil, thin-film, or wire-wound alloy resistance strain gages with well-characterized gage factors and application techniques that allow dynamic measurements up to 2000F. Foil gages in an assortment of configurations are serviceable to about 500F, steady-state temperature, and to 700F for a limited time. Thin film strain gages are used up to 1100F. Above 1100F, Fe-Cr-Al-Y and N-Cr-Al alloys and modifications are used, with trade names such as Evanohm, Nichrome, and Moleculoy. These are filament-grid wire gages with diameters of 0.5 to 1.0 mil.

The measurement of static strain in high-temperature applications introduces several complex problems. Foil gages are limited to 700F by the method of fabrication. Thin-film gages have not been developed for static strain and are used only for dynamic measurement to 1100F. The alloy wire filament gages are limited to 700F due to a phase transformation that occurs in the material in the 700F to 750F range, resulting in an unstable and unrepeatable apparent strain calibration for static strain measurement. A static

5

G9039-1A
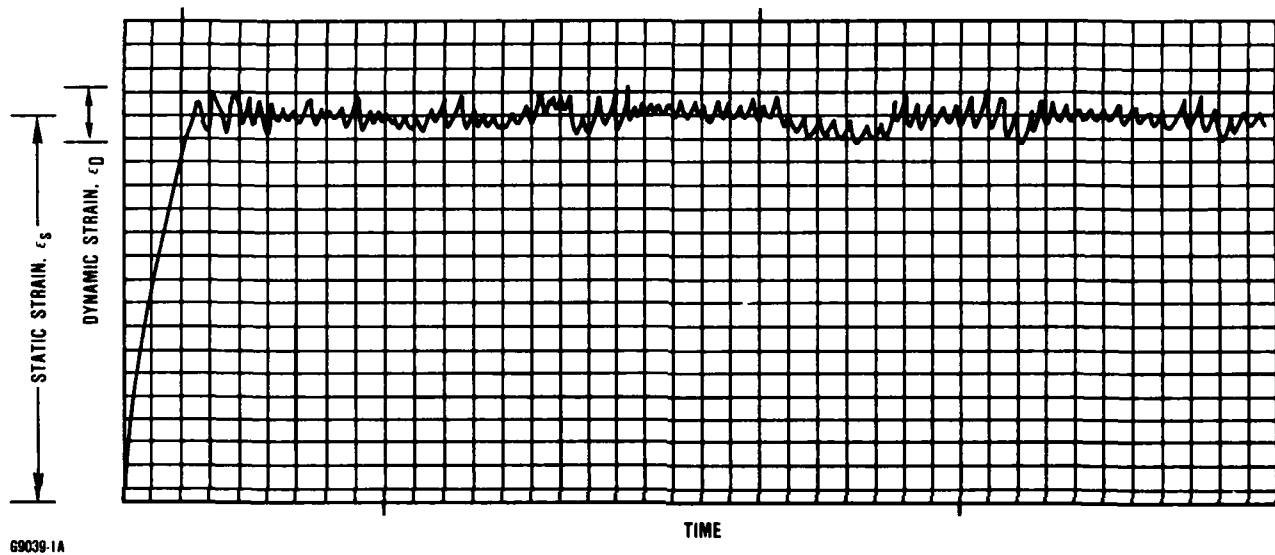
Figure 1. Differences Between Static and Dynamic Strain.

strain gage that would increase the temperature capability above 750F would be highly desirable.

GED has been investigating the application of magnetics to strain measurement since the early 1980s. The theory behind this sensor lies in the magnetostrictive response of a material to variations in strain. This new magnetic domain strain gage concept can potentially fill the technology gap outlined above and provide an alternative to the resistive strain gage suitable for static strain measurement at elevated temperatures.

2.2 Magnetic Strain Measurement Theory

The initial work at GED investigated the Barkhausen effect, including large and small Barkhausen jumps. This is a wave propagation phenomenon in which a magnetic wave velocity is measured. The wave velocity in a ferromagnetic material will change in response to strain in the material.

Evaluation of test data from initial bench tests in Phase I produced a theory explaining the phenomenon that deviates from the Barkhausen effect. Some basic concepts had to be examined to better understand magnetic phenomena and the potential application as a strain measurement system. The first task was to look at characteristic B-H, or hysteresis, loops that can be derived for a magnetic material (Figure 2).

The B-H loop is a representation of the response of a magnetic material to the application of a magnetic field (H) in the same way that a stress-strain curve represents the mechanical response (strain) of a material to stress. From basic physics, it is known that a current flowing in a coil creates a magnetic field. When this field is applied to a magnetic material, the magnetization vector in each magnetic domain wants to align with the field, producing
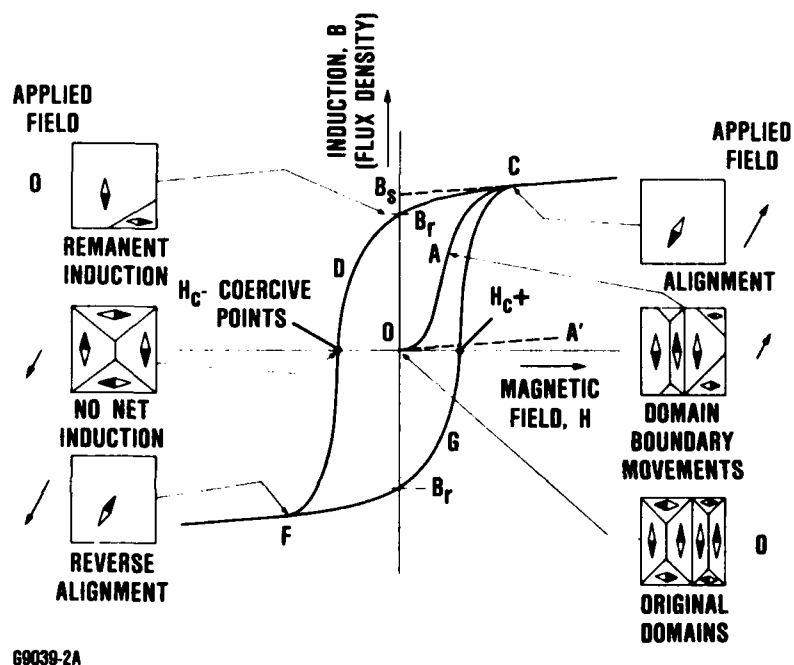
Figure 2. Magnetic Hysteresis Loop.

a magnetic induction or flux (B). An adequate magnetic field fully aligns all the domains in the material, producing saturation (point C of Figure 2). If the current in the coil is then reversed, the magnetization follows the path C-D-F (Figure 2), producing reverse alignment of the domains at point F. The coercivity point is defined by the field, H_c-, needed to reverse half the domains, thereby reducing the net flux to zero. An alternating current applied to the field coil will continuously drive the domains between saturation in the forward and reverse directions, thereby cyclically traversing the B-H loop, C-D-F-G-C.

The magnetic strain sensor concept is based on the observation that the coercive field, H_c, can be altered by stressing the magnetic material. The induced alignment of the magnetic domains due to the excitation current through the coils is shown in Figure 3. This phenomena is graphically shown in Figure 4, which demonstrates the field strength changing from H_c+ to H_c- with applied alternating current, for the general case:

$$H = \frac{Ni}{\ell} \text{ (for a long solenoid)}$$

Where:

H   =   Ampere-turns per meter

N   =   Number of turns

i   =   instantaneous current

ℓ =   length of coil

When a second coil is added to the system (Figure 5), it will pick up an induced voltage that corresponds to dB/dt and the alignment of the domains from saturation in the positive and negative

9
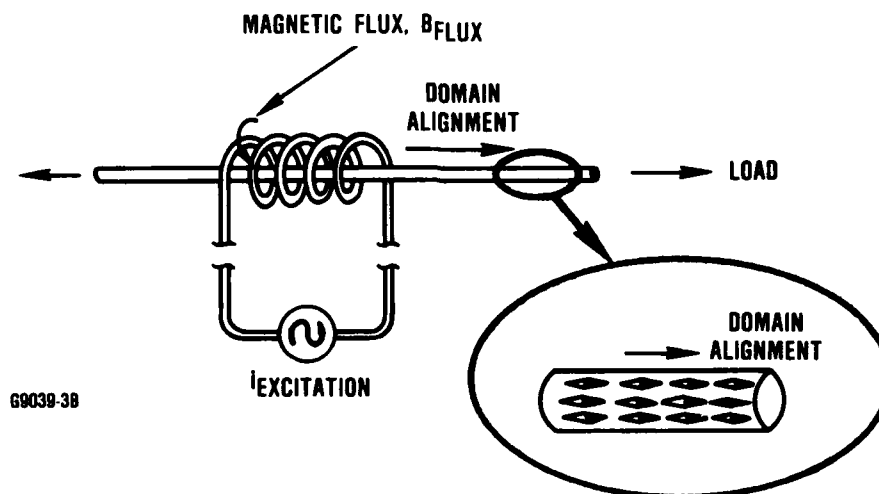
Figure 3. Excitation Coil/Wire System.
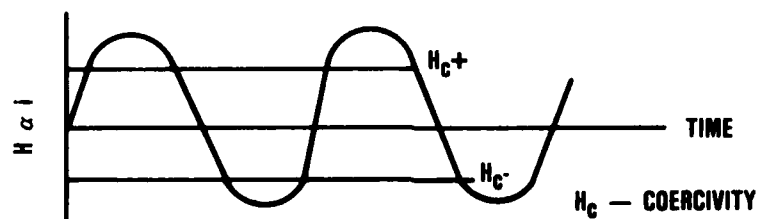
Figure 4. Alternating Excitation.

G9039-5B

^{i}EXCITATION
(DRIVE COIL)

SIGNAL
VOLTAGE, V_S
(PICKUP COIL)

LOAD
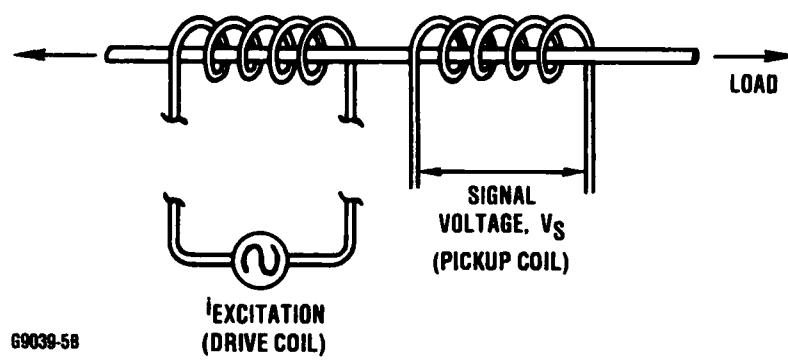
Figure 5.   Excitation and Sensing Coil System.

direction. The induced voltage in the second pickup coil corresponds to the rate of change in the magnetic flux, or dB/dt, according to Faraday's Law.

$$V_S = -NA \, dB/dt$$

V	=	induced voltage
N	=	number of coil turns
A	=	coil area
B	=	magnetic flux density
t	=	time

As the alternating current drives the domains to saturation through the coercive point, as shown in Figure 4, the induced voltage spike on the sensing coil occurs at the point where the slope of dB/dt is highest. With very little magnetic hysteresis, the dB/dt spike is very sharp and well-defined. This is shown in Figure 6.

The sensor material is required to have a square B-H loop with little magnetic hysteresis, that will give a well-defined voltage spike at the coercive point, or maximum dB/dt change. This peak in dB/dt occurs at the steepest point in the B-H loop or at the coercive point. A shift in coercivity, thus phase, shifts the dB/dt peak. As strain is applied to the system, the coercivity and location of the voltage spike occurrence changes relative to the zero strain reference, as shown in Figure 7. This results in the measured time delay (Δt).
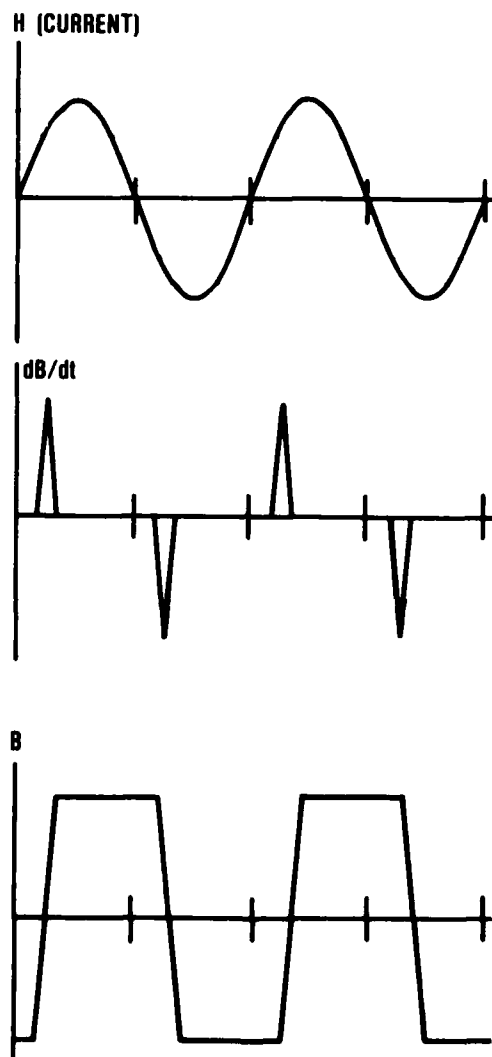
Figure 6. Time Plot of Magnetic Field, Induced Voltage and Magnetic Induction or Flux.

H (CURRENT)

+Hc

-Hc

H_c — COERCIVITY

dB/dt

B

NO
LOAD

dB/dt

Δt

LOAD

B

TIME

TIME

G9039-6A
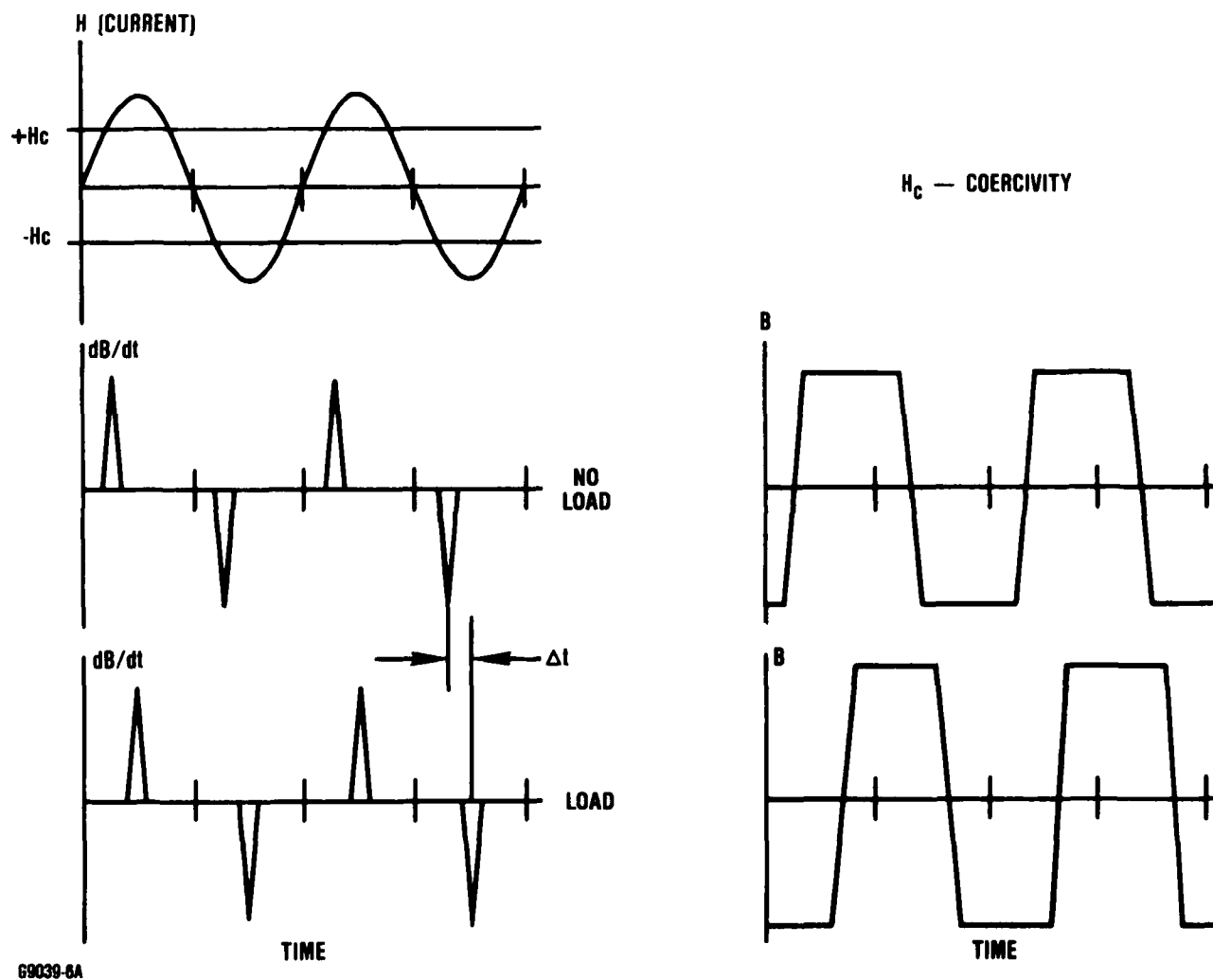
Figure 7. Shift in Time of the Induced Voltages.

Using these magnetic principles, the sensor concept is a thin-film multilayer gage system using a magnetic alloy as the element and an integral excitation and sensing coil. This alloy could exceed the 700F limit of resistance gages and provide an output signal that would be compatible with digital data-acquisition methods.

2.3 Material Selection

Material selection for the sensing element is the critical component in this system. Characteristic B-H loops for ferrous materials are not always square, and are not all suited for this application. Two B-H loops are shown in Figure 8. One loop is square and well defined while the second has a poorly-defined dB/dt transition. A square B-H loop is indicative of a material with high magnetic remanence. The slope dB/dt approaches ∞ producing a very sharp well defined signal pulse.

A contributing factor to the material selection is permeability (μ):

$$\mu = B/H$$

This relates the induced magnetic flux to the applied field in the sensing element. The permeability of amorphous materials is characteristically very high, allowing a relatively easy induction of domain alignment.

15
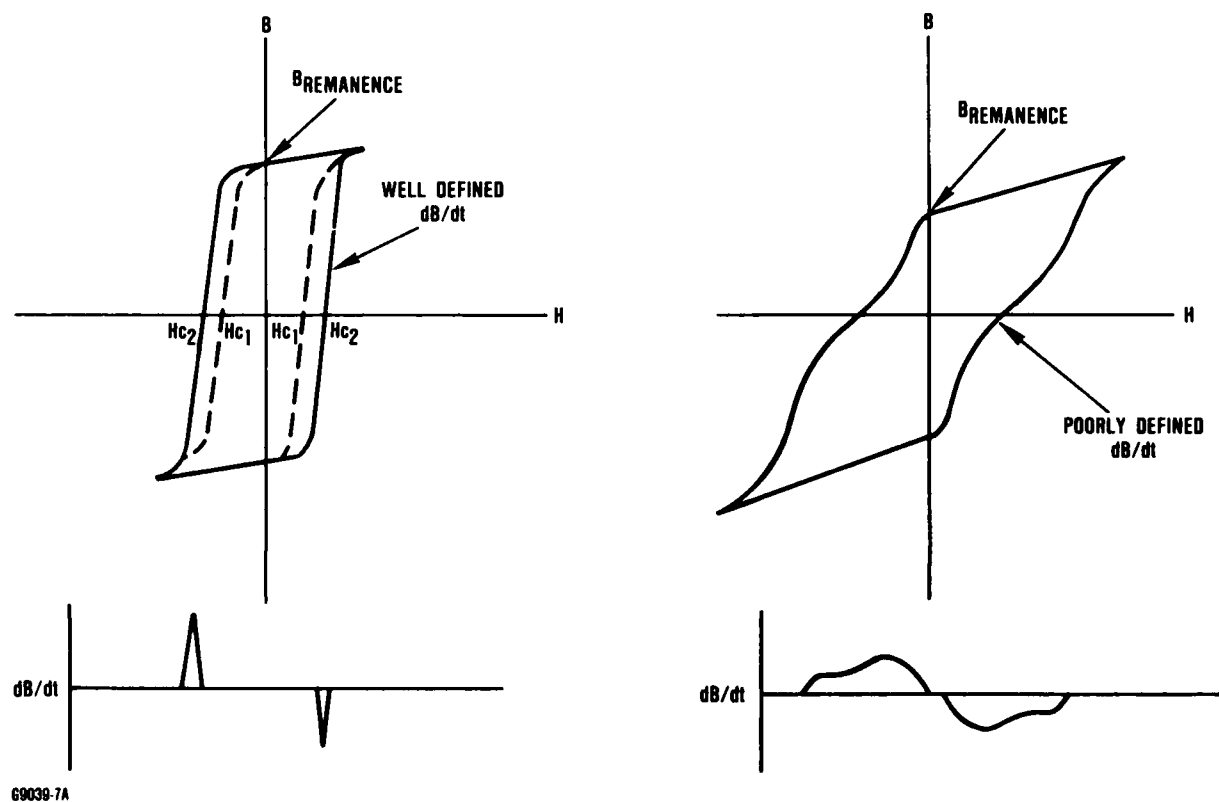
Figure 8.   B-H Loops.

Metallic glass is produced by rapid quench to form an amorphous structure. Amorphous metallic glass, developed by Allied-Signal, Inc., for the fabrication of transformers and magnetic devices has several advantages over crystalline materials. This material has a very square B-H loop resulting in a good dB/dt induced-voltage spike.

These new alloys are noncrystalline and have stable magnetic characteristics up to the Curie point, or transition from ferromagnetism to paramagnetism. In addition, the recrystallization (transformation from amorphous to crystalline structure as a time-dependent phenomena) occurs in the same temperature range as the Curie point. The 85-percent iron, 10-percent boron and 5-percent silicon metallic glass currently used has a Curie point of 850F and a recrystallization temperature of 825F.

Crystalline alloys would not be compatible with desired sensor characteristics for the following reasons:

o   Crystalline materials with desired magnetic properties are generally mechanically soft and have a yield point of 20 ksi.

o   Hardened crystalline magnetic alloys require 10 to 100 times higher drive current than amorphous materials to reach magnetic saturation.

Noncrystalline alloys offer several advantages:

o   Amorphous alloys are elastic to their yield limit, which is approximately 100 ksi.

o   Amorphous alloys have negligible magnetocrystalline anisotropy, with magnetic properties dominated by stress-induced anisotropy over a wide range of stresses.

17

o   The microstructure of amorphous materials is conducive to superior soft magnetic properties, as shown by their characteristic B-H loops.

o   Continued alloy development may raise the Curie point to the 1000 to 1100F range.

Amorphous metals are unique in that they are mechanically hard (high strength) but are magnetically soft. Since they easily change magnetization, they can readily be adopted to this application. A photograph of a characteristic amorphous material B-H loop is given in Figure 9.

The magnetic strain gage would have other benefits over the resistive strain gage. These benefits lend themselves well to propulsion engine development and diagnostic analysis:

o   The signal can be processed using digital techniques

o   The gage can be fabricated by thin-film techniques

o   The gage can exceed current temperature limitations of resistive static strain measurement

A critical issue is the difference in the metallic glass characteristics due to variations in machine application techniques. Differences in sputtering methods will result in varied film stresses and material characteristics. Of specific interest for the measurement of tensile versus compressive static strain is the residual film stress that occurs as a result of the deposition process.
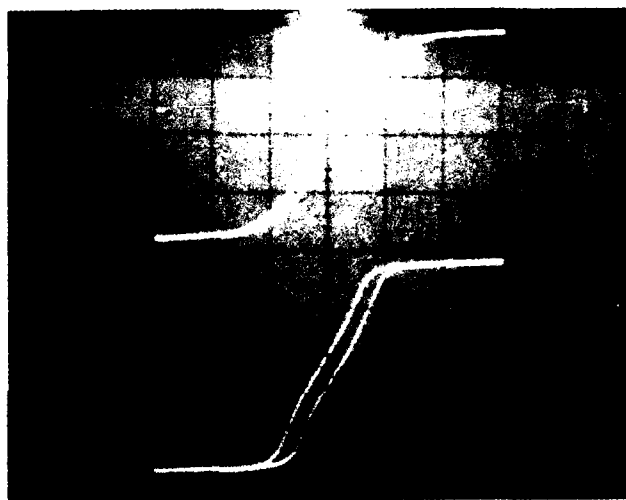
Figure 9. B-H Loop Photograph.

Internal film stresses occur as a result of the machine sputtering characteristics. The sensor element must have consistent properties from run to run.

In addition, both positive and negative magnetostrictive materials should be considered. The Fe-B-Si metallic glass used for this program has a positive magnetostrictive constant as shown in Figure 10. Positive magnetostriction has an increasing H_C with tensile loading. Below zero residual film stress, the B-H loop becomes poorly defined. Conversely, a negative magnetostrictive material has increasing H_C with compressive loading. Residual film stresses introduced into the sensor during fabrication must address the expected measurement range and sign. For example, a residual film stress of 50-ksi tension in the Fe-B-Si metallic glass would allow measurement from 50-ksi compression to 50-ksi tension.

2.4 Project Structure

The project was structured to progress from theory development and verification to a multitasked, parallel-path, thin-film systems development. Figure 11 is a flow chart of the program showing the items critical to the prototype fabrication.
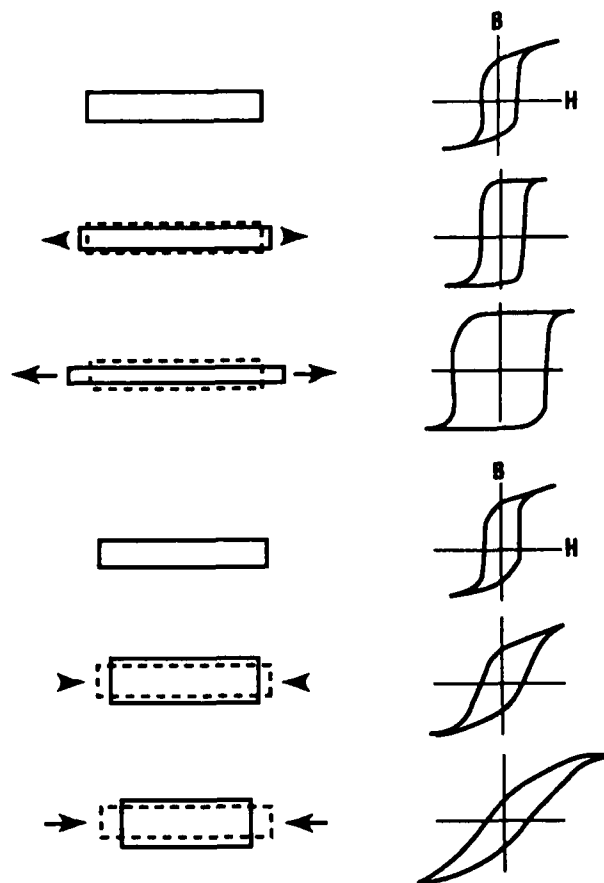
G0700-158

Figure 10.   Response of a Positive Material to Tensile and
              Compressive Strain.

```
┌─────────────┐      ┌─────────────┐      ┌─────────────┐
│   PHASE I   │      │   PHASE II  │      │  PHASE III  │
│ THEORY AND  │─────▶│  THIN-FILM  │─────▶│ INTEGRATION │
│   TESTING   │      │ DEVELOPMENT │      │             │
└─────────────┘      └─────────────┘      └─────────────┘
       │                    │                    │
       ▼                    ▼                    ▼
┌─────────────┐      ┌──────────────┐     ┌──────────────┐
│             │      │DEMONSTRATE AND│    │METALLIC GLASS│
│    WIRE     │      │ TEST SPUTTERED│    │  EVALUATION  │
│ EVALUATION  │      │ METALLIC GLASS│    │              │
└─────────────┘      └──────────────┘     └──────────────┘
       │                    │                    │
       ▼                    ▼                    ▼
┌─────────────┐      ┌──────────────┐     ┌──────────────┐
│             │      │  THIN-FILM   │     │  INTEGRATE   │
│   RIBBON    │      │ DESIGN AND   │     │  COILS AND   │
│ EVALUATION  │      │  PROTOTYPE   │     │METALLIC GLASS│
└─────────────┘      └──────────────┘     └──────────────┘
       │
       ▼
┌─────────────┐
│PHASE II AND III│
│THIN-FILM DESIGN│
└─────────────┘
```
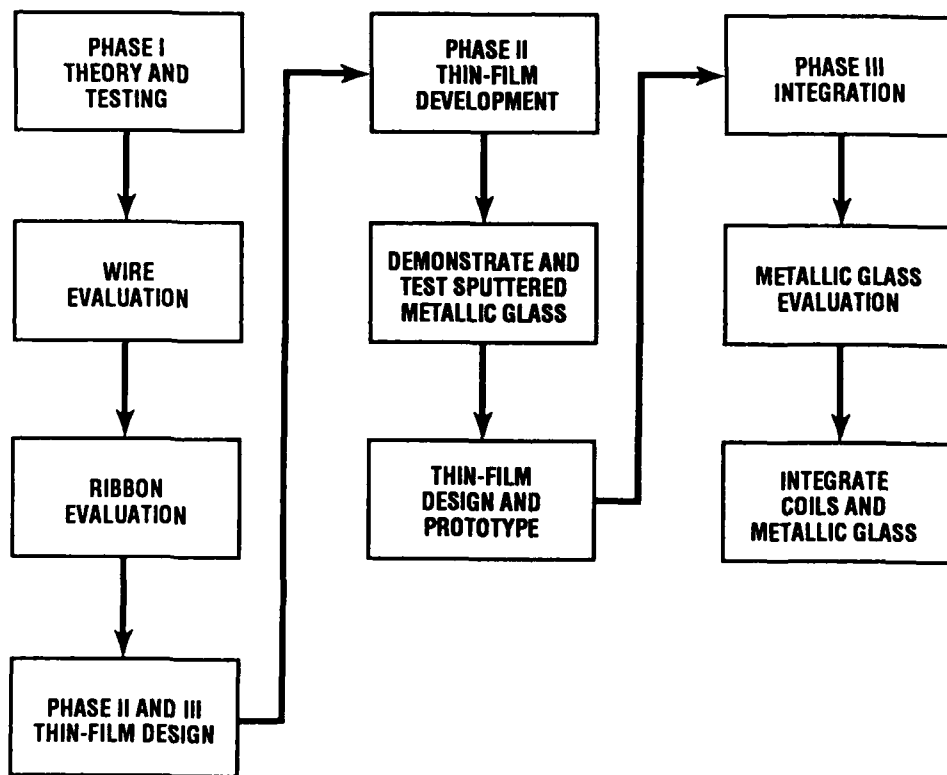
G0158-10

Figure 11. Magnetic Domain Strain Gage Program Flowchart.

3.0 EXPERIMENTAL PROCEDURE

3.1 Phase I Literature Search and Feasibility Study

3.1.1 Literature Search

The Magnetic Alloys Research Group of the Allied-Signal Metals and Ceramics Laboratory was responsibile for the program's literature search. A number of journal articles on the Barkhausen effect, propagation of domain walls and magnetomechanical coupling with an emphasis on metallic glasses were assembled and reviewed to increase Allied-Signal's understanding of the physics underlying the gage concept.

Analysis of magnetic data taken revealed that the propagation of domains of the sort observed in the classic Sixtus – Tonks experiments occurs over a fairly narrow range of applied magnetic fields; generally of the order of 0.05 – 0.5 Oersteds Oe (4.0 – 40 Amps/meter), for Fe-based amorphous wire. For smaller fields, only small nonpropagating changes in magnetization occur, as the applied field is insufficient to nucleate reverse magnetic domains. For larger fields, the magnetization process involves domain wall motion which is either completely transverse to the wire direction or has a very high axial velocity. In either case for high applied field, there is no resolvable propagation delay seen between the induced voltage pulses on physically separated coils.

In the intermediate (Sixtus – Tonks) region, there is considerable stress dependence to the propagation velocity in both amorphous wires and ribbons given various annealing treatments.

In another phase of the work, a current pulse was applied to a magnetic wire and the voltage induced in a small pickup coil wound around the wire was measured. This provides a determination of the transverse magnetization loop. Sharp pulses were seen, indicative

23

of rapid magnetization near the coercive field. Considerable dependence of pulse initation on the B-H curve was seen, indicating that the coercivity of this material is strongly dependent on tension.

The initial concept was to use the stress dependence of the propagation velocity of magnetic domain walls through a magnetic material. This concept requires that the magnetization occur through large Barkhausen jumps. The second concept, developed in the course of Phase I, employs the stress dependence of the magnetic coercive field.

The initial concept requires the use of at least two coils: a drive coil and one or two detection coils. However, the method is limited by the narrow range of parameters of excitation amplitude and stress over which true Barkhausen domain propagation occurs. This implies a limited range and lack of linearity of response. The problem of immunity to extraneous magnetic or electric fields, which may cause noise problems, also had to be assessed.

In the second concept, the magnetic material is driven through its hysteresis loop by application of a magnetic field either from an external drive coil or by passing an electrical current through the magnetic material. The response is seen as a voltage induced in a pickup coil due to the changing magnetization, as implied by Faraday's law. Pulses are induced, centered at the times at which the time-varying applied magnetic field equals plus and minus the coercive field. As the coercive field shifts due to applied stress, the phase of the pulses relative to the applied field shifts, which can be sensed either using an oscilloscope trace or using delta t electronics circuitry. In using the technique of passing current through the wire, ohmic heating can be a problem. A gated burst drive circuit was fabricated to apply large excitation current

levels and to limit the extent of heating, as one only needs to traverse the magnetization loop once to determine coercivity.

3.1.2 Wire and Ribbon Candidate Materials

The initial selection of magnetic materials included the following:

o   Balco 70 percent Ni - 30 percent Fe

o   Amorphous Fe wire (metallic glass)

o   Cobalt based wire

Initially, amorphous metals (metallic glasses) were selected as test cases to minimize the effects of magnetocrystalline anisotropy and crystallographic texture, both of which would complicate the interpretation of data. Materials were being studied in both the as-cast state and after magnetic annealing. An annealing yoke of mild steel was designed and built in the Allied-Signal Corporate Research apparatus shop to allow ribbon-form samples, 1/4 to 1 inch wide by 8 inches long to be annealed in a transverse field. This yoke is depicted in Figure 12. The testing of ribbons was important, because the magnetic effects seen in this geometry are expected to more closely approximate what would be seen in a thin film than a wire sample.

The test program revealed that the amorphous metallic glass in both the wire and ribbon format exhibited the characteristics desired for a magnetic domain strain gage. The following is a list of the advantages of an amorphous metallic glass material.

o   Crystalline alloys with desirable magnetic properties are generally soft-elastic limit 20 ksi.

Figure 12. Annealing Yoke (Designed and Fabricated by
Allied-Signal Labs) (Alnico magnets shown Hi-pole
up -- Transverse to ribbon)

o   Hardened crystalline alloys require 10-100 times higher drive current than amorphous.

o   Amorphous alloys are elastic almost to the yield limit (>100 ksi).

o   Desirable magnetic properties can be enhanced by heat treat or applied magnetic field during deposition.

o   Alloying with cobalt can raise curie temperature to 950-1100F.

o   Microstructure of amorphous material is conducive to superior magnetic properties.

3.1.3 Test Rig/Electronics/Setup

The test fixture was redesigned and modified to increase sensitivity and accuracy. A new load cell was procured to improve the low end accuracy and the fixture modified to allow dead weight calibrations. An oven was designed and fabricated, utilizing a tungsten halogen heat source, to provide an environmental chamber to characterize thermal responses. The test fixturing is shown in Figures 13 and 14.

An electronic circuit was designed and fabricated to read out the pulse time (delta t) which greatly expedited the data acquisition/reduction time during the running of the pulse tests. An additional circuit was designed and fabricated to input a high-amplitude periodic pulse current to excite the magnetic domains and propagate the domain wall to the receiving coil.

27

P-1121:0310
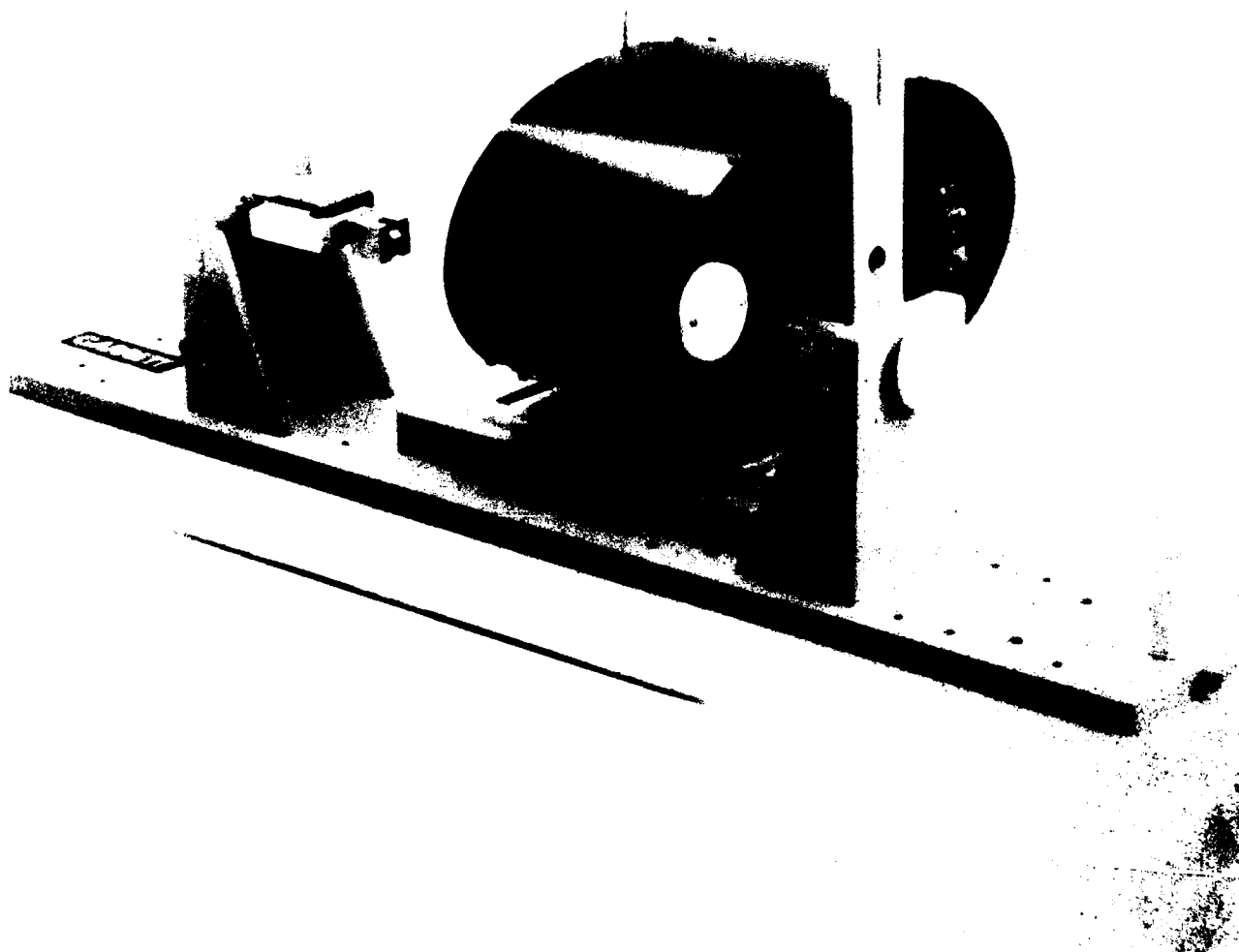
**Figure 13.   Wire Test and Evaluation Fixture With Tungsten
Halogen Heater.**
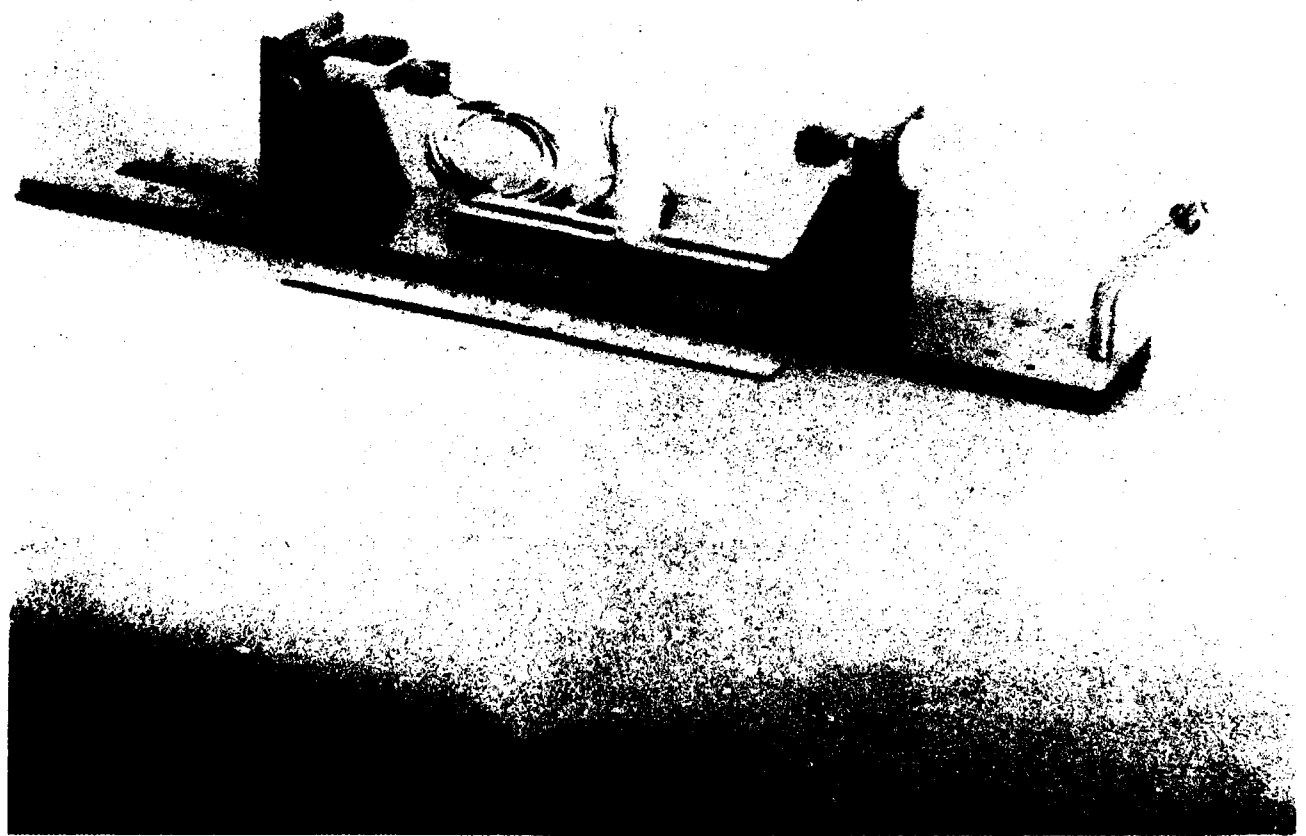
Figure 14. Wire Test and Evaluation Fixture Without Heater.

3.1.4 Test/Evaluation

The initial testing was based on the assumption that the gage would operate by sensing the velocity of a propagating magnetic domain wall, which separated regions of aligned and anti-aligned magnetization. After some preliminary testing with a two coil apparatus, it became apparent that a more clearly defined signal pattern would facilitate analysis. Hence, the GED Instrumentation Lab switched to a 3-coil configuration. Each coil had 25 turns and the coils were separated by about 1 cm. Coil 1 was used for initiating a propagating magnetic domain wall. The propagating wall produced a changing magnetization which induced a voltage successively in coils 2 and 3 according to Faraday's law. It was postulated that the time delay between the arrival of the domain wall at coils 2 and 3 determined the propagation velocity and that the velocity was dependent on the tension in the wire. These assumptions closely paralleled the results of the classic Sixtus-Tonks experiment. It was determined that the theoretical prediction of the propagation phenomenon was indeed operative, but only over narrow ranges of applied magnetic field and stress. Outside these ranges, it was difficult to quantify any difference in the time of arrival of pulses at coils 2 and 3, thus limiting the usefulness of a gage operating in this mode. Therefore, it was concluded that a simple magnetic domain reversal was being measured and not a propagating domain. However, it was noted that under an imposed stress in the magnetic wire there was a measurable shift in the phase of the pulses at coils 2 and 3 relative to the phase of the drive current in coil 1. More detailed measurements revealed that this phase shift was quite linear with applied stress over a wide range, affording a workable basis for a strain gage which was employed for the remainder of the contract effort.

B-H loops have been obtained in a conventional way by integrating the induced voltage (proportional to dB/dt) of the pick-up Coil 2 and displaying it parametrically versus the current drive.

The application of tension results in two obvious changes in the loop: an increased squareness ratio (ratio of the remanent induction to the saturation induction) and an increase in the coercive field, H_c. These results were in accord with the theory for a positive magnetostriction material.

Two constraints in the design of a practical strain gage system were identified:

o   Because the coil-magnetic material combination is an inherently nonlinear inductive load, a-c circuit theory implies that the pulse being launched has a finite rise time instead of being infinitely sharp.

o   Because of this finite rise time and the inherent dispersion of the induced pulse, there is uncertainty and a limit to the resolution to which the postulated velocity can be determined.

Figures 15(a) and 15(b) illustrate how the Sixtus - Tonks experiment can be accomplished in two ways. In Figure 15(a), the solenoid is used to provide a magnetic field H(t) which is switched periodically, as seen in Figure 16(a). An induced voltage is seen on each of the pickup coils; Figure 16(b) and 16(c). For each H transition, two pulses are seen on the pickup coils; the first is synchronous with the transition, and the second is due to the switching of the magnetic domains at that coil.

In the second scheme, shown in Figure 15(b), the driving field is applied as a current pulse $I_D(t)$ on the drive coil. The field (H) falls off with distance z from the drive coil as $1/z^3$. Hence domain propagation is seen only over the distance along the wire in which H falls within the Sixtus - Tonks Limits. The exact distance is dependent on specific material parameters, but is of the order of 1 cm.
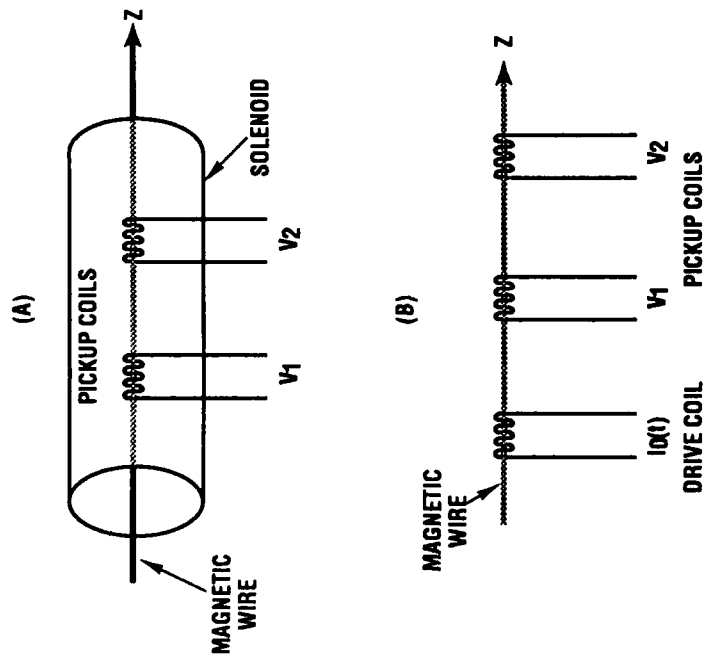
31

(A)

(B)

H(t)

V1(t)

V2(t)

FIGURE 16

(A)

PICKUP COILS

V2

V1

SOLENOID

MAGNETIC
WIRE

Z

(B)

MAGNETIC
WIRE

I0(t)

DRIVE COIL

V1

V2

PICKUP COILS

Z

FIGURE 15

G0158-8
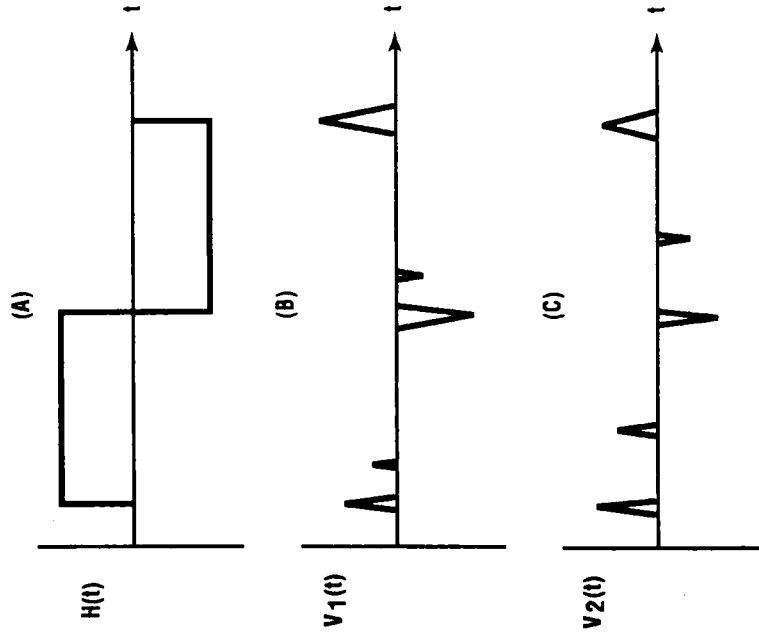
Figures 15 and 16.   Magnetic Domain Pulse Propagations.

The amorphous metallic glass wire demonstrated superior performance over the other wire candidates tested and the results are shown in Figures 17 and 18. The wire gages supported the theory development in the Phase I portion of the program. Metallic glass ribbons were used to simulate the behavior of thin film depositions. The results of delta time measurements versus applied stress are shown in Figures 19 through 28.

3.2 Phase II Development - Sensor Material

3.2.1 Sensor Material

The amorphous iron/boron/silicon alloy material was selected as the best candidate from Phase I. Phase I concentrated on tests involving wire and ribbon gages, whereas Phase II focused on thin film deposition of the same amorphous material.

The objective of the Phase II effort was to evaluate thin films of the amorphous iron/boron/silicon material sputtered on quartz substrates as shown in Figure 29. Once the sputtering targets were fabricated, the thin film deposition onto quartz substrates was initiated.

Allied-Signal Corporate Research Labs successfully applied aluminum oxide via chemical vapor deposition (CVD) onto titanium substrates for use on the program. Successful thin film coatings of metallic glass onto quartz and the CVD coated titanium were received from XiMagnetics. The coatings received from Damaskos initially appeared to be successful but later proved defective in repeatability and reliability testing. The 8-inch-diameter metallic glass target that Damaskos was using cracked during sputtering operations, and it is suspected that the resultant coatings are contaminated with the bonding material that affixes the target to the backing plate. Scanning Electron Microscope (SEM) evaluations were done to confirm and evaluate the Damaskos coatings.
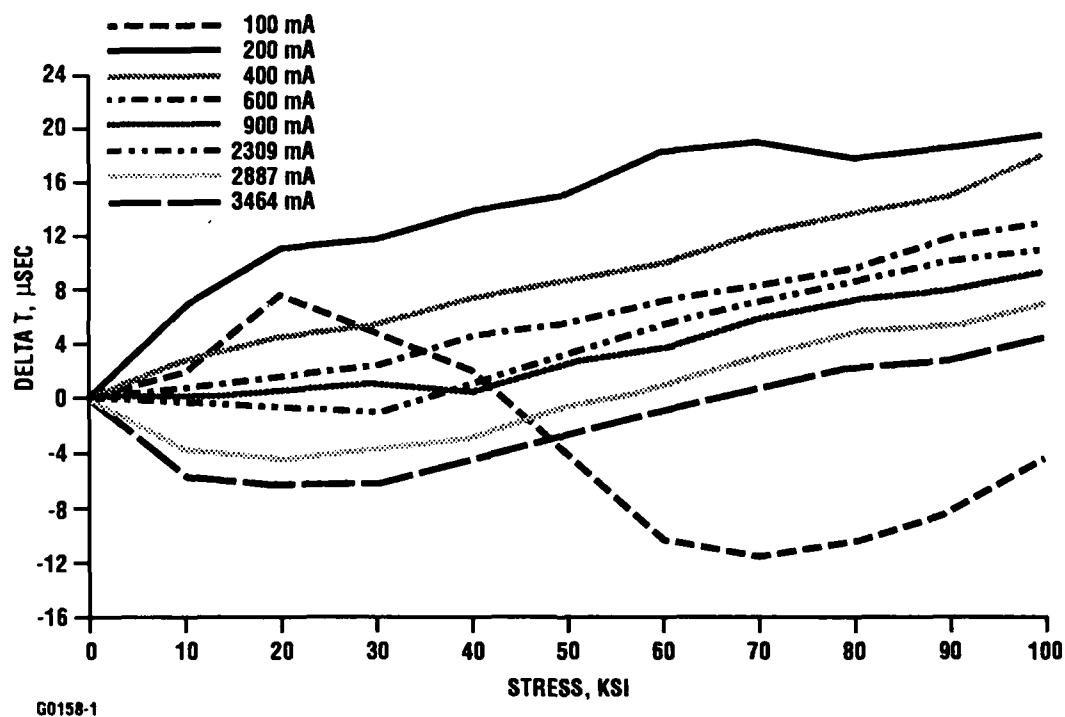
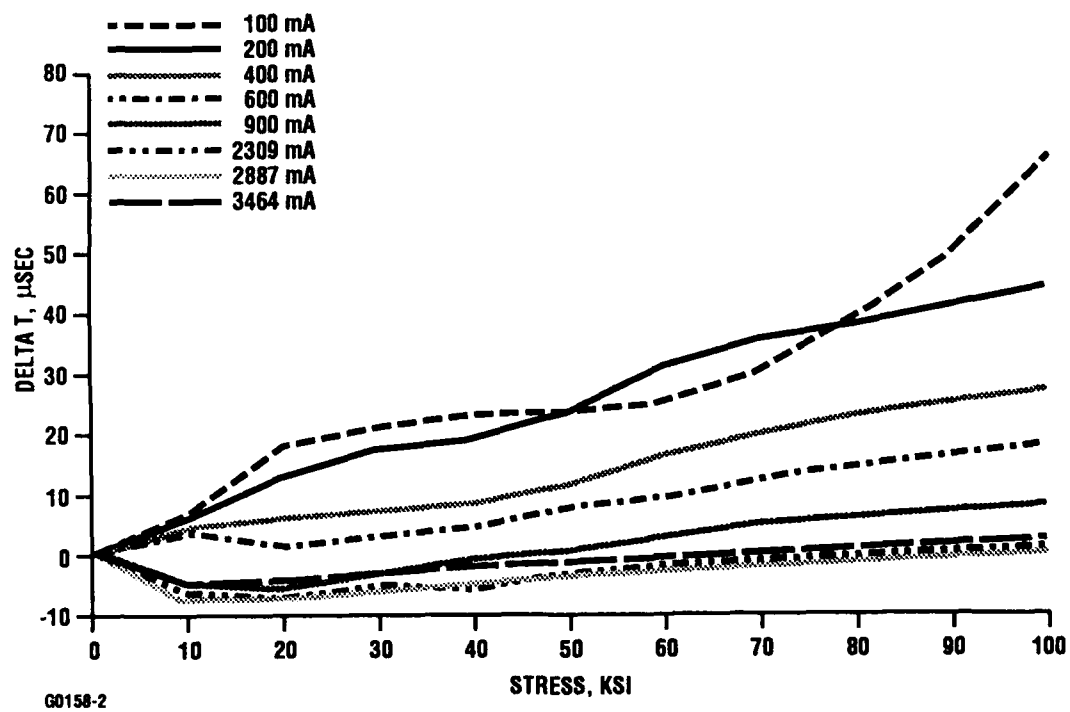Figure 17. Two-Coil Amorphous Wire Gage Response - Maxima.

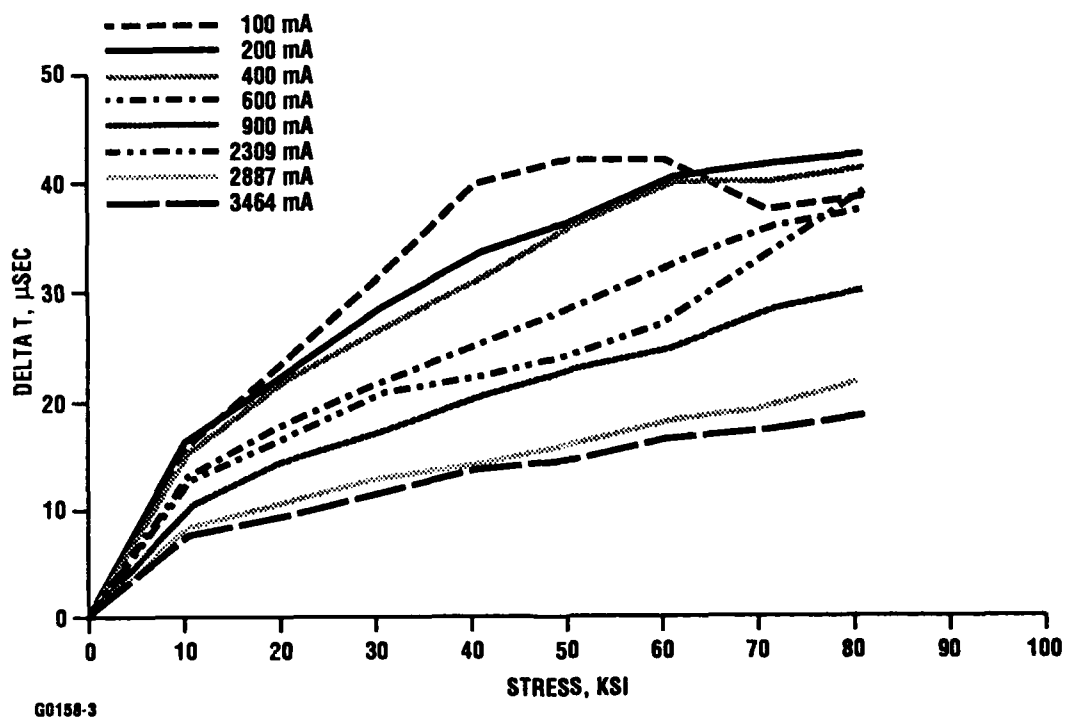Figure 18.   Two-Coil Amorphous Wire Gage Response - Minima.

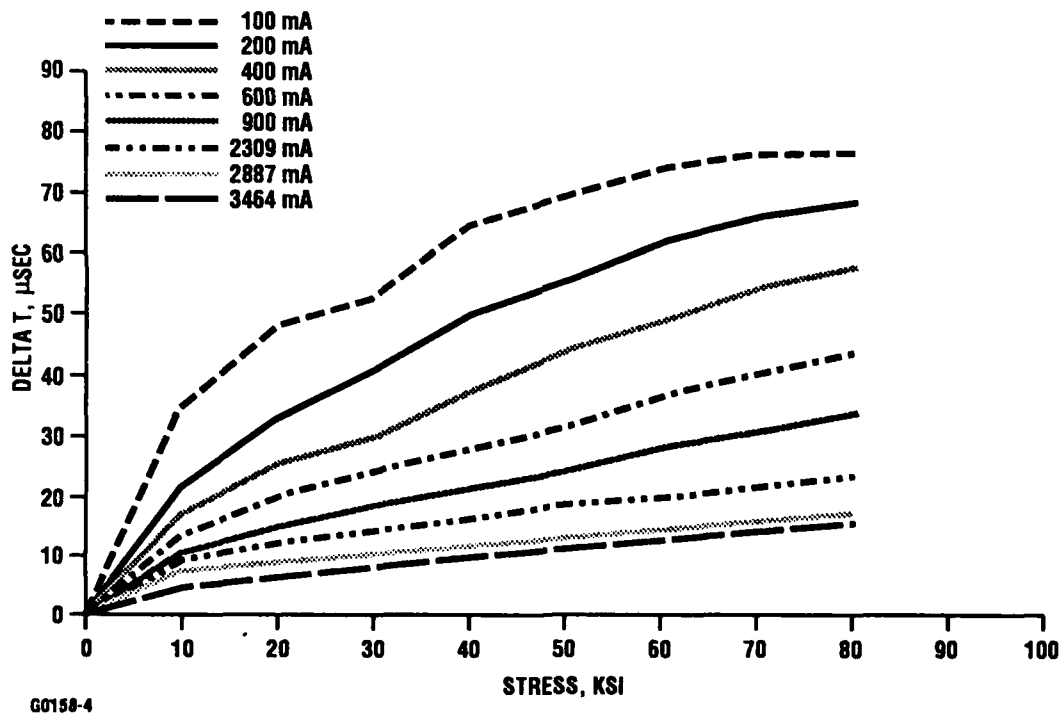**Figure 19. Two-Coil Amorphous Ribbon Gage Response - Maxima.**

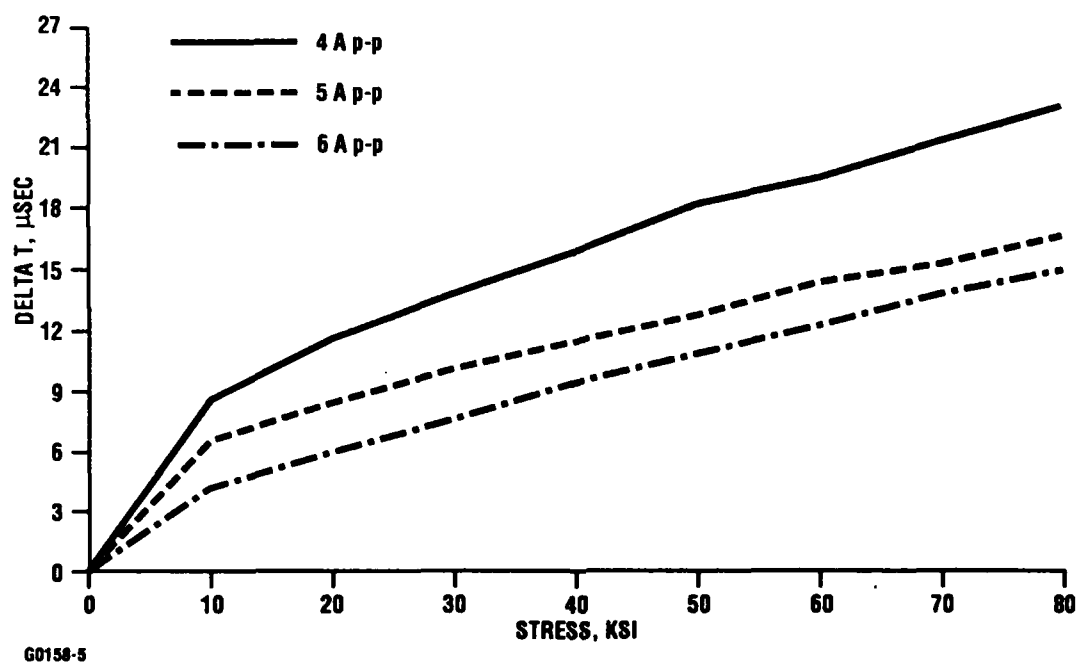Figure 20. Two-Coil Amorphous Ribbon Gage Response - Minima.

Figure 21. Two-Coil Amorphous Ribbon Gage Gated Burst Response - Maxima.
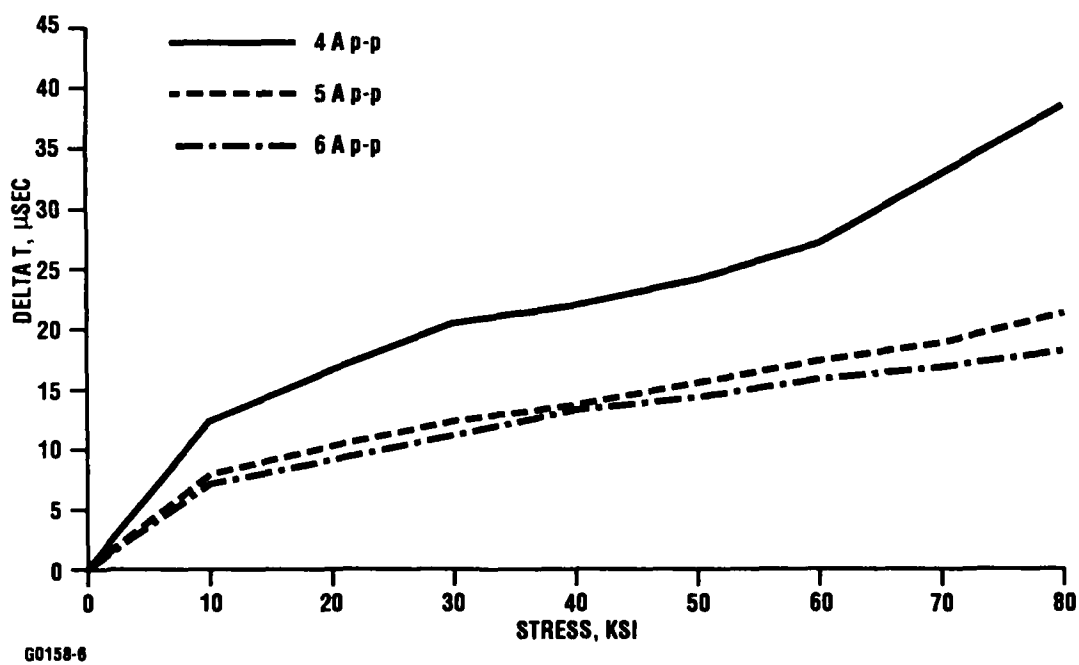
Figure 22. Two-Coil Amorphous Ribbon Gage Gated Burst
Response - Minima.

TEMPERATURE/SCATTER TEST
200 F

Figure 23. 200F Temperature/Scatter Test Results.

Figure 24. 300F Temperature/Scatter Test Results.

41
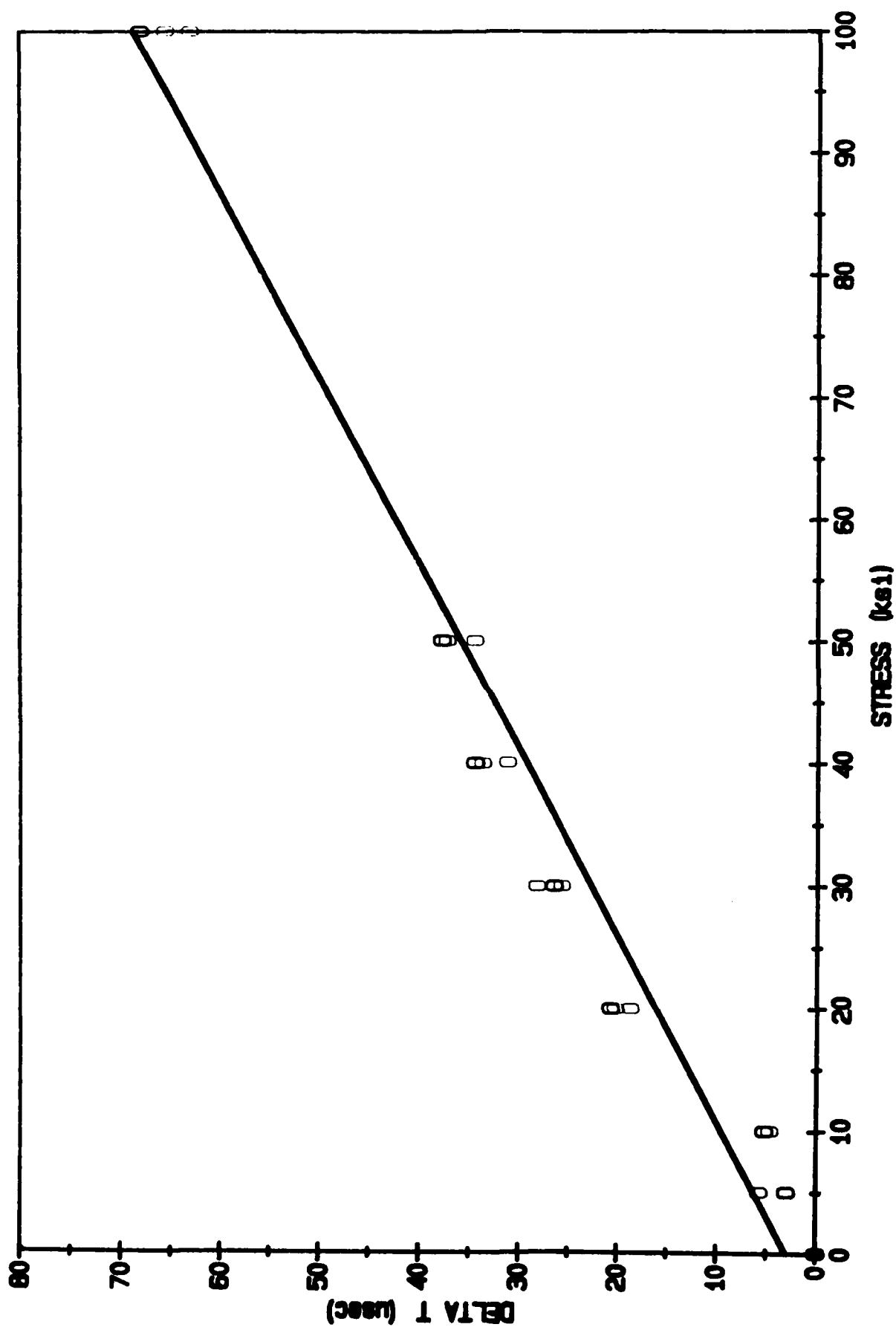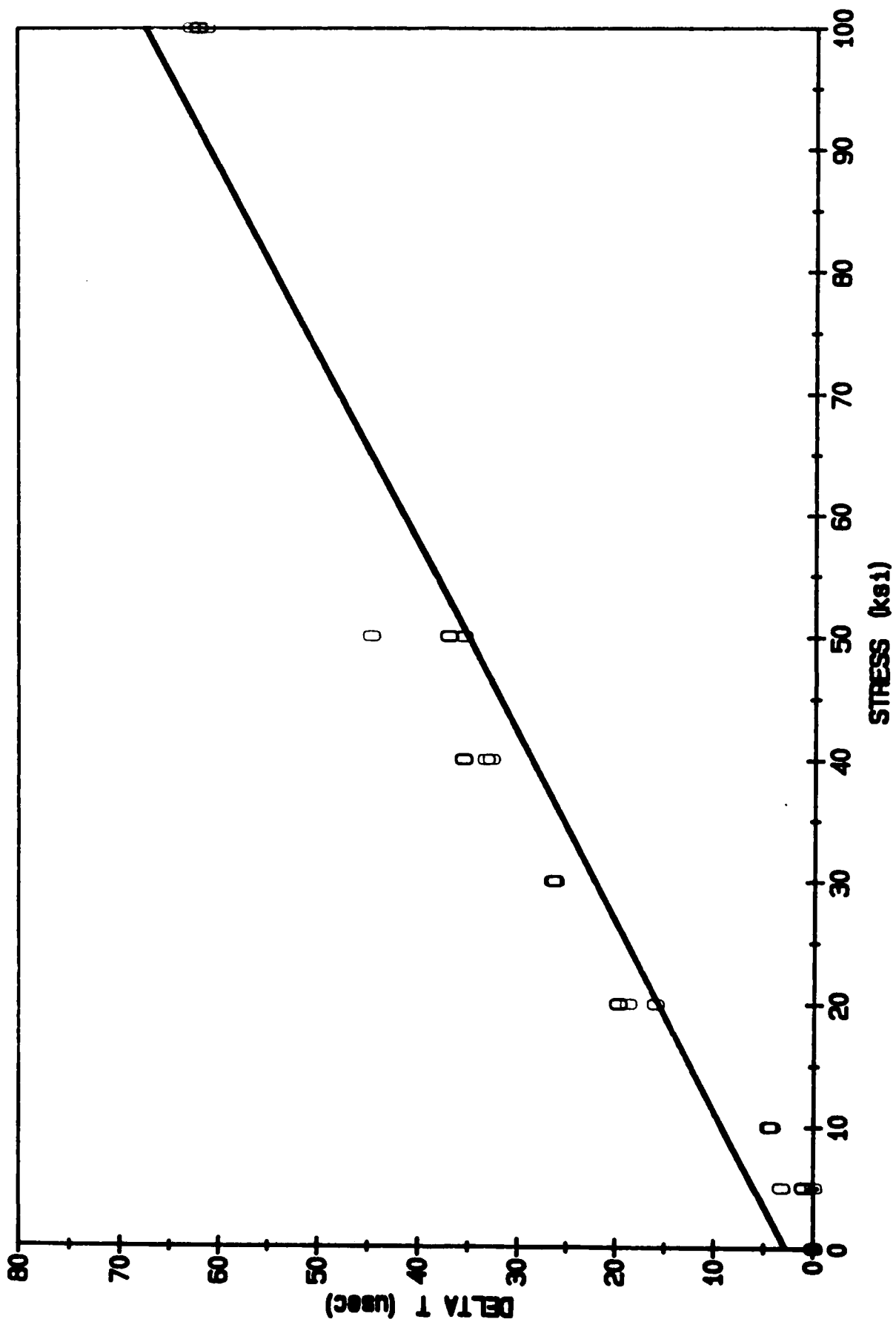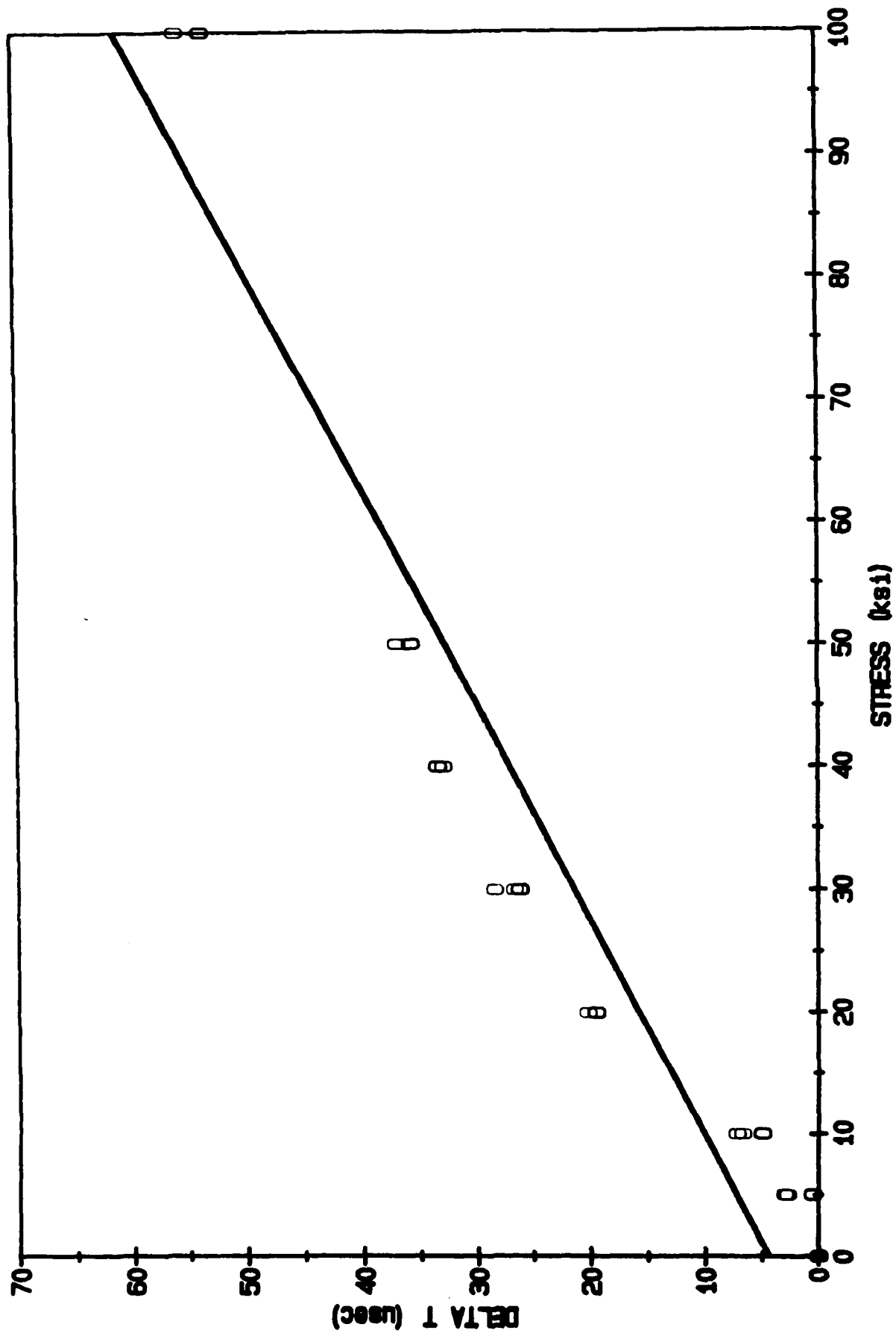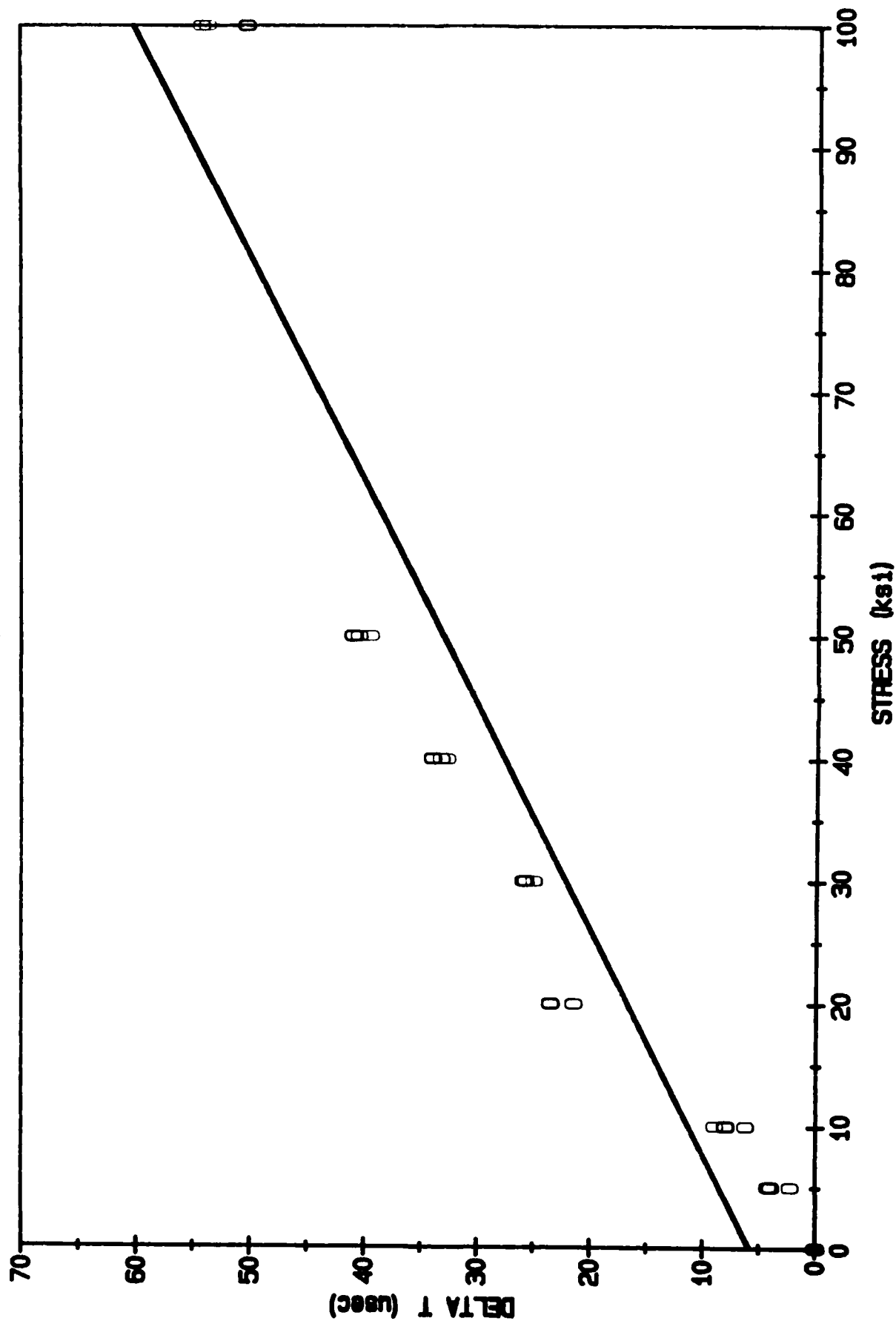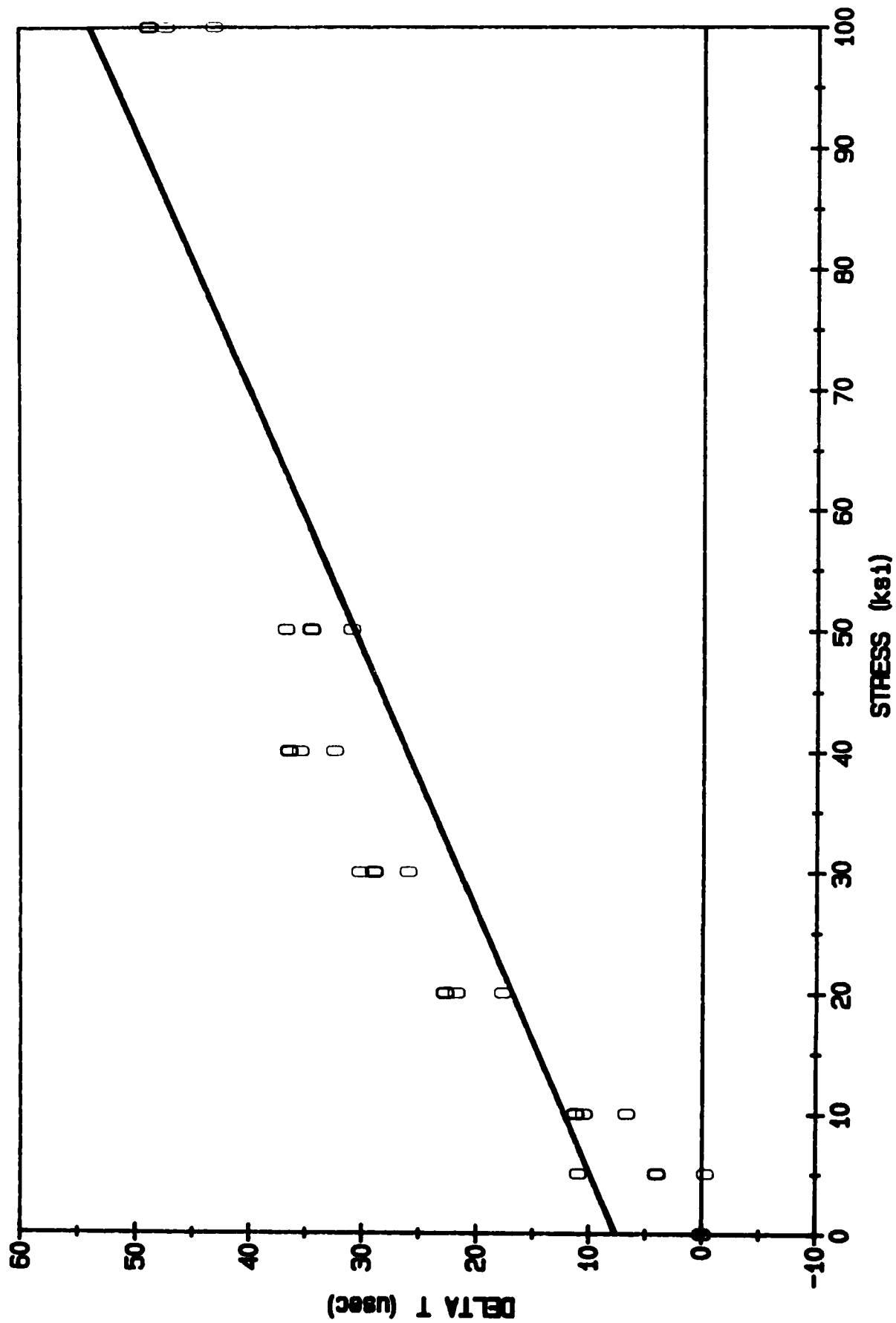
Figure 25. 400F Temperature/Scatter Test Results.

42

TEMPERATURE/SCATTER TEST
500 F

Figure 26. 500F Temperature/Scatter Test Results.

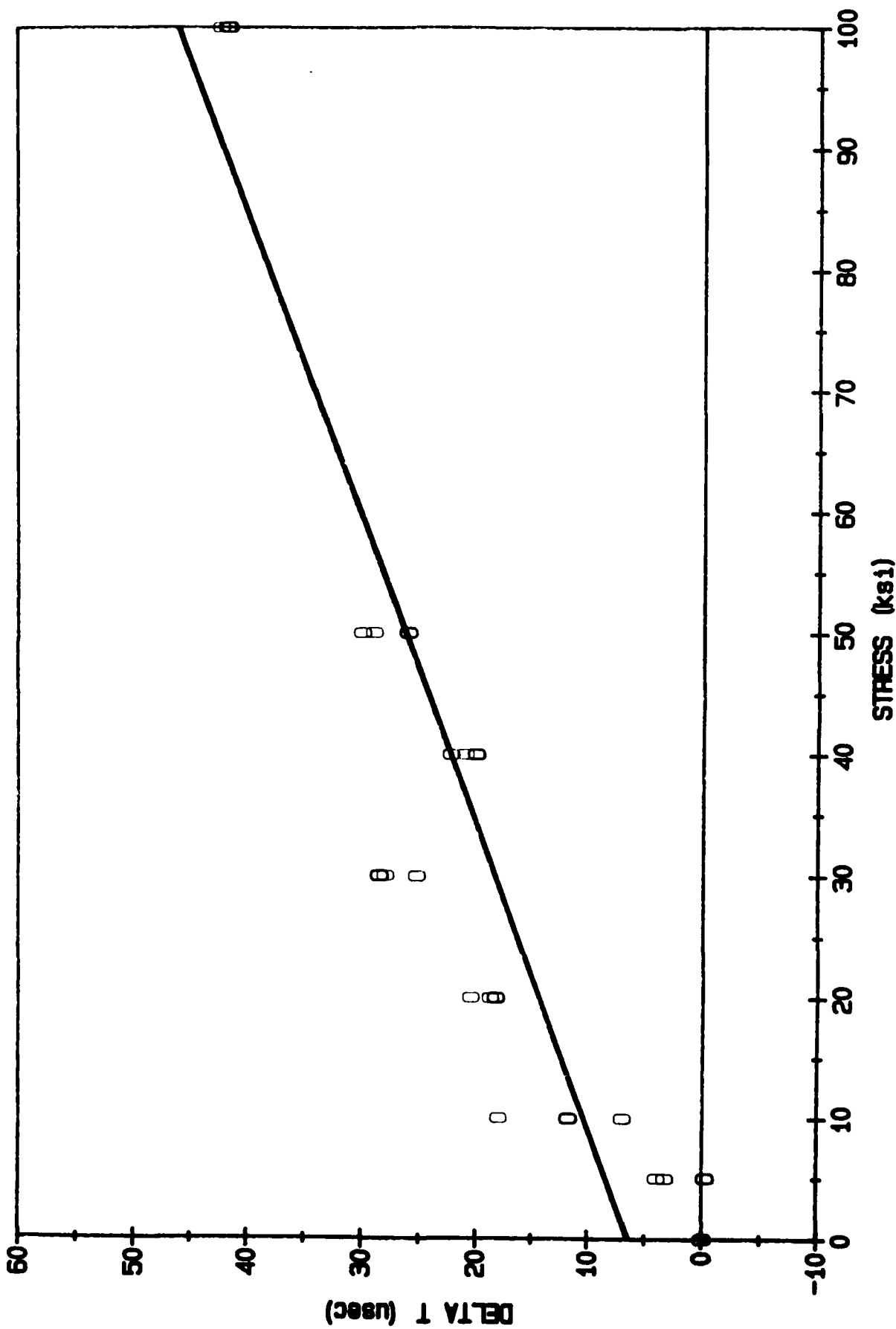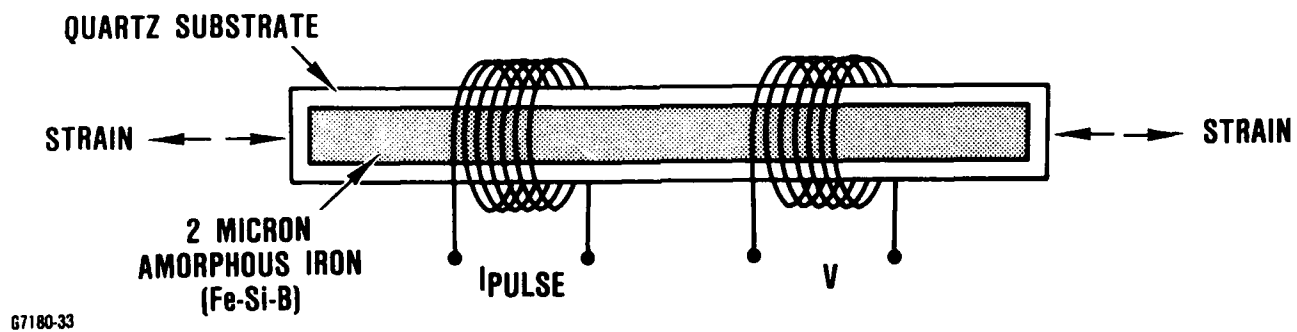Figure 27. 600F Temperature/Scatter Test Results.

44

Figure 28. 700F Temperature/Scatter Test Results.

QUARTZ SUBSTRATE

STRAIN

2 MICRON
AMORPHOUS IRON
(Fe-Si-B)

G7180-33

IPULSE

V

STRAIN

Figure 29. Phase II Prototype Sputtered Gage.

Material morphology is critical to the design and success of a thin film gage. Initial testing of these films was accomplished by winding a standard copper coil around a sputtered amorphous sample. This enabled GED to evalaute the amorphous material in a gage configuration.

Dr. John L. Wallace of XiMagnetics, under the sponsorship of the U.S. Department of Energy (DOE), documents the difficulty of fabricating targets of iron-boron-silicon and proposes an alternate means of producing an amorphous coating, of this same alloy, by a reactive sputtering technique. This method is documented in Appendix A; however, it was not used in this program.

3.2.2 Coil Development

Phase II investigated, as a parallel effort, the other technologies (aluminum oxide insulation layers, antidiffusion layers, thermal layers, gold coil sputtering and photomasking techniques) needed for the eventual fabrication of an entire gage design (Figure 30) that would occur in Phase III of this program. This included the aluminum oxide, coil fabrication technologies, interlayers, bond coats, photofabrication development, step coverage, diffusion analysis and photomasking requirements.

GED was notified by Engelhard in August of 1988 that they had decided to close their precision thin film coatings division. Engelhard was considered by GED to be the primary coating vendor for the gage development. The other coating vendors involved in the program (Damaskos and XiMagnetics) were contacted to see if they could pick up the work that Engelhard was scheduled to do. Other vendors also were contacted, including American Microcomponents in Milpitas (Silicon Valley), California, which was recommended by Engelhard.
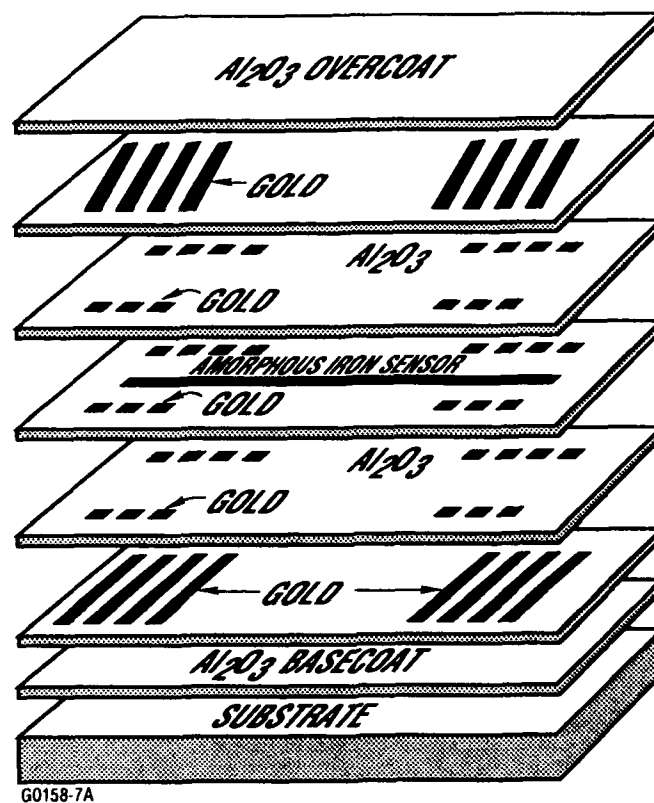
Figure 30. Cutaway of Phase III Thin Film Strain Gages
(Simplified Illustration, see Page 78 for
Full Complement of Depositions).

American Microcomponents (AMCI) was selected to complete the coil development portion of the job and Figures 31(a) and 31(b) illustrate their successful sputtering of the entire coil system.

AMCI evaluated improvements in interlayers, diffusion barriers and bond coats that were required for a successful gage design. AMCI purchased targets of gold, titanium tungstenate, silicon dioxide, and paladium for the coil and coating development.

Contact with XiMagnetics was maintained by GED for possible metallic glass deposition in Phase III should time and sputtering difficulties preclude successful completion at AMCI.

3.2.3 Test/Evaluation

A thin film sensor evaluation fixture was fabricated to test the thin film specimens. Figures 32(a), 32(b), and 33 are photographs of the fixture and the test setup. Metallic glass quartz specimens coated by Damaskos and XiMagnetics were tested on this fixture.

These tests revealed that the coatings were amorphous in structure and the coercivity measurements are similar to those experienced in the wire/ribbon portion of the Phase I activities. Figures 34 through 38 are graphs of delta time measurements versus applied stress. Each figure contains maxima and minima traces determined from pulses of both positive and negative polarities as shown in Figure 7. In principle the phase shifts should be identical, since the positive and negative coercive points (illustrated in the B-H loop of Figure 2) are equivalent. The apparent differences in phase shift between the polarities can arise from several sources, including:

o   Lack of precision or experimental error in the determination of peak position;
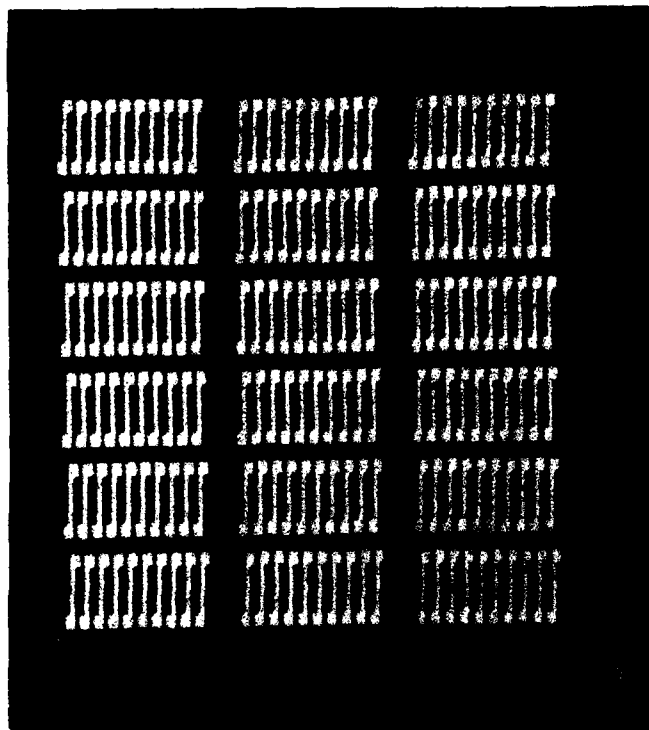
Figure 31(a). Lower Coil Array Sputtered at AMCI.
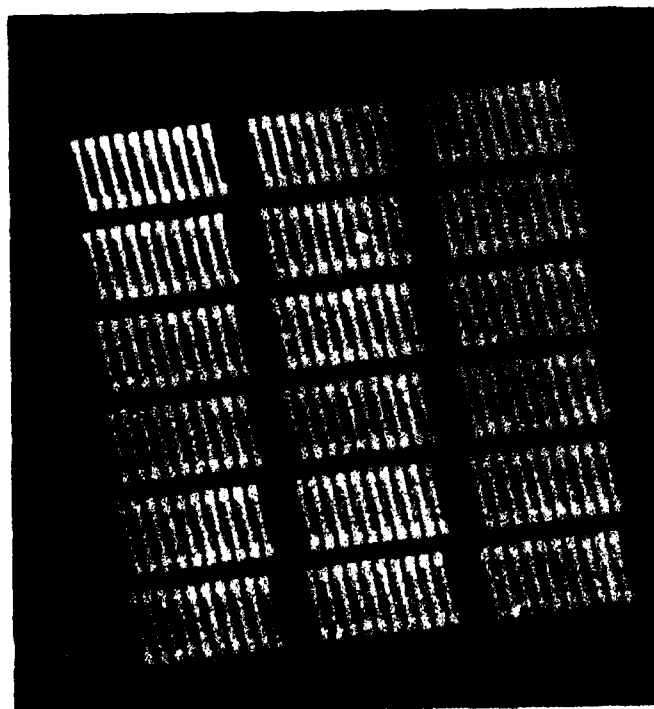
Figure 31(b). Completed Coil Array Sputtered at AMCI.
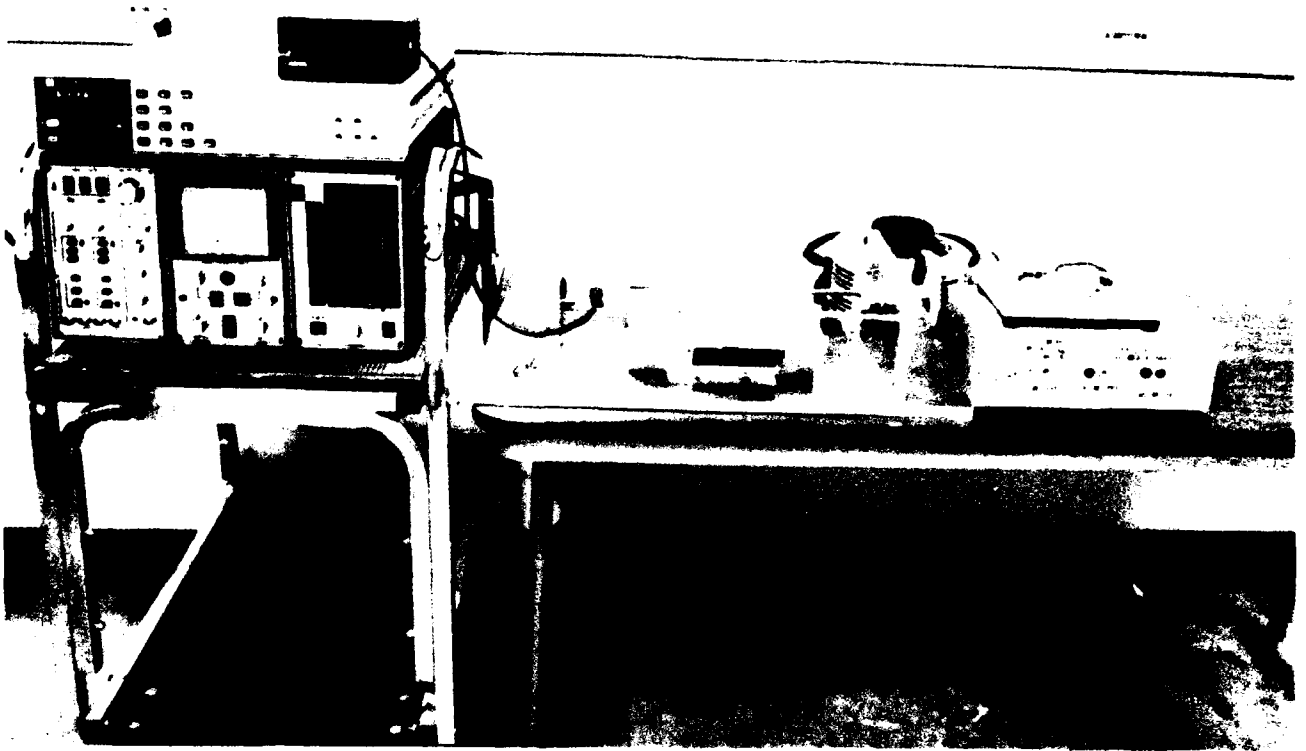
Figure 32(a).   Test Setup with New Thin Film Evaluation Fixture.
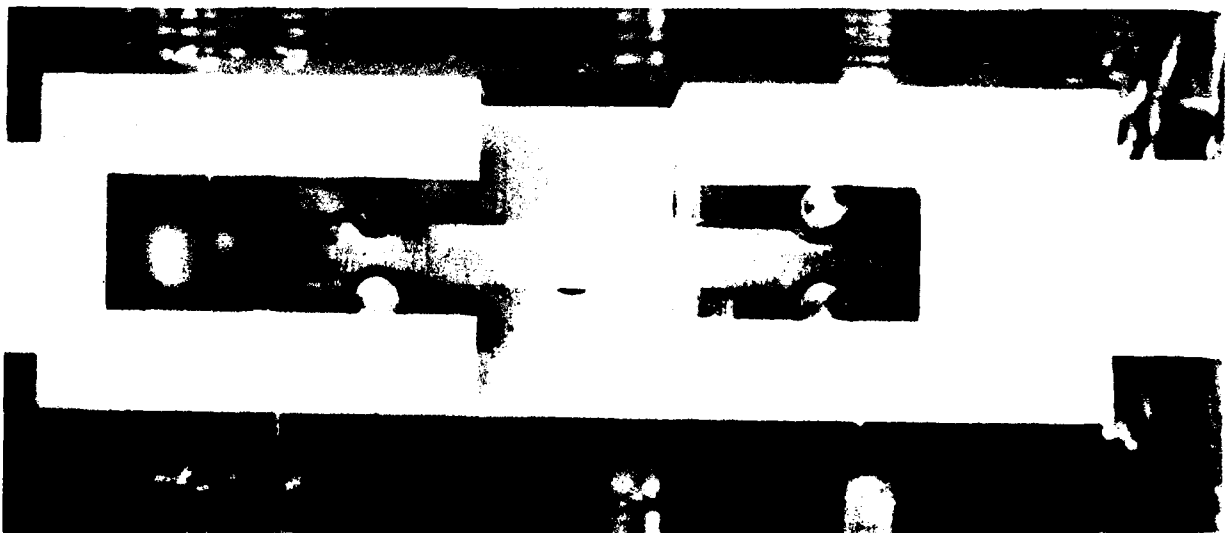
Figure 32(b).   Specimen Holding Fixture.
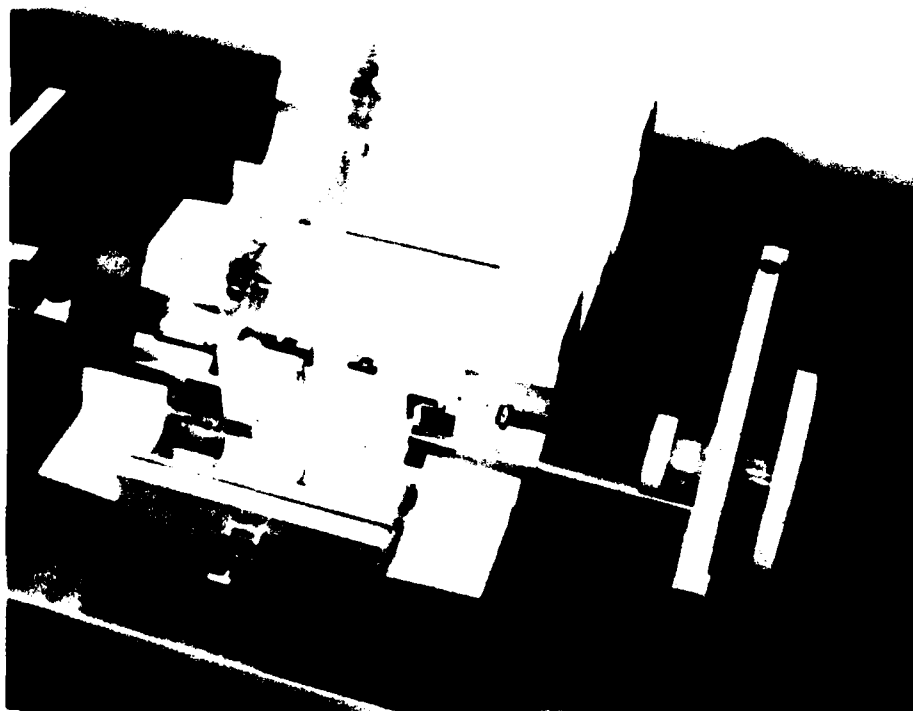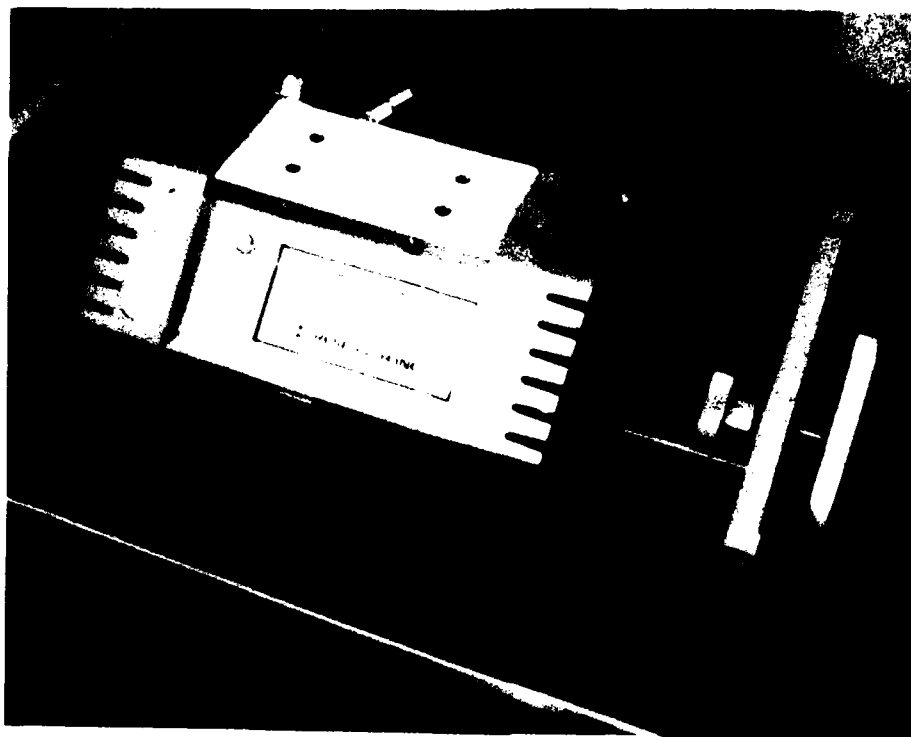
Figure 33. Radiant Heating Oven in Thin Film Evaluation Fixture (Closed and Opened Positions).
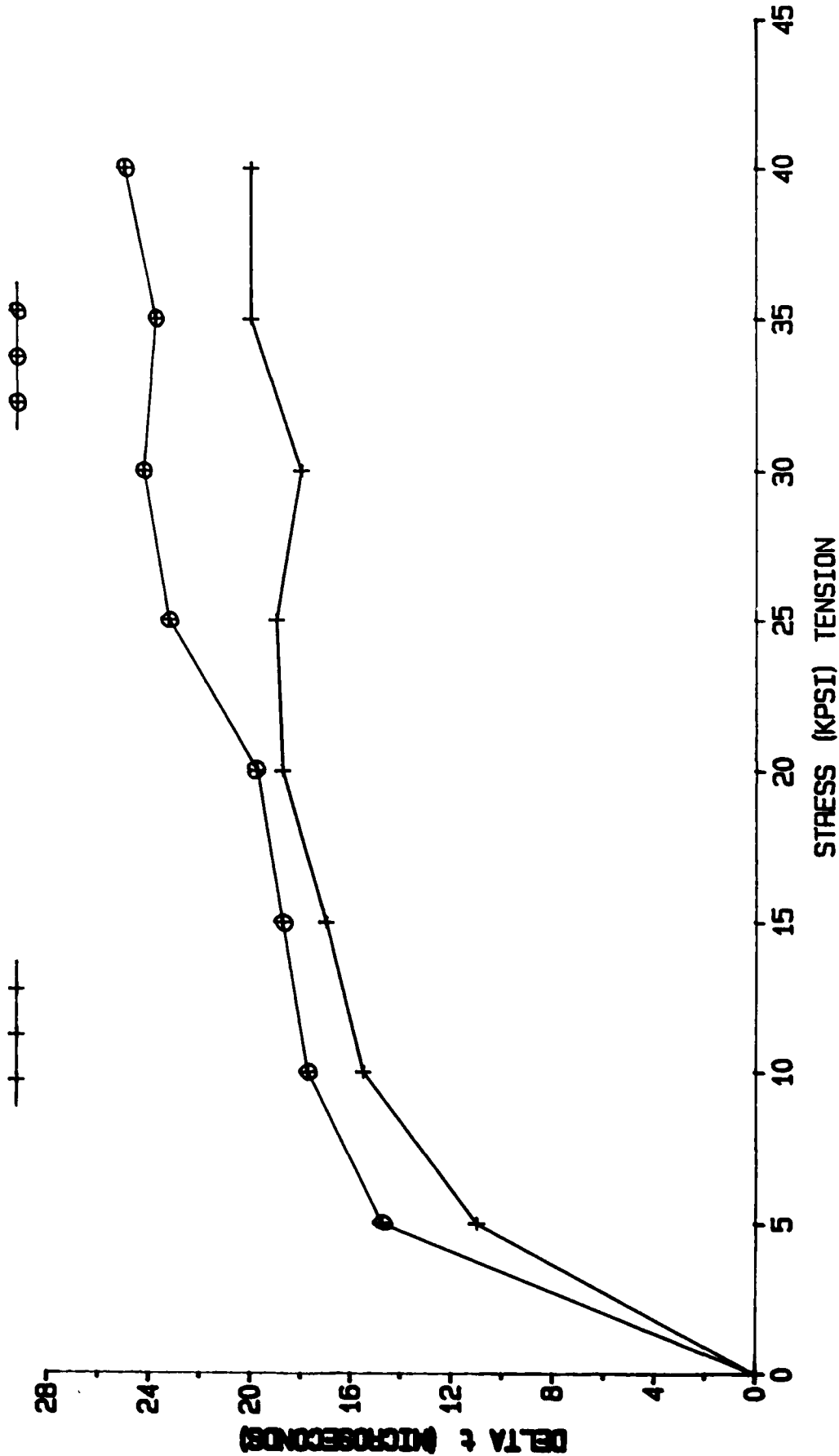
Figure 34. Thin Film Gage Response - Titanium Substrate - 500 mA.
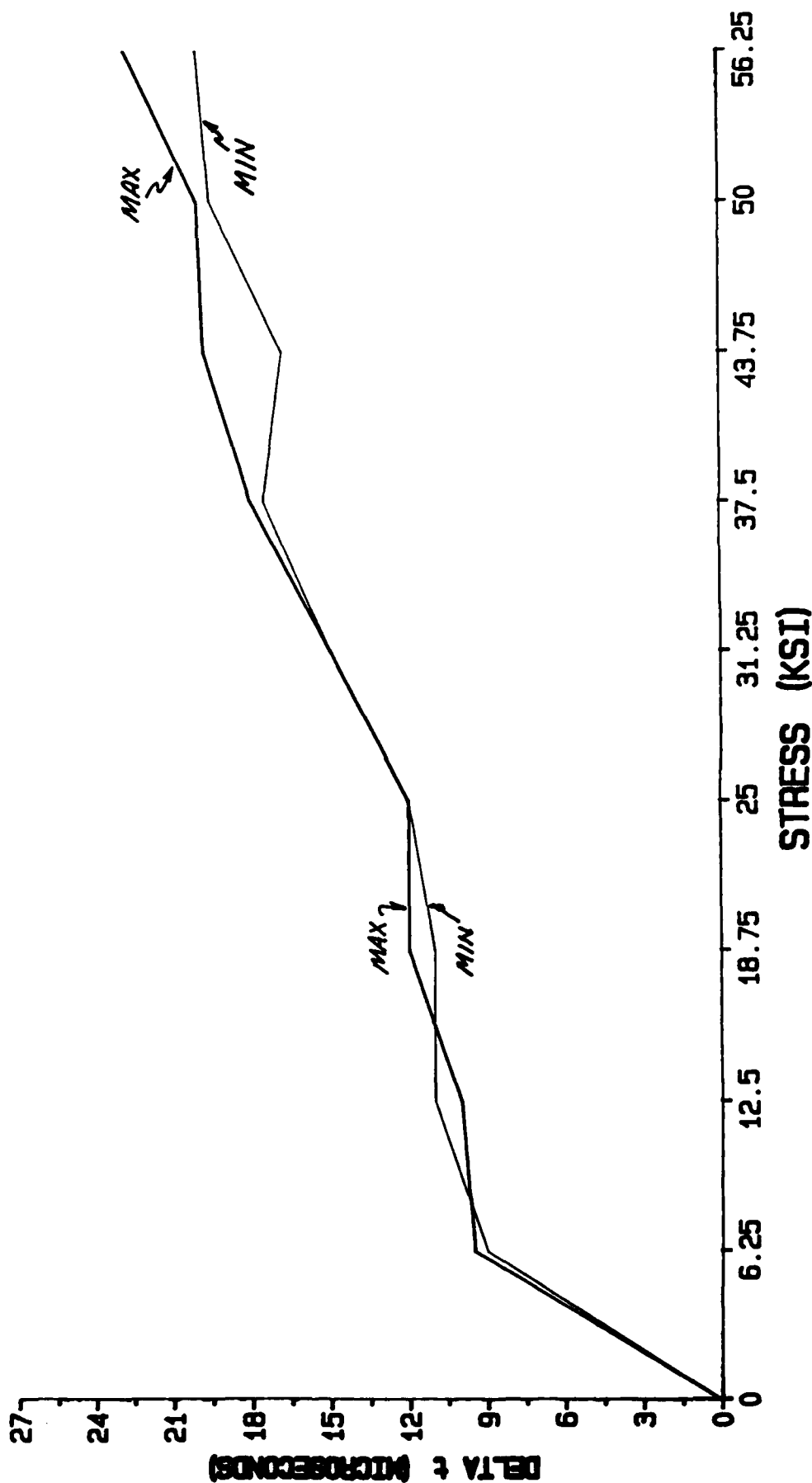
Figure 35. Thin Film Gage Response - Titanium Substrate - 520 mA.

54
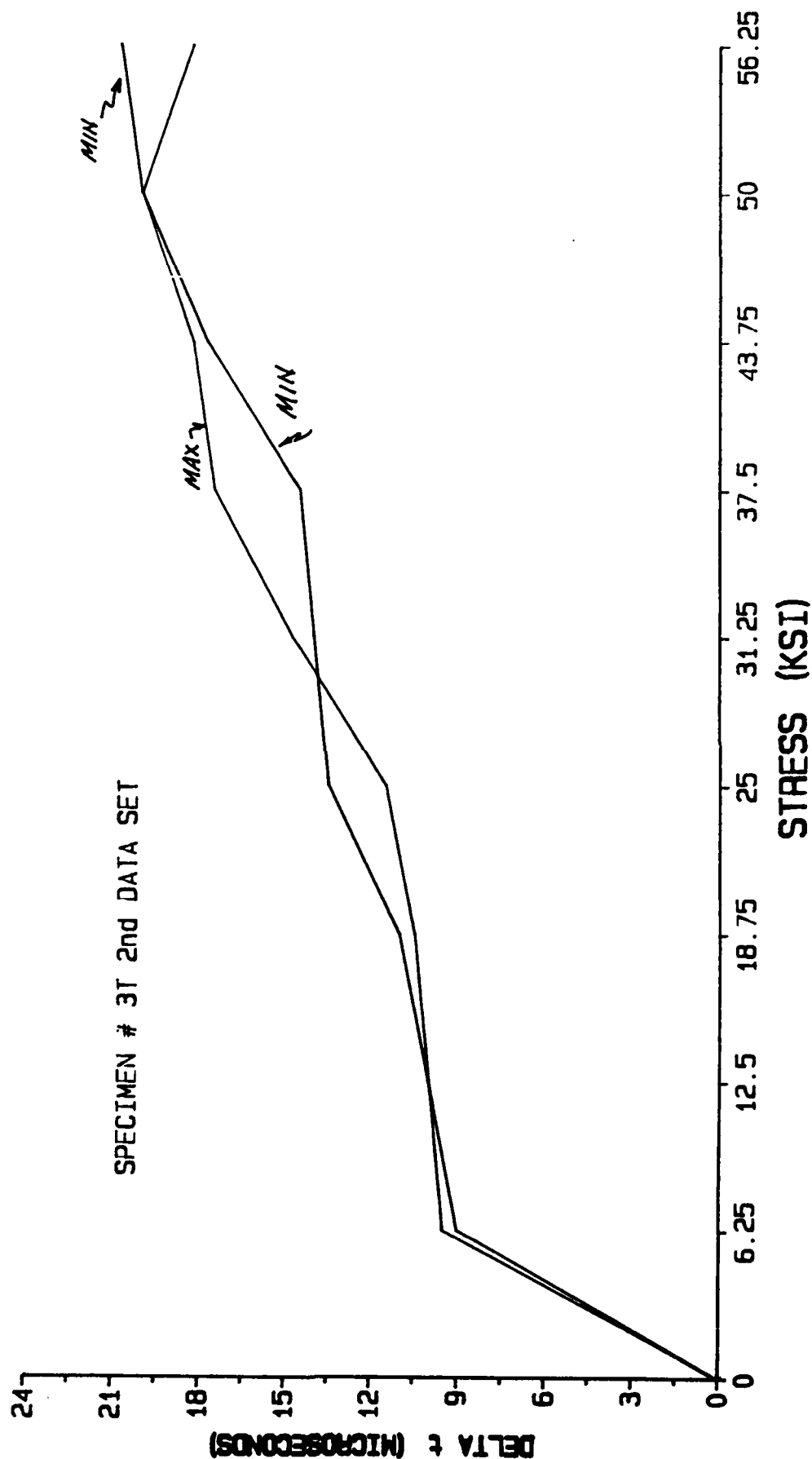
Figure 36. Thin Film Gage Response – Titanium Substrate – 520 mA.

55
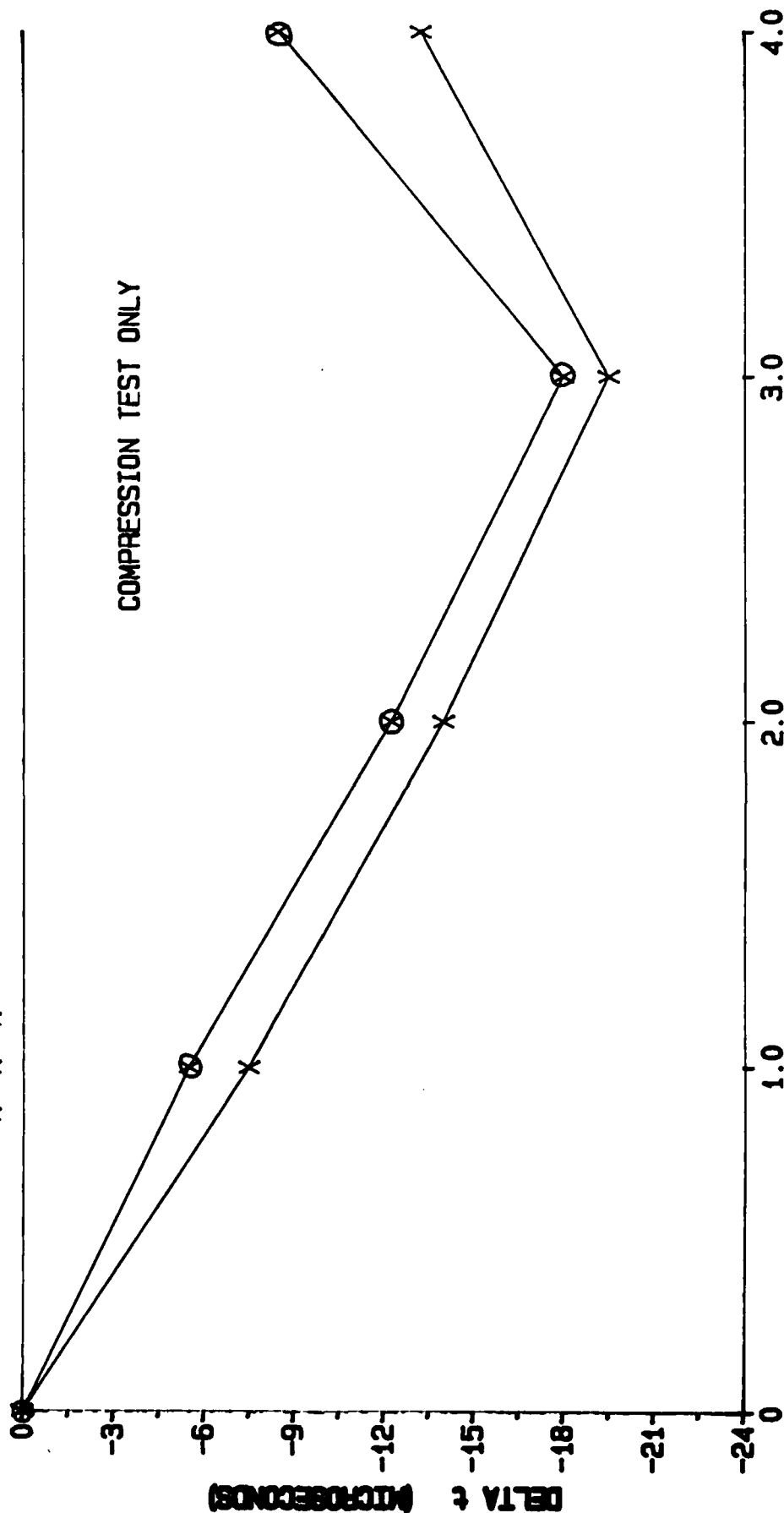
Figure 37. Thin Film Gage Response - Quartz Substrate - 380 mA.
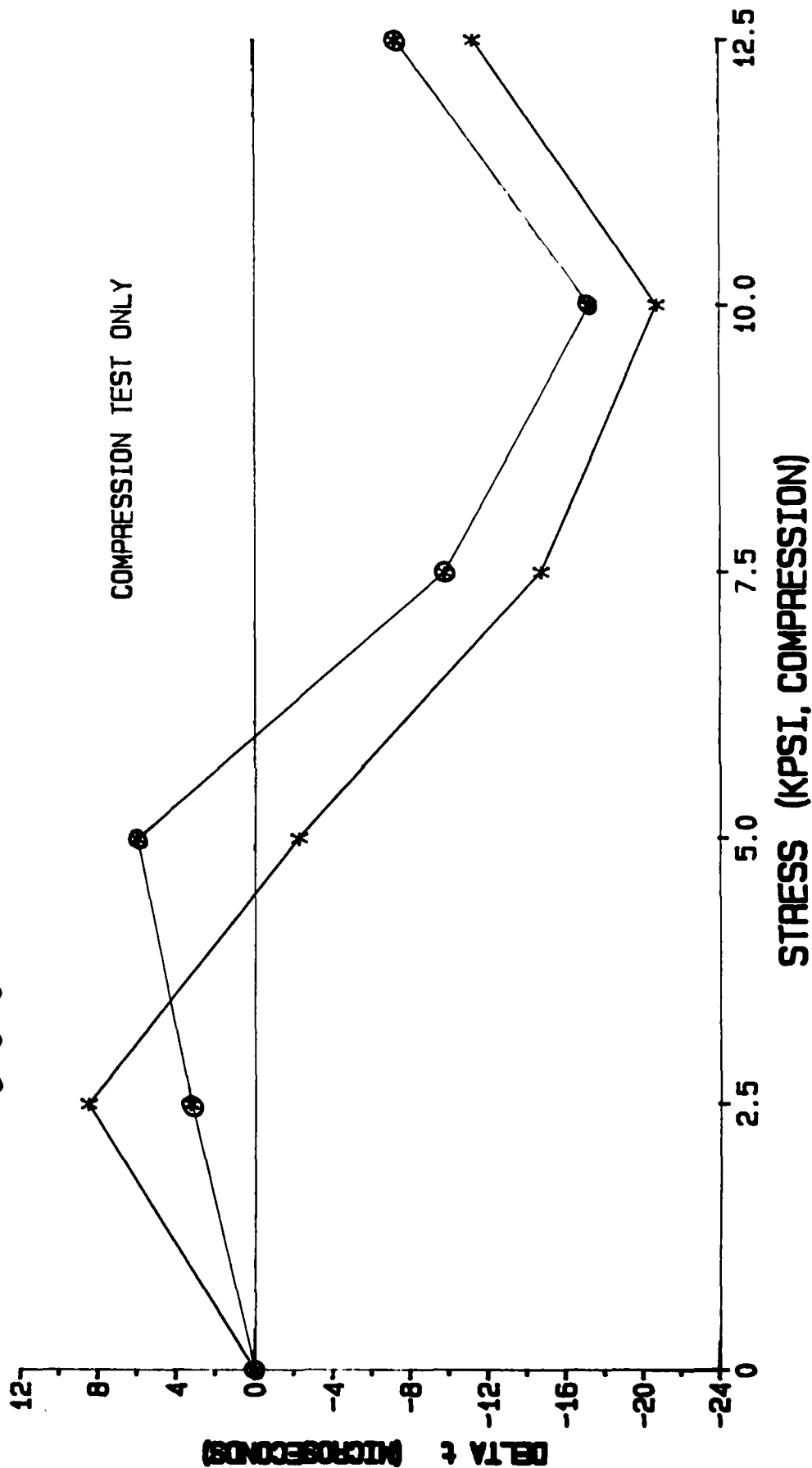
Figure 38. Thin Film Gage Response - Quartz Substrate - 300 mA.

57

o   A Bias caused by external fields, such as earth's field;
    or

o   Use of insufficient drive field to saturate fully the mag-
    netization, resulting in an asymmetric minor hysteresis
    loop.

The effects are felt to be minimal and can be overcome by proper design of the peak detection circuitry and use of an adequately large drive field.

Gage sensitivity was similar to what was experienced in the Phase I tests of wire and ribbon gages. It was noted during the testing that some specimens responded better than others when cycled in compression and tension. The Allied-Signal Magnetic Alloys Research Group analyzed the data and determined that these specimens had a residual tensile strain in the film from the deposition process. An examination of Figure 37 reveals that the residual tensile strain in the metallic glass was approximately 3000 psi, and it was only after this load was applied that the film began showing a compressive response. It must be noted that since metallic glass is a positive magnetostrictive material, the films would respond minimally to a compressively applied load. It was decided that a predetermined residual tensile strain should be introduced into the film as it is deposited to allow improved compressive and tensile load measurements. Dr. Fish's analysis, discussion and recommendations can be found in Appendix B.

Mixed results were obtained from the two vendors. XiMagnetics specimens demonstrated good data signals, whereas Damaskos coatings were very erratic in signal quality, reliability and repeatability. Efforts to improve the signal quality, such as etching the metallic glass to remove edge effects, together with epoxy overcoatings to prevent oxidation, were not successful. A materials analysis on the coatings applied by both vendors was performed to determine if

contamination in the Damaskos coatings was the cause of the anom-
alies. Both the GED Materials Lab and the Allied-Signal Research
Center were involved with the analysis. Damaskos noted on their
coating runs that cracks seen in the metallic glass target, made
bonding agent contamination suspect. XiMagnetics used a cast metal-
lic glass target, whereas Damaskos used a target fabricated by
powder metallurgy.

Testing of the existing metallic glass specimens was completed
at GEd with inconclusive results. Insufficient sampling, oxidized
specimens and contamination precluded the acquisition of a good data
base for the magnetic sensor material. All the specimens were pho-
tographed and the results cataloged.

In a parallel effort, AMCI, with consultation by GED, developed
the complex interlayer sputtering techniques necessary for the coil
fabrication and testing, and the subsequent integration of the
metallic glass sensor element.

Extensive interlayer development was necessary to overcome the
following problems inherent in the multi-layer thin-film fabrica-
tion:

o   Thermal mismatch and gradients at temperature which can
     debond the coatings

o   Migration of one constituent or element from layer to
     layer causing shorts, inclusions, or failure of the sensor
     and coil

o   "Planarization" of the metallic glass layer in the thin-
     film circuit (Sputtering techniques that planarize coat-
     ings over irregular surfaces, such as the coil configura-
     tion, were addressed.)

The bulk of the Phase II and Phase III efforts were accomplished at the AMCI facility including coil evaluation and testing. Results were extremely favorable for a complete gage to be built in Phase III. The initial coil system was tested to 800F with current levels up to 700mA applied. There were no failures in the coil system. AMCI conducted an exhaustive evaluation of the bond and diffusion layers required for the total gage system fabrication. The multilayer coil system was fabricated and evaluated. Problems in step coverage and diffusion were noted and resolved.

All necessary photomasks were designed and fabricated. AMCI successfully sputtered the entire coil system on aluminum oxide plates, including all the necessary interlayers, diffusion barriers, and bond coats. Step by step evaluations of the prototype coils were accomplished at AMCI.

Evaluation of the metallic glass sensor needed to include the following issues and properly address sensor performance, calibration, and repeatability:

o   Repeatability of output with cyclic loading

o   Run-to-run variations in the sputtering process

o   Temperature calibration or apparent strain evaluation for metallic glass

o   Current capacity and requirements for magnetic saturation of the material

o   Determination of the residual film stresses and the effect on the calibration curves

o   Material characteristics and the determination of the Curie and recrystallization points

o   The effects of stray magnetic fields

3.3 Phase III Fabrication and Test

3.3.1 Integrate Technologies

Phase II provided the following basis for the follow-on Phase III:

o   XiMagnetic demonstrated that metallic glass (Iron-Boron-Silicon) sensor material can be sputtered.

o   Sputtered thin film specimens were successfully tested.

o   The sputtered thin film coil technology was developed.

o   Sputtered coil specimens were verified to 800F.

o   The current capacity of coils was demonstrated.

Phase III was constructed to integrate the technologies developed in Phases I and II into a prototype, Magnetic Domain Strain Sensor. The first completed arrays of gages are shown in Figure 39 and include the following:

(a) Arrays of the lower portion of coils including the metallic glass sensor all deposited on an alumina substrate.

(b) Same as above but with insulation over the metallic glass sensor and etched coil connectors

(c) Arrays of completed magnetic domain strain gages on alumina substrate.
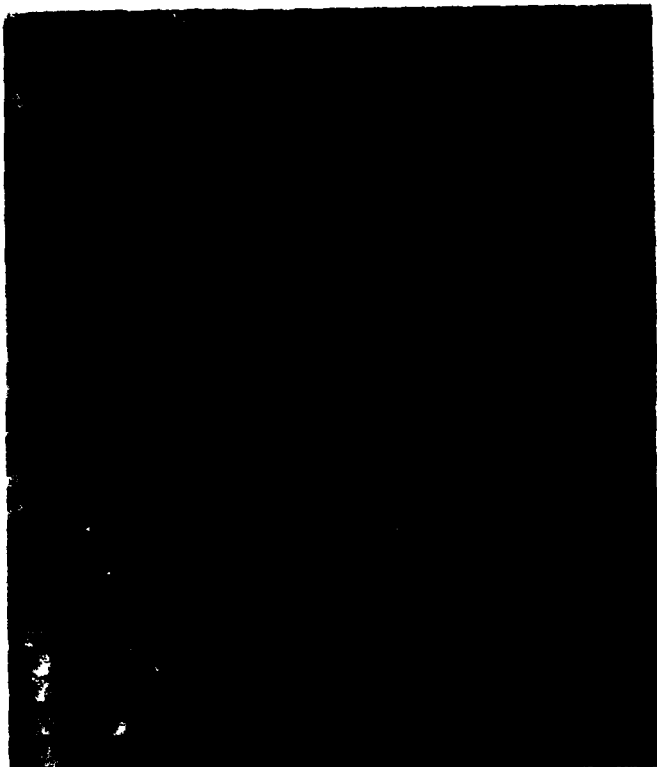
(A) Lower Coil Array With Metallic (B) Lower Coil Array With Metallic
    Glass Sensor Material   Glass Sensor Material and
                                        Etched Coil Connectors
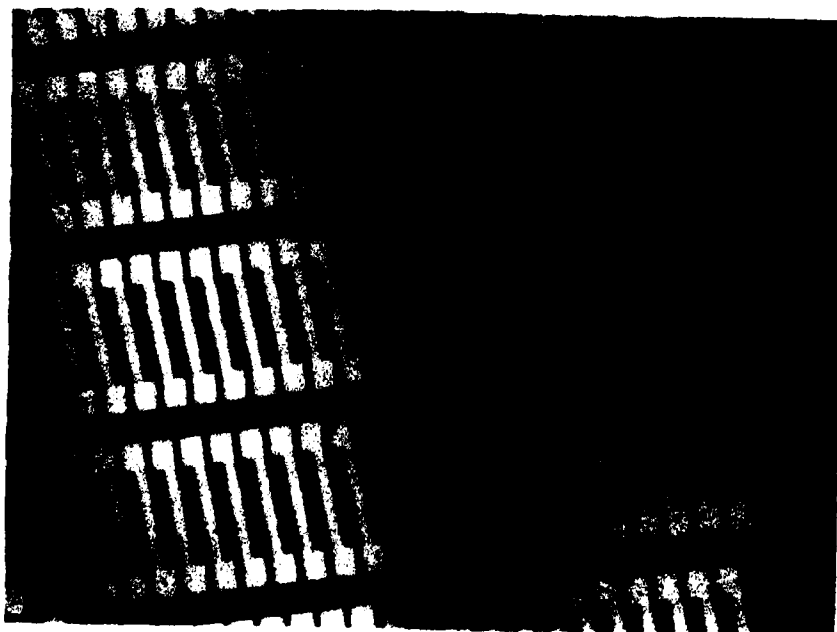
(C) Completed Gage Arrays (26 Separate Depositions)

Figure 39.   Three Additional Arrays of Thin Film Specimens
             Received from AMCI.

The completed gages required 26 separate coating depositions of metallic materials, insulation layers, and diffusion barriers to produce the desired results.

3.3.2 Test/Evaluation

Tests performed by GED on three iron-boron-silicon specimens, sputtered by AMCI, revealed that the metallic glass deposition was partially crystalline, which resulted in poor gage response. AMCI, with the assistance of GED, varied the process parameters in an attempt to produce an amorphous film of metallic glass. The process of cooling the anode was improved, in an attempt to keep the metallic glass from crystallizing.

The efforts expended to improve AMCI's process parameters in an attempt to produce an amorphous film of metallic glass were unsuccessful. XiMagnetics, which successfully deposited the metallic glass sensor material in Phase II of the program, was contracted to assist in the final gage fabrication. AMCI sputtered the layers of the gage array up to the point where the metallic glass sensor material is required. The partially completed gage array was hand carried from AMCI to XiMagnetics in Pennsylvania. The metallic glass was deposited by XiMagnetics and the gage array was then returned to AMCI to deposit the upper layers of the coil. XiMagnetics also coated pull specimens with the iron-boron-silicon for evaluation at GED. The specimens were subjected to a Looper analysis and the results indicated that the coatings were amorphous metallic glass (square B-H loop).

The metallic glass pull specimens sputtered by XiMagnetics were wrapped with wire coils at GED and tested. The results are shown in Figures 40, 41, and 42. The test results were indicative of an amorphous metallic glass coating; however, there is a suspicion that the variations encountered in repeatability tests on specimens Tl-1 and Tl-2 (Figures 40 and 41) can be attributed to the test fixture
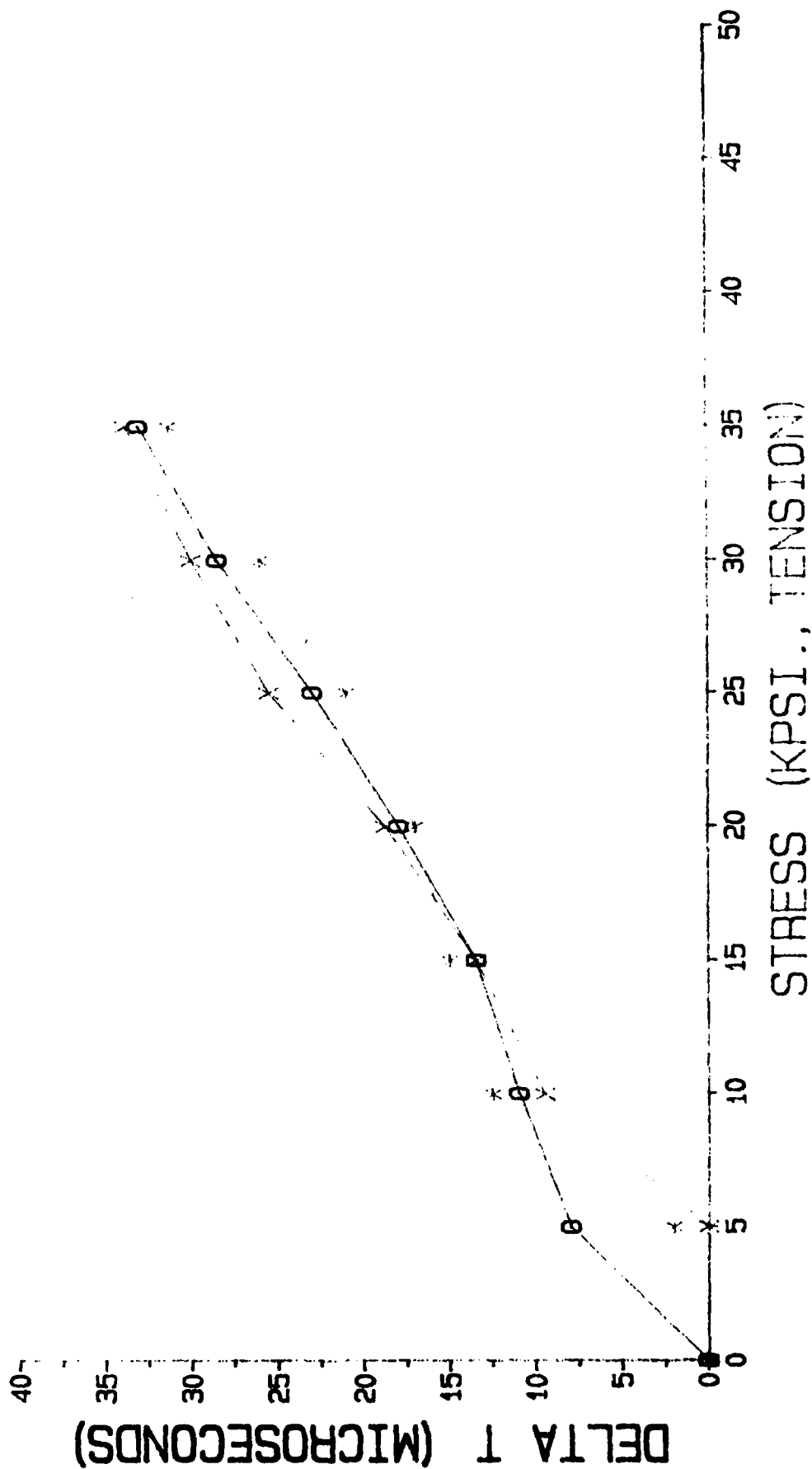
Figure 40. Gage Response of XiMagnetics Metallic Glass Sensor Specimen T1-1.

64
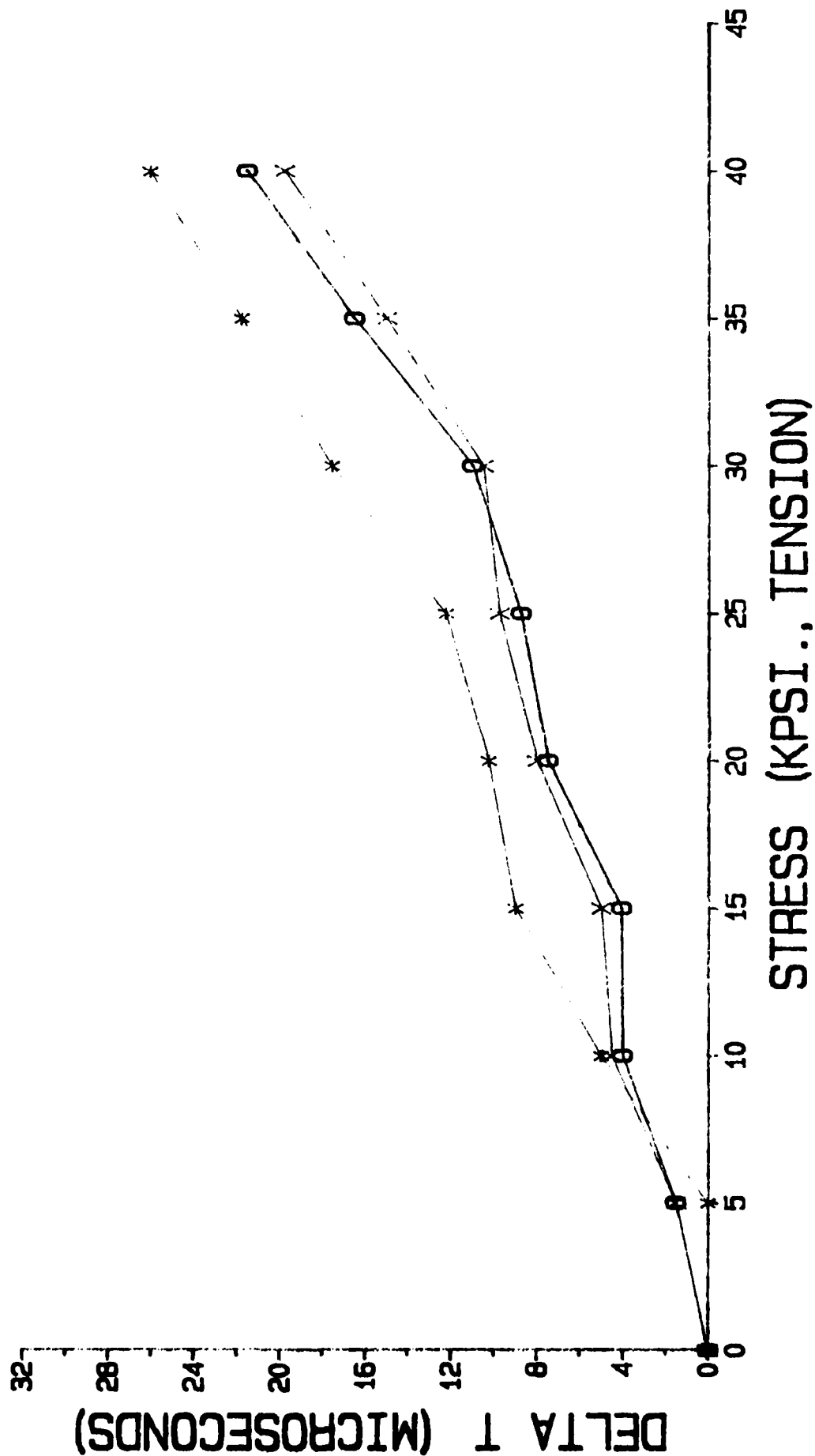
Figure 41. XiMagnetics Metallic Glass Sensor Specimen T_{1-2}.

65
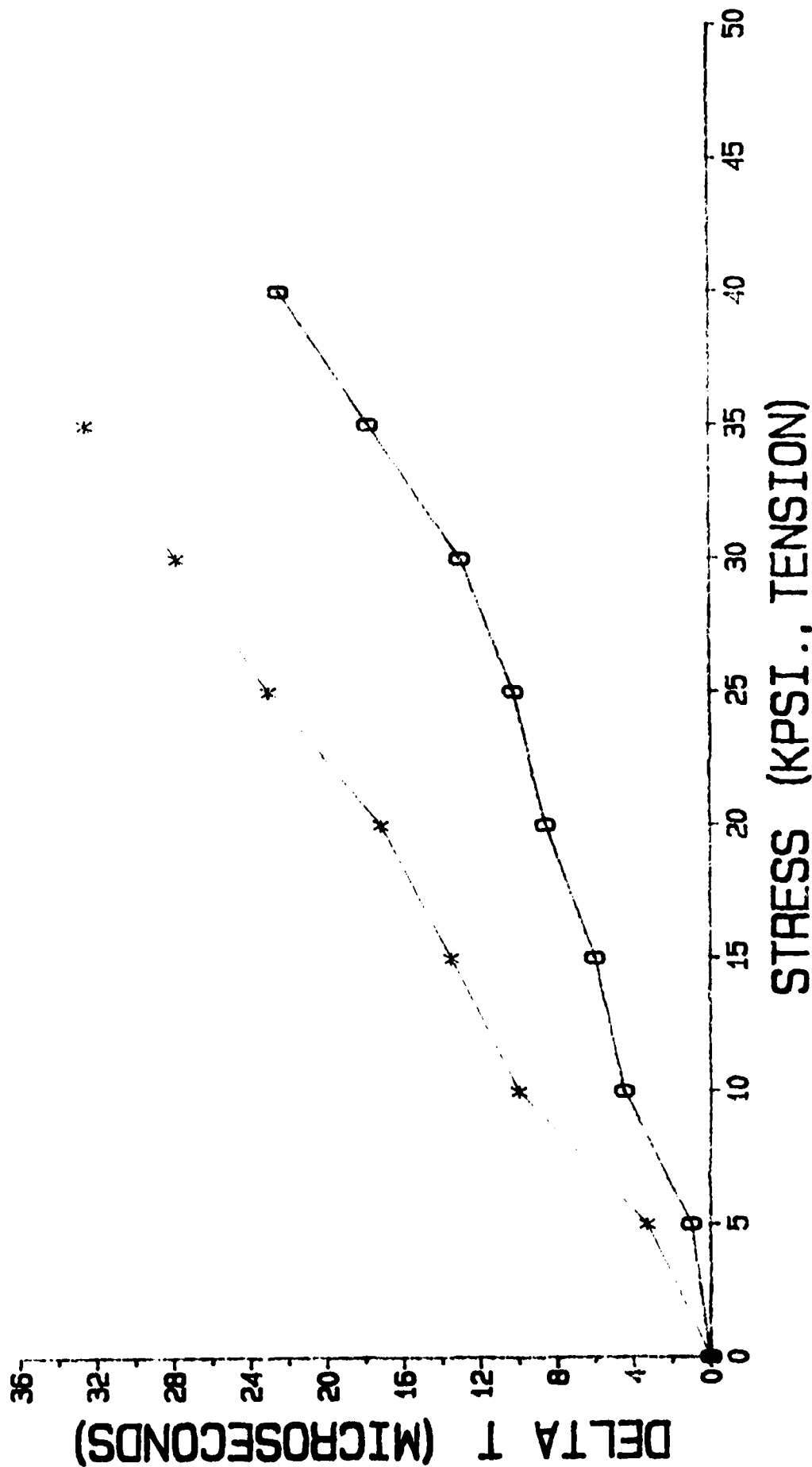
Figure 42. Gage Response Comparison of XiMagnetics Metallic Glass Sensors Specimens T1-1 and T1-2.

which has degraded over the period of test activity. Prior to testing, the full gage arrays were diamond saw cut to produce individual test specimens. These in turn were bonded to metallic test pieces suitable for use in the evaluation rig.

The testing of the XiMagnetics' amorphous metallic glass coated titanium pull bars produced excellent results at Allied-Signal Labs. There is strong evidence that the XiMagnetics amorphous metallic glass coatings on the thin film gage arrays was also successful.

Tests performed at GED on the full thin film gage with the XiMagnetics amorphous metallic glass were disappointing. Currents of up to 1 ampere through the sending coil could not induce the desired voltage in the pickup coil. The specimens were then sent to the Allied-Signal Labs for their evaluation. They were able to produce an induced voltage in both the pull bar and thin film gage. The specimens were then annealed while applying a magnetic field to help align the domains and repeated his tests. The response improved somewhat in both specimens and graphs of the response as well as the sine wave drive current applied is shown on Figures 43 through 50 for the unannealed as well as the annealed samples. The test setup used is more sensitive than the GED test apparatus. The wrapped wire coils around the thin film gage produced the signals generated. It appears that the problem with the thin film gage is not with the metallic glass sensor coating but with the thin film coil configuration. The number of coils and the spacing used in the thin film configuration should be redesigned to improve magnetic saturation in the sensor material. The coil spacing chosen, however, was based on needed insulation resistance requirements at the high operating temperatures of the gage. In addition, it is felt that the thin film processes required to build the multilayer gage resulted in the metallic glass deposited between coil turns, thus causing loss of magnetic saturation as shown in Figure 51.

V/D 2.5000e-1
Vx 1.70000e-2

V/D 1.2500e0
Vy -4.883750e0

Vx

Vy

TL
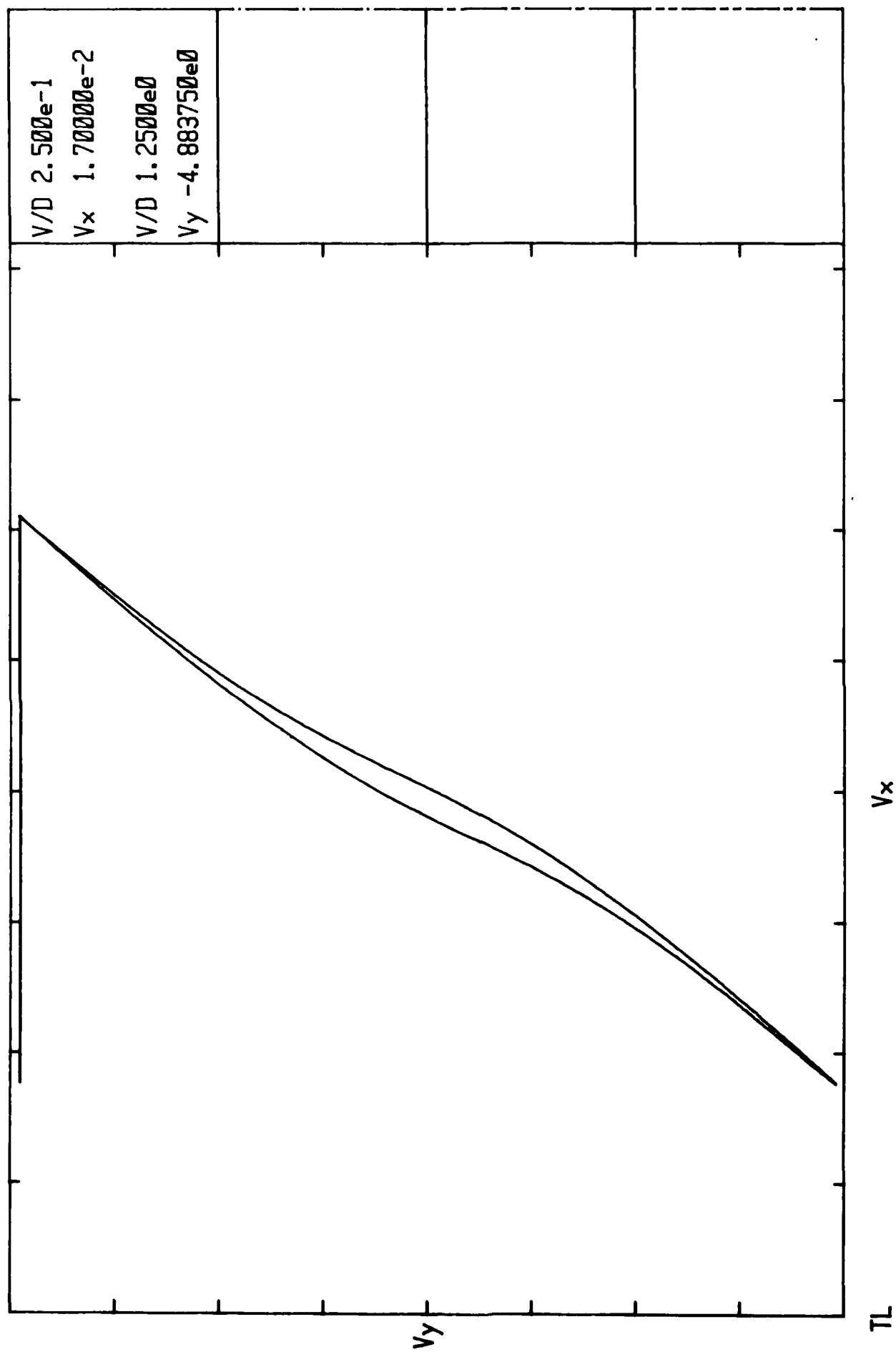
Figure 43. B-H Loop for Unannealed Gage (Record 18, 12/19/89).

68

V/D	2.500e-1
Vy	1.7000e-2
T/D	2.500e-4
TL	-4.25e-5

V/D	2.500e-2
Vy	-1.090625e-2
T/D	2.500e-4
TL	-4.25e-5

——— DRIVE - 26.25 Oe/DIV
—·—·— PICKUP ACROSS 100 TURNS

Vx
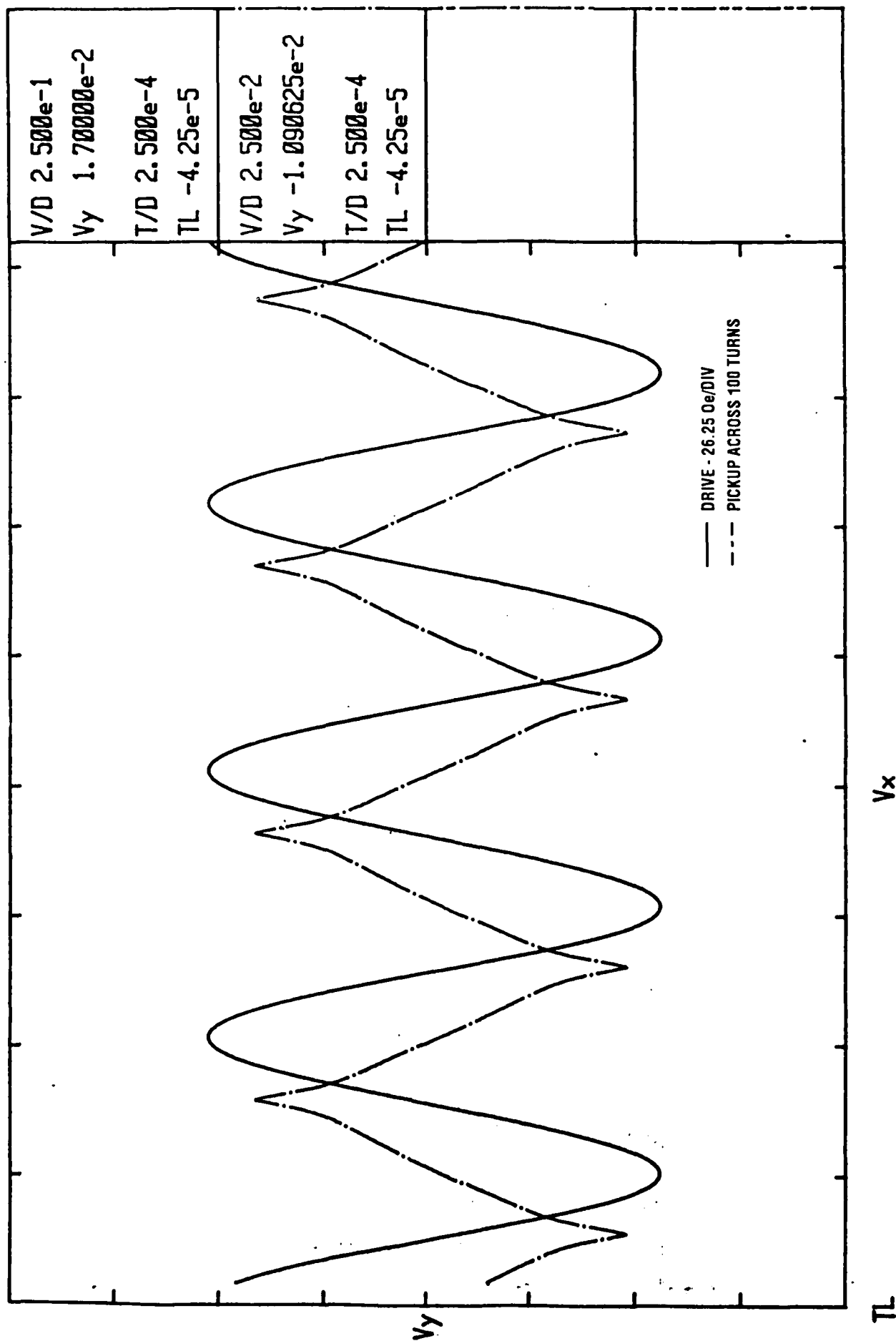
Figure 44. Drive (H) and Pickup (dB/dt) Waveforms.
(Record 17, 12/19/89)

69

V/D 2.500e-1
Vx 1.40000e-2

V/D 2.500e0
Vy -6.06250e0

V_x

V_y

TL
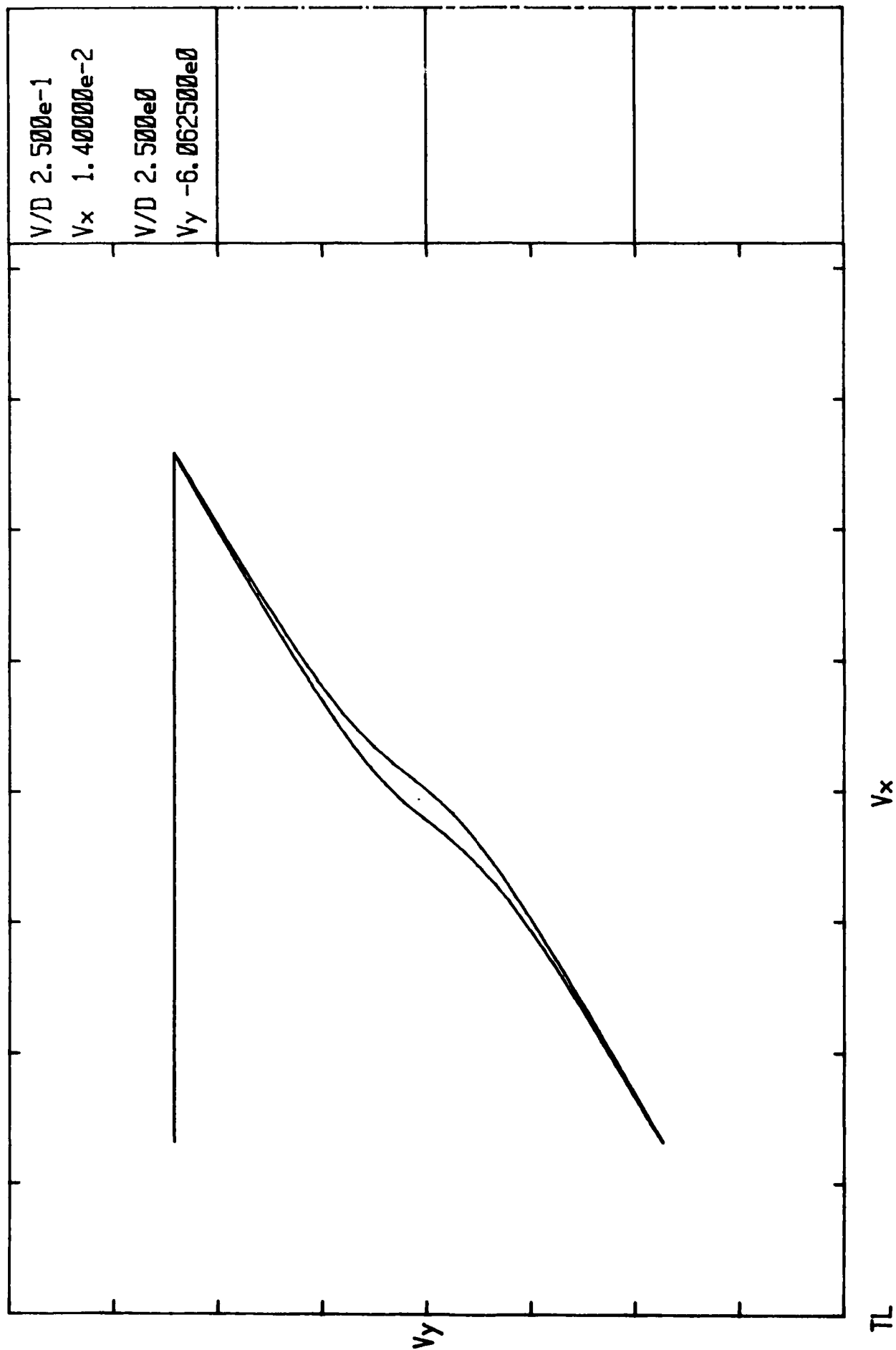
Figure 45. B-H Loop for Unannealed Gage 300C/1Hour/Hparallel.
(Record 16, 1/19/90)

70

V/D 2.500e-1
Vy -4.7125Øe-2
T/D 2.500e-4
TL -1.665e-4

V/D 2.500e-2
Vy -1.56125Øe-2
T/D 2.500e-4
TL -1.665e-4

DRIVE - 26.25 Oe/DIV
PICKUP ACROSS 100 TURNS
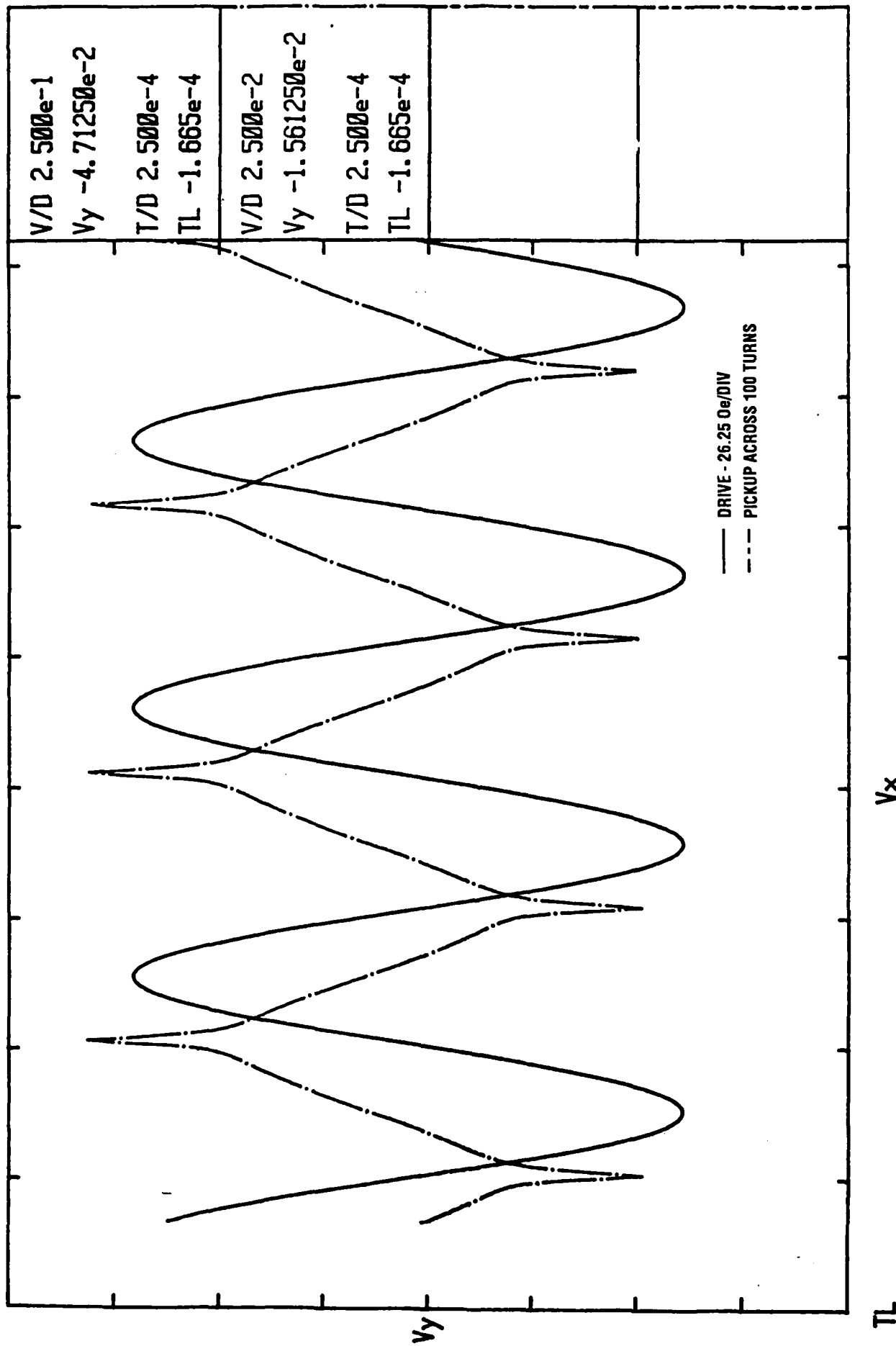
Figure 46. Drive (H) and Pickup (dB/dt) Waveforms.
(Record 15, 1/9/90)

	ANISTROPY FIELD (Oe)	COERCIVITY (Oe)
"Ti" UNANNEALED	27.1	1.6
"Ti" ANNEALED	12.7	0.7
GAGE UNANNEALED	18.0	2.9
GAGE ANNEALED	14.8	2.9

V/D 2.5000e-1
Vx 1.70000e-2

V/D 6.250e0
Vy -1.791250e1

V_x

V_y

TL
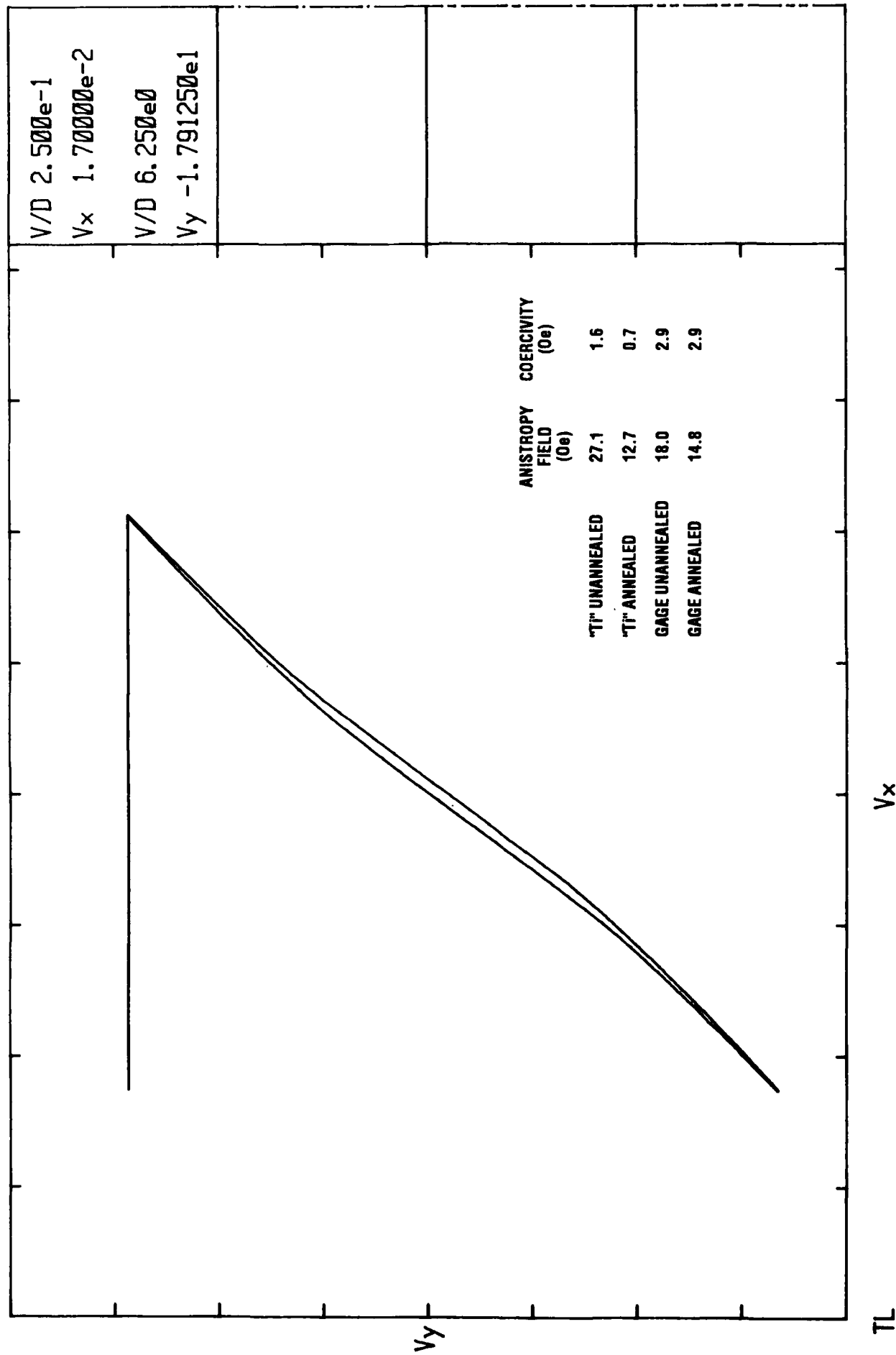
Figure 47. B-H Loop for Unannealed Titanium Bar (Sample B).
(Record 16, 12/19/89)

| V/D 2.500e-1 |
| Vy 1.7000e-2 |
| T/D 2.500e-4 |
| TL -4.25e-5 |
| V/D 5.000e-2 |
| Vy -7.0000e-3 |
| T/D 2.500e-4 |
| TL -4.25e-5 |

—— DRIVE - 26.25 Oe/DIV
—·— PICKUP ACROSS 100 TURNS

Vx

Vy

TL
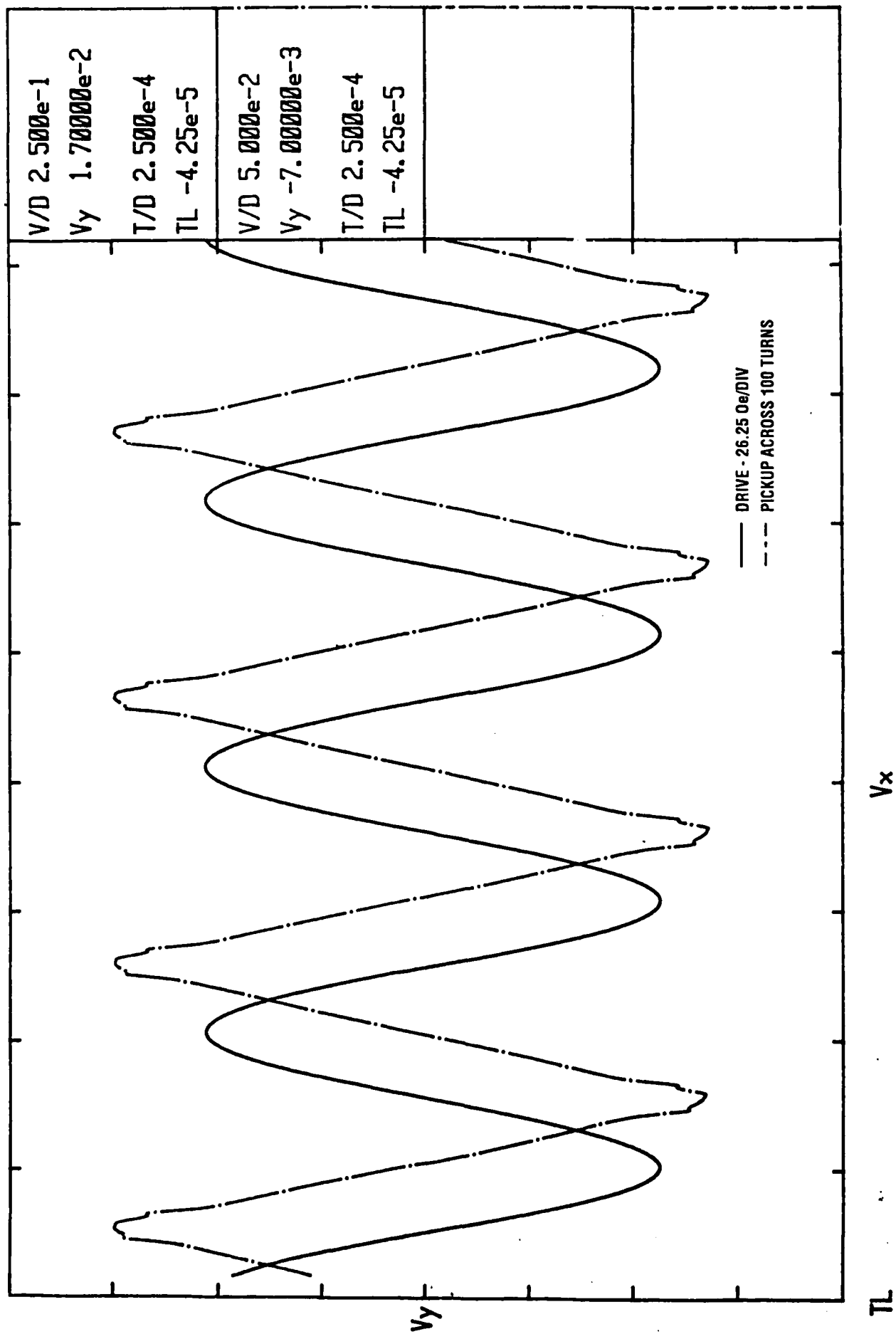
Figure 48. Drive (H) and Pickup Waveforms.
(Record 15, 12/19/89)

73

V/D 2.500e-1
Vx 1.0500e-2

V/D 1.000e1
Vy -2.355000e1

Vx

Vy

74

TL
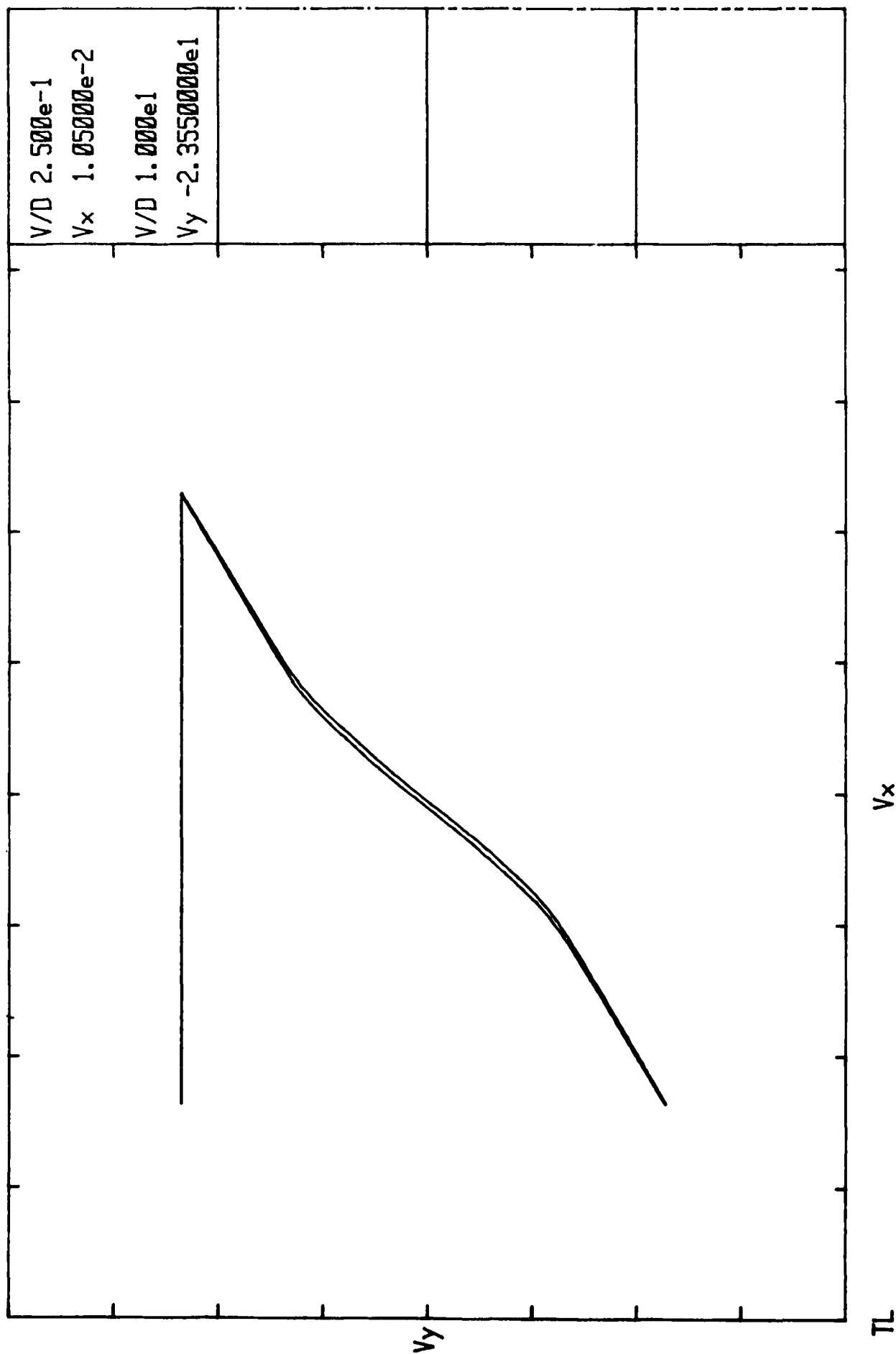
Figure 49. B-H Loop for Annealed Titanium Bar (Sample B).
(Record 16, 1/14/90)

V/D	2.500e-1
Vy	1.0500e-2
T/D	2.500e-4
TL	-4.25e-5

V/D	1.000e-1
Vy	-1.5600e-2
T/D	2.500e-4
TL	-4.25e-5

——— DRIVE - 26.25 Oe/DIV
—·— PICKUP ACROSS 100 TURNS

Vx

Vy

TL
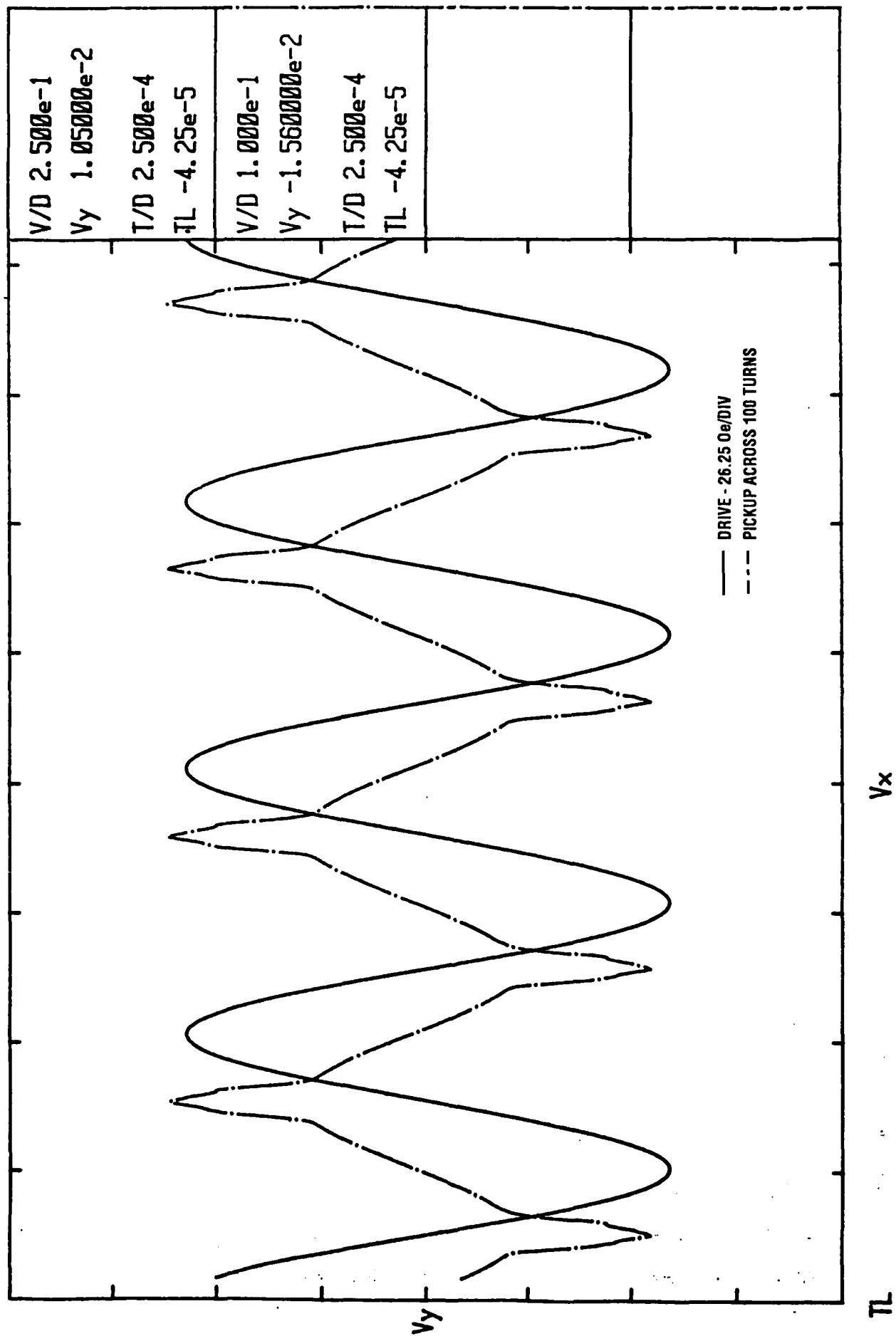
Figure 50. Drive (H) and Pickup Waveforms.
(Record 5, 1/14/90)

75

INSULATION
BARRIERS

COILS

METALLIC
GLASS SENSOR

SUBSTRATE

G0700-159
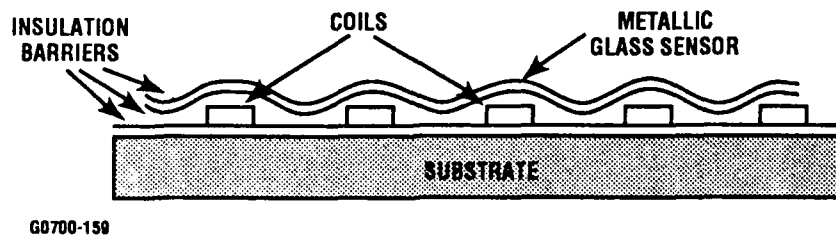
Figure 51. Cross-Sectional View Through Multi-Layered Gage
Illustrating the Sensor Layer Undulating in and
Around the Coil Layers.

These losses are believed to be the reason behind the poor gage response. The gage works well when wire coils are substituted for the thin film coils. A major effort is required to redesign the coil configuration and to change the thin film processes to avoid the intertwining problem described above. Unfortunately, the program schedule and available resources will not permit this significant redesign effort.

It is felt that the primary purpose of this program has been achieved in demonstrating the feasibility of the Magnetic Domain Strain Sensor.

4.0 CONCLUSION

4.1 Thin Film Gage Fabrication

The use of thin films in the fabrication of any sensor on an engine component is a very exacting and precise process. The integration of a coil with a sensor element in this strain gage introduced a series of new challenges to be addressed:

o   Diffusion barriers

o   Thermal expansion mismatch layers

o   Insulation layers

o   The metallic glass sensor element

o   The coil gage elements.

Resistive thin film dynamic strain gages fabricated at GED consist of four layers. Comparatively, the magnetic strain gage incorporated 26 sputtered layers as shown below.

	Al_2O_3	(Aluminum Oxide)
	SiO_2	(Silicon Dioxide)
	Al_2O_3	
	TiW	(Titanium-Tungsten)
	Pd	(Palladium)
Upper Coil ———⟶	Au	(Gold)
	Pd	
	TiW	
	Al_2O_3	
	SiO_2	
	Al_2O_3	
	Nichrome ⟵——— Bond Coat	
Sensor Element ———⟶	Fe-B-Si	(Iron-Boron-Silicon)
	Nichrome ⟵——— Bond Coat	
	Al_2O_3	
	SiO_2	

26 Layers
Final Gage

78

Al_2O_3

TiW

Pd

Lower Coil ⟶ Au

Pd ⟵ Bonding Layer

TiW ⟵ Thermal Layer

Al_2O_3 ⟵ Insulation Layer

SiO_2 ⟵ Diffusion Layer

Al_2O_3

Titanium Bond Coat

/S/U/B/S/T/R/A/T/E/

NOTE:

Each aluminum oxide-silicon dioxide double layer is 0.5 to 0.75 micrometer thick.

Many iterations were required before the above deposition procedure was determined. A conservative approach was taken in the design of the photomasks used for the sputtered coils. Spacing between coils was generous to ensure that there would not be any dielectric breakdown at the elevated operating temperature of the gage.

Due to the high cost of research sputtering, especially multilayered systems such as these, only a limited number of samples could be procured. Sensor oxidation, caused by the iron constituent, occurred on one of the final gage arrays received from AMCI. The use of nonoxidizing environments must be considered for any future work.

The sputtering of metallic glass as the sensor element was difficult. The only successful coatings were applied at XiMagnetics. Engelhard, Damaskos, and AMCI were not able to produce viable sensor elements. This points out a deficiency in technology and understanding of the physics in sputtering of amorphous materials.

79

Corrective action may include changing sputtering gas pressures, a cooled anode, reactive sputtering, target composition, or target integrity.

The use of magnetics for the measurement of strain requires considerable development before qualifying as a production-viable gage. Several unresolved questions, areas of technique, and design have been identified for future work. The primary focus of any follow on development must focus on the coil technology.

As with any development program, the results often vary from the expectation and the path had to be modified along the way as problems were defined and uncovered. We have advanced and demonstrated a new concept in strain sensors. The future work outlined will uncover new challenges toward the goal of an improved static strain measurement device.

4.2 Technical

The operation of the magnetic strain gage relies on the stress dependence of the magnetic coercive field H_c, i.e., the reverse magnetic field required to reduce to zero the internal magnetization M of a magnetic material previously magnetically saturated. H_c is conventionally determined from a B-H loop, the parametric representation of the magnetic induction $B = (H + 4\pi M)$ as a function of a cyclically varying excitation H(t). The B-H loop crosses the H-axis (B=0) at the points in time where $H(t) = \pm H_c$.

In practice, H(t) is applied to a magnetic material by passing a cyclically varying electric current (sine, square, or tri-angular waveform) through a set of windings around the material. For a long, thin sample, H (in amp-turns/meter) is given by

$$H(t) = ni(t)/l,$$

Where n/l is the number of windings per unit length and i(t) is the current. B(t) is determined indirectly from its time derivative, dB/dt. By Faraday's law, the voltage V(t) induced in a coil of N turns tightly encircling a magnetic material of cross-section A is

$$V(t) = -NA \ dB/dt.$$

A second set of windings is used as a pickup coil to sense this voltage. The time integral $\int V(t)dt$ can be performed either electronically or numerically from a digitized waveform to obtain B(t).

The geometry of the present strain gage is somewhat removed from the idealized, text-book case described above, so the experimentally obtained numerical values for dB/dt and H differ slightly from those predicted. Nevertheless, the functional forms and dependences on n, l, N, and A are correct to an excellent approximation. H_c thus can be determined as the values of H(t) at which the dB/dt waveform exhibits sharp positive and negative peaks, since the B-H loop is most nearly vertical at those points. (Integration to form and display the B-H loop is useful as a diagnostic test but need not be accomplished in actual device operation.)

Among the anticipated departures from the idealized behavior are the following:

o   If the "bar" shaped magnetic sensor is not infinitely long, the B-H loop is sheared over by demagnetizing effects as shown in Figure 52(a). This phenomena can be visualized with the aid of the flux lines depicted in Figures 52(b) through (e). The flux lines of H are noted to change direction at the boundary. The relationship:

$$B \ = \ H \ + \ 4\pi \ M$$

81
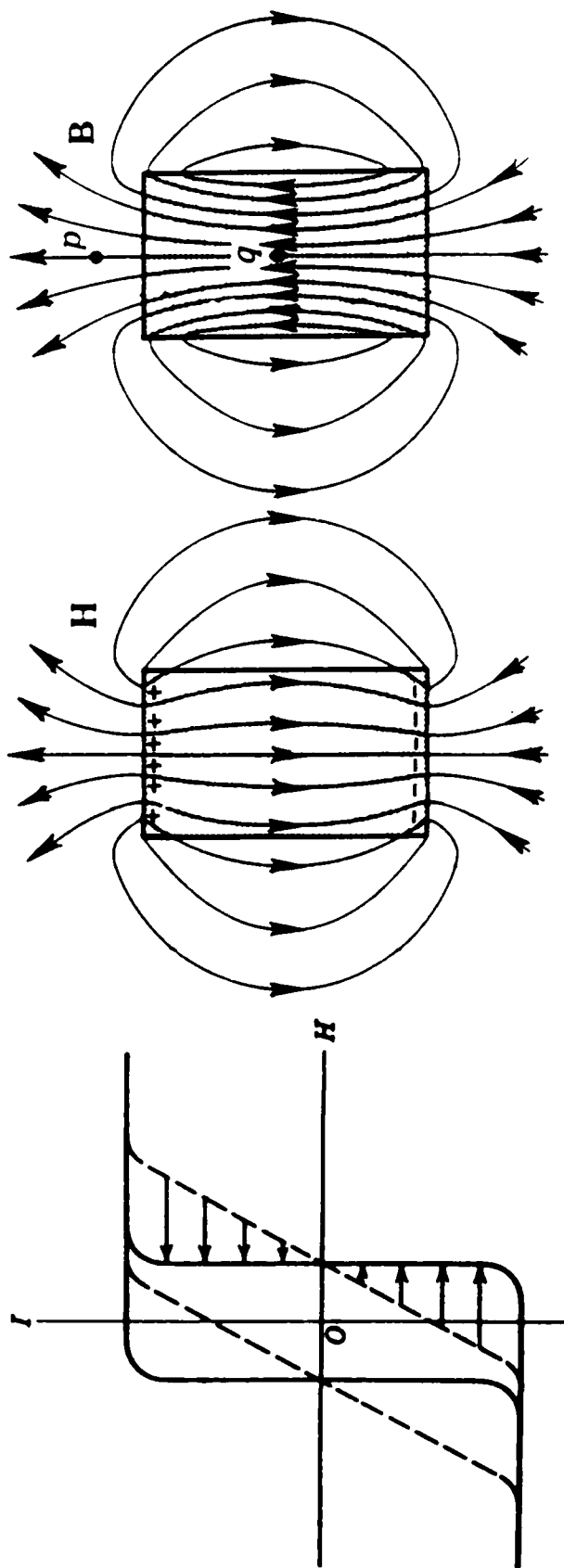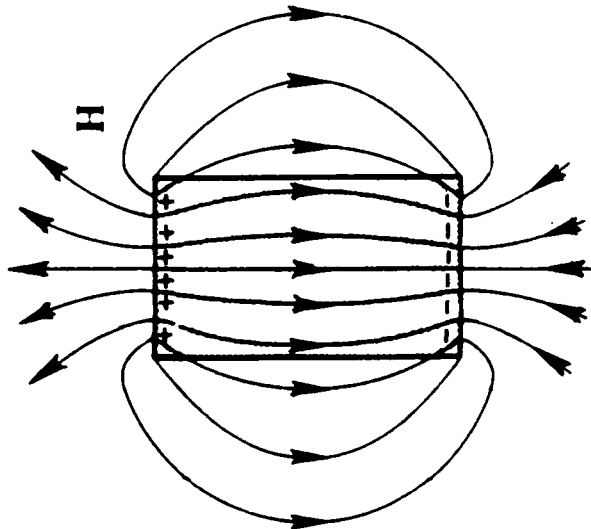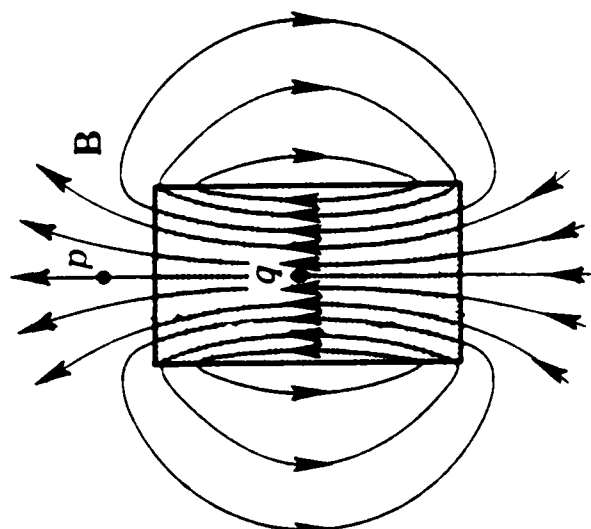
(b) THE LINES OF H AND (c) THE LINES OF B FOR A MAGNET.
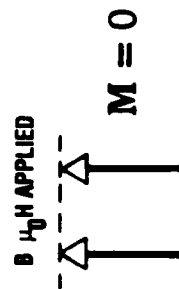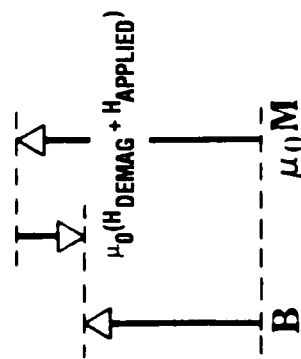
Figure 52. Shearing of a Magnetization Curve.

82

Where:

    B   =   Induction (Flux Density)

    H   =   Magnetic Field

    M   =   Magnetization

is shown to be satisfied for (d) a particular outside point p and (e) a particular inside point q. The field H inside the magnetic material equals the vector combination of the applied field ($H_{applied}$) opposed by the demagnetizing field ($H_{demag.}$). The demagnetizing field may be pictured as arising from free magnetic poles as shown in (b) leading to the sheared B-H loop shown in (a). The shearing effects were minimized by making certain that the ratio of sample length to the square root of the cross-sectional area was greater than 200 to 1. It would be preferable to have a ratio greater than 1000 to 1, or to go to a continuous loop sensor in the shape of a picture frame, with the coils wrapped along each of the long axes.

    o   If the H drive windings are not uniformly distributed over the sample, some nonuniformity of H field may result, tending to spread out the dB/dt peaks. Also, it becomes difficult to obtain an absolute determination of H, though H does not need to be known for device operation and strain calibration.

    o   The air-core mutual inductance of the H and dB/dt coils adds a small induced voltage in the dB/dt coil which is not affected by the magnetic material. This superposes a linear component on the anticipated B-H loop as shown in Figure 53.

    o   The accuracy in determining the amplitude of B is limited by the accuracy of the determination of cross-sectional

INHERENT LOOP OF MATERIAL

$2 \times B_{SAT}$

AIR CORE CORRECTION

APPARENT LOOP

$2 \times B_{SAT}$

G0700-165
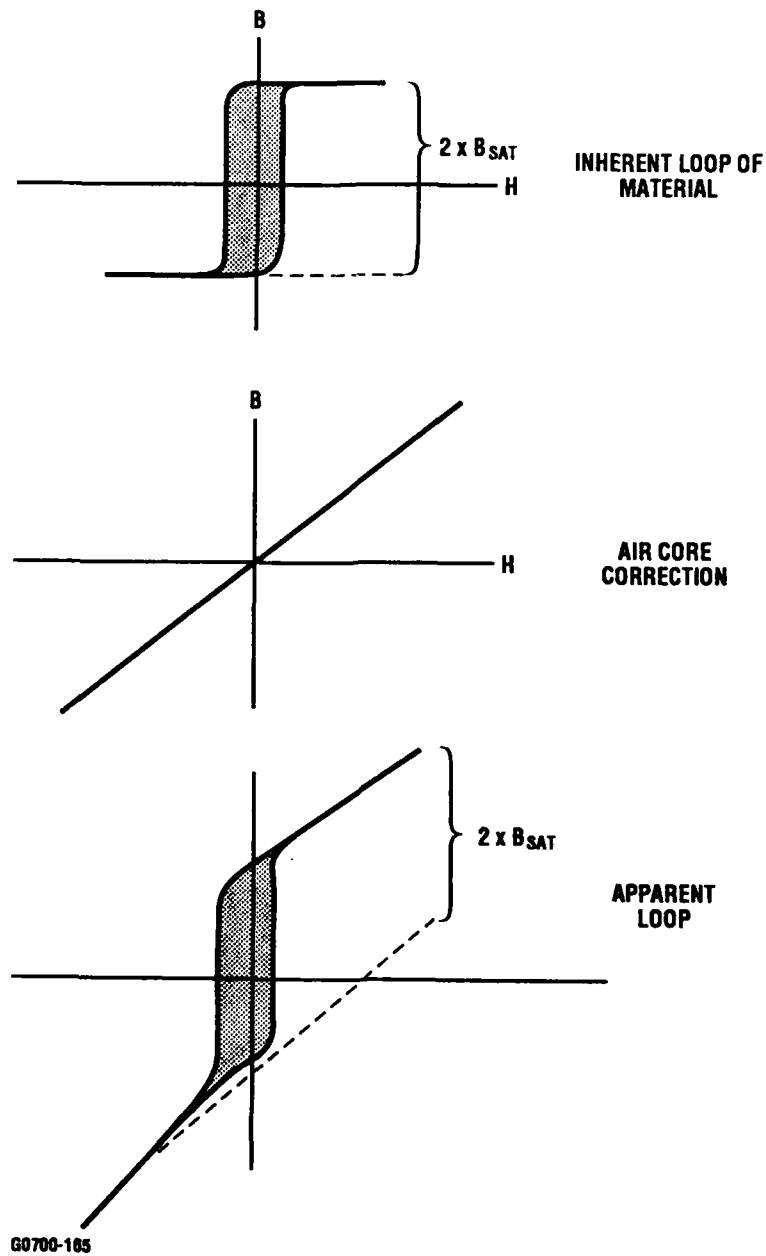
Figure 53.   Air-Core Mutual Induction Correction in B-H Loop.

84

area A, again a factor important only for diagnostics and not for device operation and strain calibration.

A series of tests has established the performance of each of the different constituents of the strain gage.

First, the magnetic quality of the thin films of amorphous metal produced in the program has been established. The B-H loops of films deposited on Ti gage bars were measured using long solenoid and a ten-turn coil wound directly onto the Ti bar for the H drive and dB/dt pickup, respectively. The use of the solenoid gave an accurately determined and uniform H field through the whole sample. This test focused attention on the material itself without any possible complication from the associated issues of the thin-film winding performance. The relatively large ratio of the cross-sectional area of the nonmagnetic material to the magnetic material enclosed in the dB/dt coil results in a substantial linear addition to the B-H loop as discussed above, for this test simulation geometry. Nonetheless, the B-H loop shows the expected shape for the soft magnetic film, with good saturation characteristic and reasonable H_c and anisotropy field as shown in Figure 54. The same test was then run on an actual gage sample, again with an external pickup coil and the solenoid drive. The magnetic quantities thus determined were nearly equivalent to those for the film on the Ti bar, showing that the total gage fabrication process was compatible with the treatment needed for preparation of a good magnetic film as shown in Figure 55.

The program also attempted to improve the magnetic properties of the films, both on the Ti substrate and in actual gage configuration, by a preliminary heat treatment at 300C for 1 hour in a 2.4-kA/m (300 Oe) magnetic field directed along the long axis of the sample. The resulting B-H loops showed reduced anisotropy and coercivity, suggesting that final gages should be pretreated to obtain maximal performance as shown in Figures 56 and 57.

V/D 2.500e-1
Vx 1.7000e-2
V/D 6.250e0
Vy -1.79125e1

	ANISTROPY FIELD (Oe)	COERCIVITY (Oe)
"Ti" UNANNEALED	27.1	1.6
"Ti" ANNEALED	12.7	0.7
GAGE UNANNEALED	18.0	2.9
GAGE ANNEALED	14.8	2.9

V_x

V_y

TL
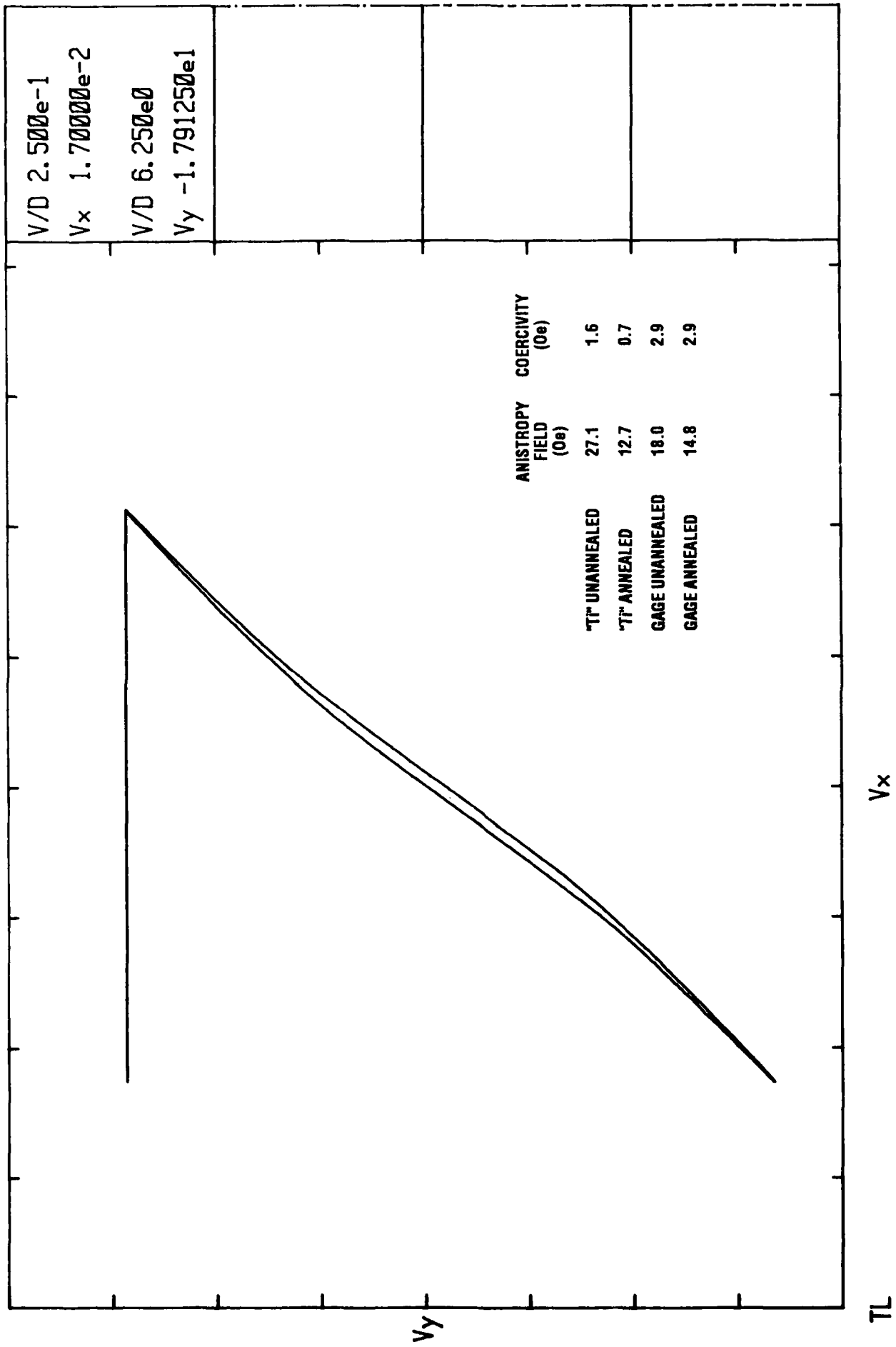
Figure 54. B-H Loop for Unannealed Titanium Bar (Sample B). (Record 16, 12/19/89).

V/D 2.500e-1
Vx 1.4000e-2
V/D 2.500e0
Vy -6.062500e0

V_x

V_y
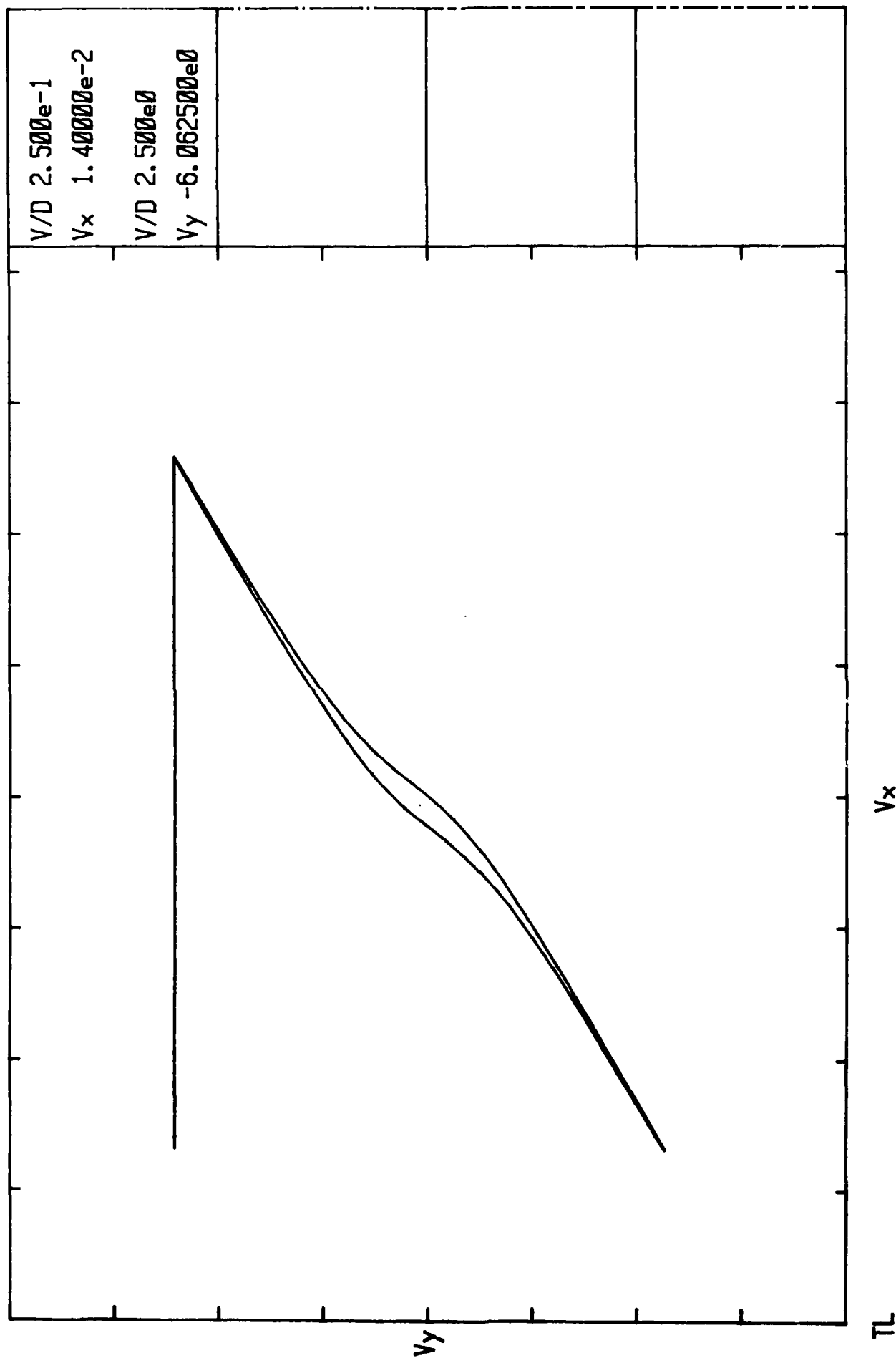
Figure 55. B-H Loop for Annealed Gage 300C/1 Hour/Hparallel.
(Record 16, 1/19/90)

V/D 2.500e-1
Vx 1.05000e-2
V/D 1.000e1
Vy -2.35000e1

Vx

Vy

88

TL

Figure 56. B-H Loop for Annealed Titanium Bar (Sample B).
(Record 16, 1/14/90)

V/D 2.500e-1
Vx 1.7000e-2
V/D 1.2500e0
Vy -4.88375e0

V_x

V_y

TL
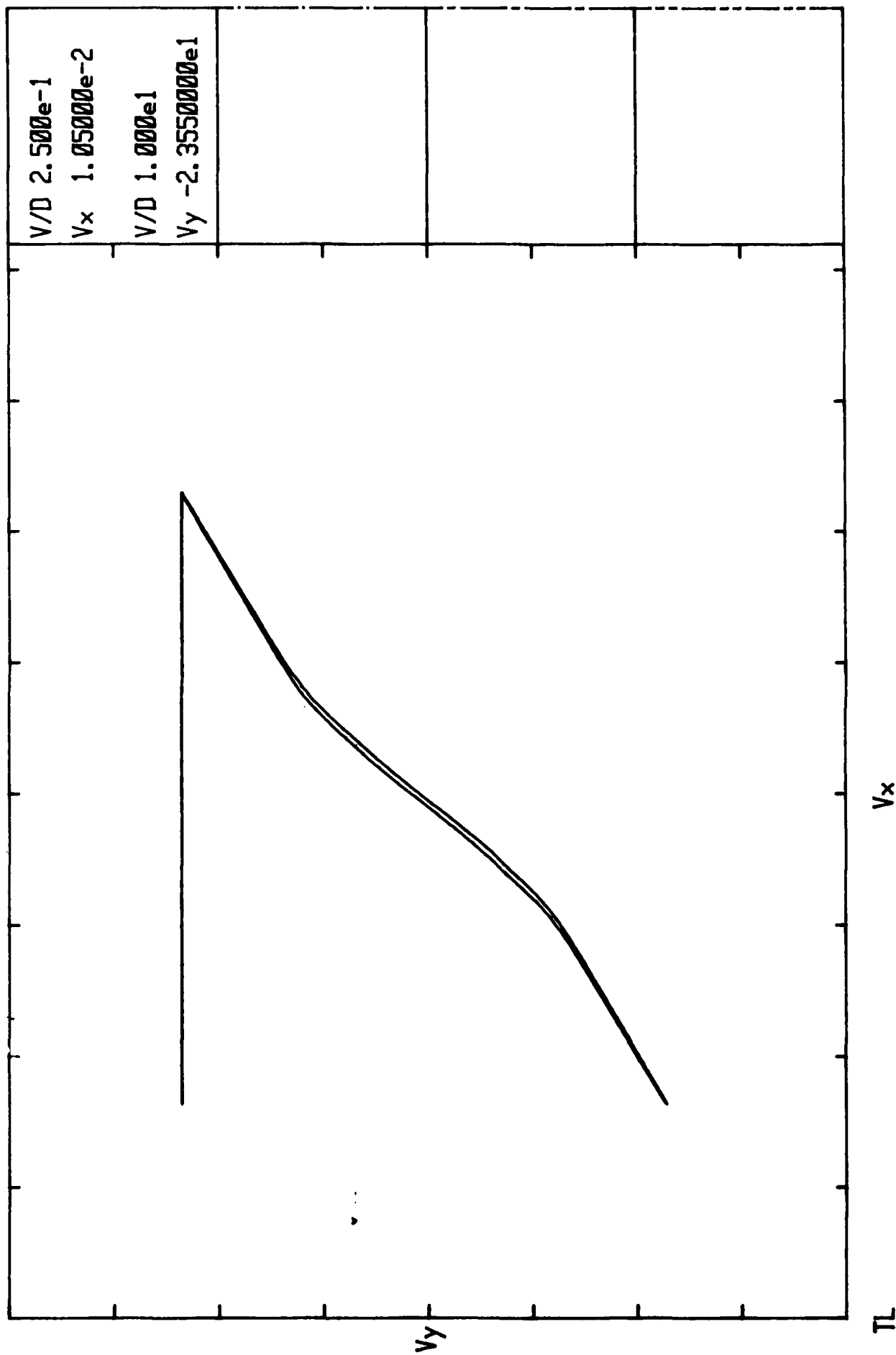
Figure 57. B-H Loop for Unannealed Gage (Record 18, 12/19/89).

Second, the actual coils in the thin film gages were validated as both drive and pickup coils. B-H loops were taken using one of the thin-film windings in conjunction with an external coil of 10 turns of No. 36 AWG copper wire. Figure 58 shows a B-H loop taken with the thin film winding as a pickup coil and the drive current applied with the external coil. The nearly identical loop of Figure 59 was taken with the roles of the two coils reversed. The i(t) and dB(t)/dt waveforms from which Figures 58 and 59 were derived are displayed in Figures 60 and 61. It should be noted that in these experiments the thin-film winding repeatedly carried some 3.75 amperes of peak current in intermittent burst of 6-10 cycles of sine wave, equivalent to a current density of 4.9×10^9 amps/cm^2, far greater than what would be normally allowed for a conductor in the steady state. It is presumed that the low average power in a burst mode operation and the heat sinking effect of the alumina substrate allowed this magnitude of current without any failure or apparent deleterious effect.

However, it proved impossible to obtain the expected B-H loops using the two thin-film coils on the one substrate. We attribute this failure to an inadequate degree of magnetic coupling between the two co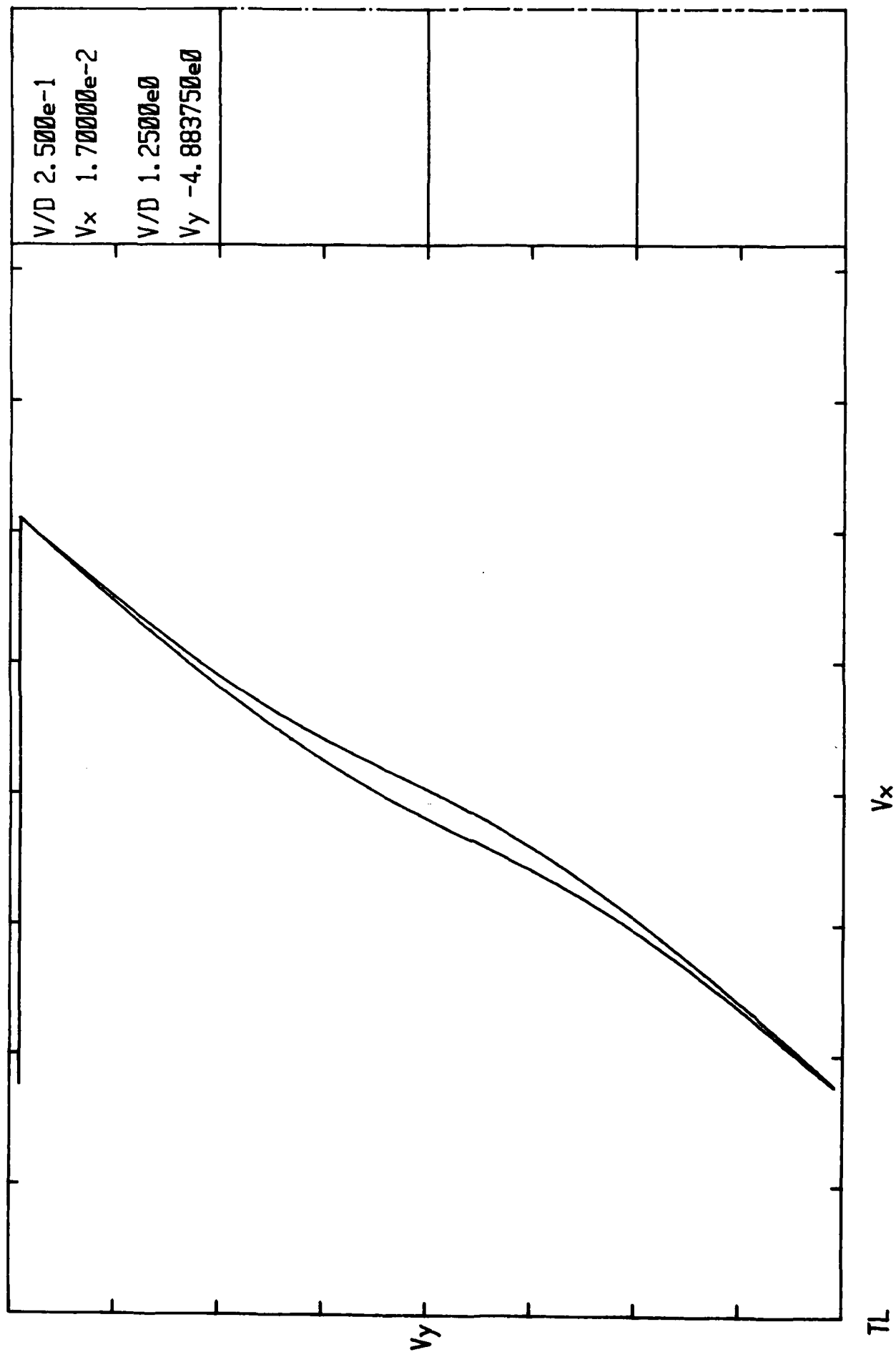ils. It was initially expected that the magnetic reluctance of the amorphous metal film would be low enough to keep most of lines of magnetic flux within the film. That expectation proved not to be the case. There apparently was a sufficiently large demagnetizing effect (presumably brought on by the length to thickness ratio and by the "railroading" effect) that the flux lines were not channeled from one coil to the next to a great enough degree to get adequate coupling. The railroading effect is illustrated in the Scanning Electron Microscope (SEM) photomicrographs shown on Figures 62 and 63.
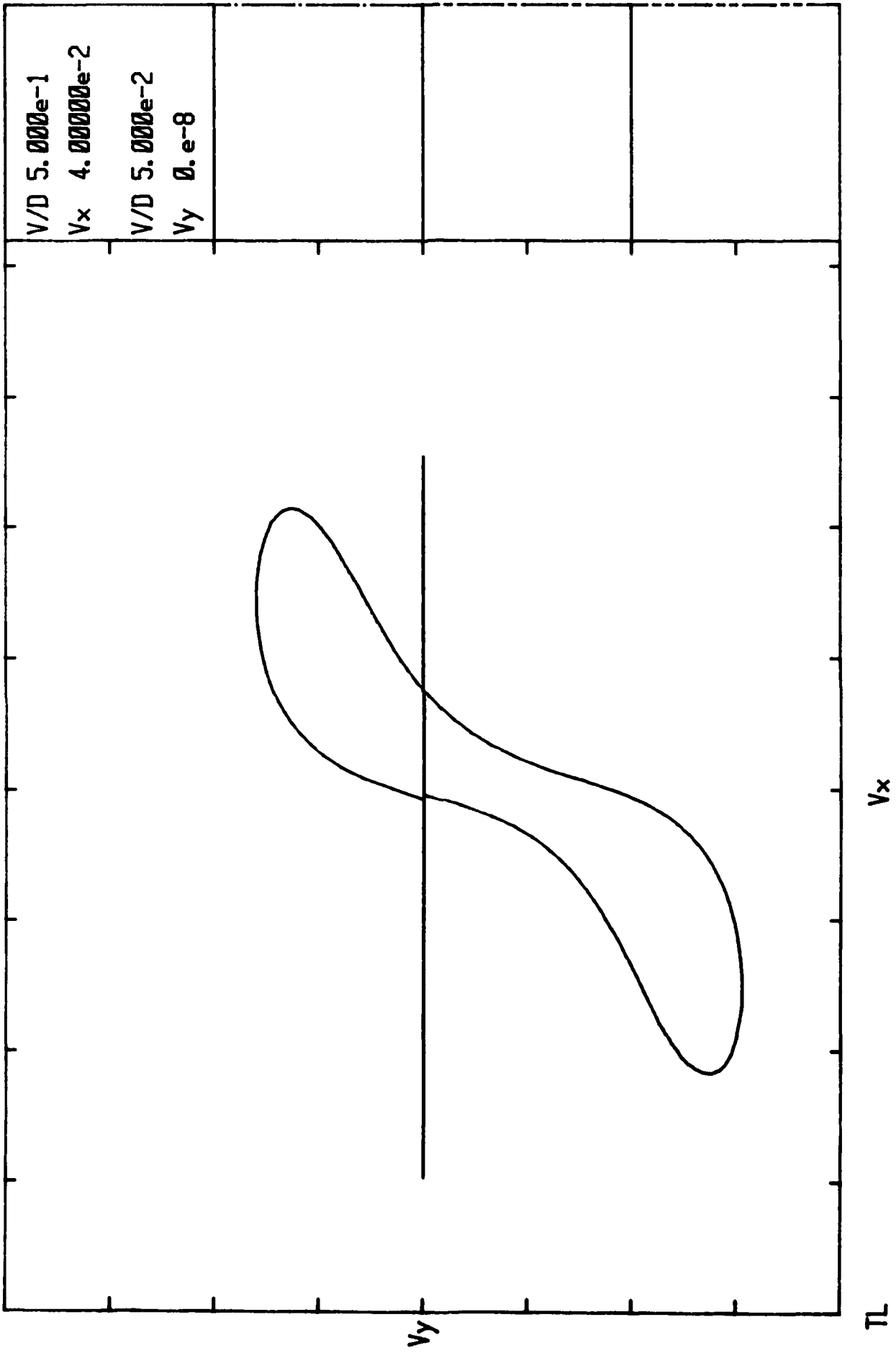
Figure 58. B-H Loop for Sample Using Drive Coil C and Pickup Coil A on Alumina Substrate.

91

V/D 1.000e-1
Vx 8.2000e-3

V/D 5.000e-2
Vy 0.e-8

Vx

Vy

TL
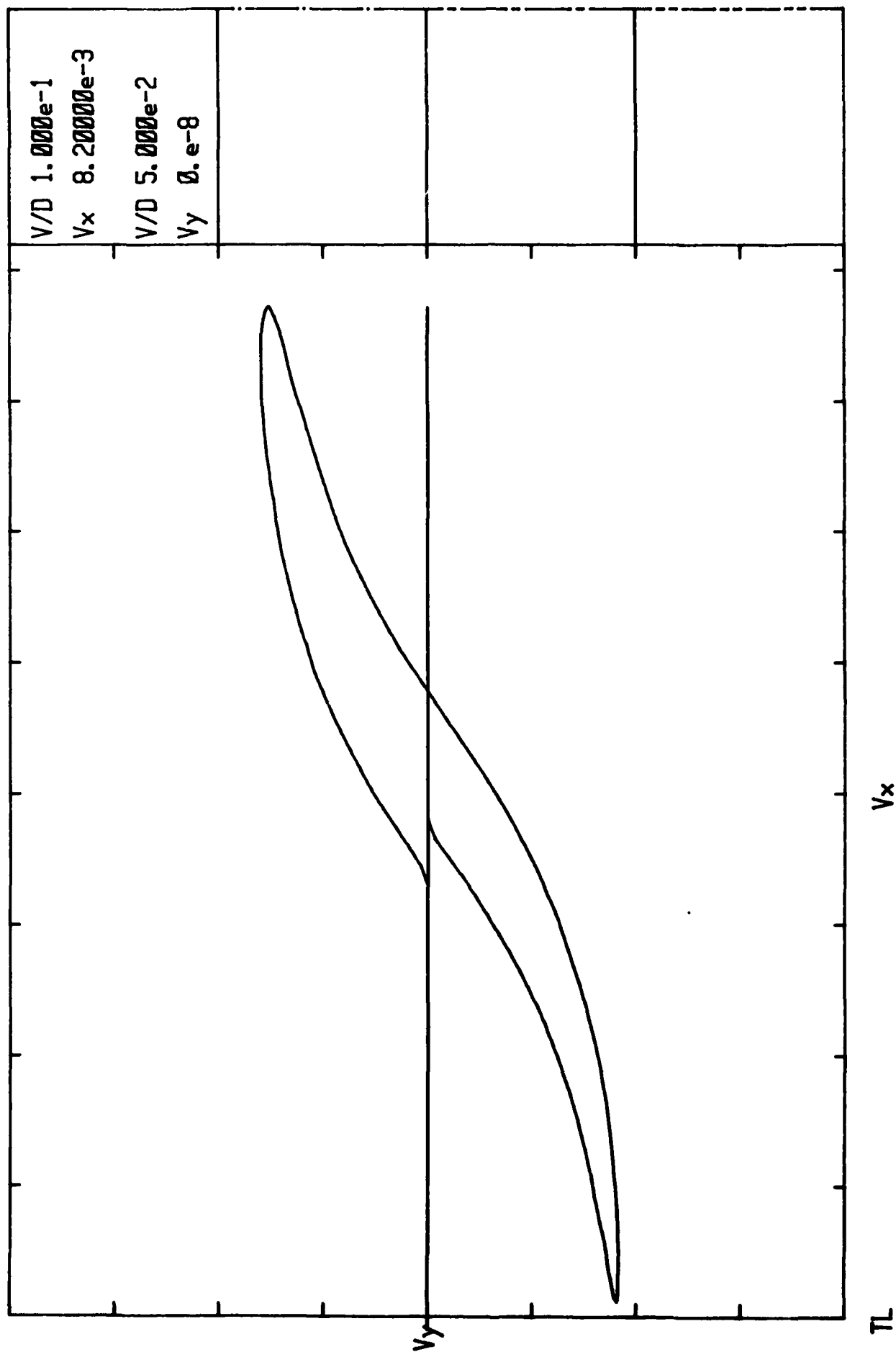
Figure 59. B-H Loop for Sample Using Drive Coil A and
Pickup Coil C on Alumina Substrate.
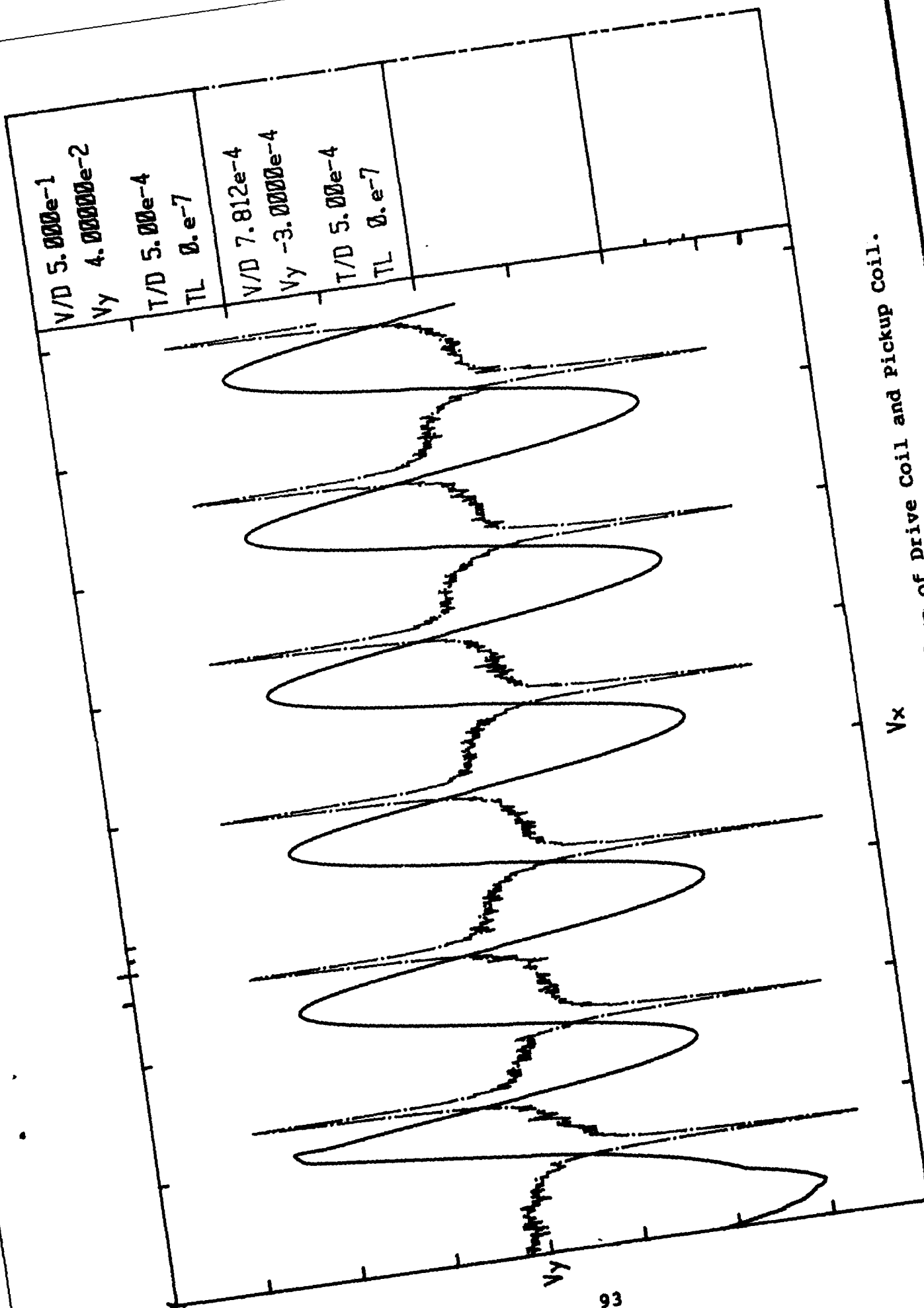
Figure 60. Real-Time Waveform of Drive Coil and Pickup Coil.

93

V/D	1.000e-1
Vy	8.2000e-3
T/D	5.00e-4
TL	0.e-7
V/D	3.906e-4
Vy	-3.5000e-4
T/D	5.00e-4
TL	0.e-7

V_x

V_y

TL

94

Figure 61. Real-Time Waveform of Drive Coil A and Pickup Coil C.
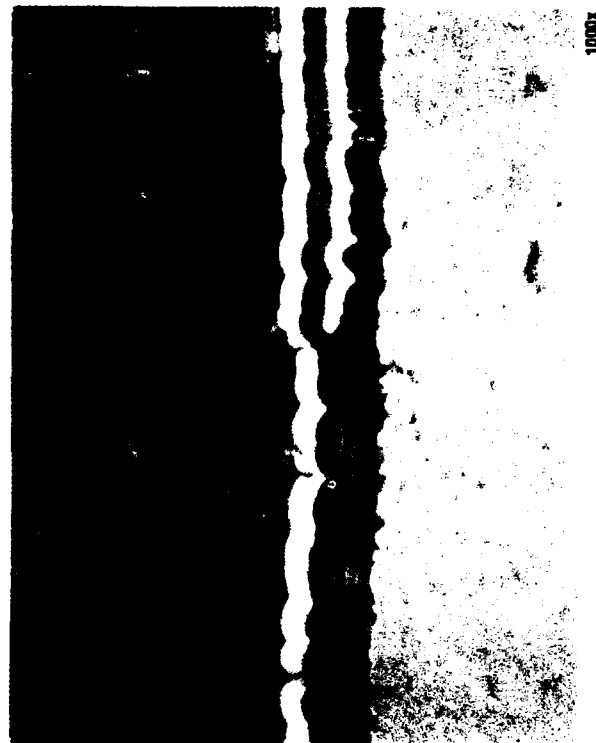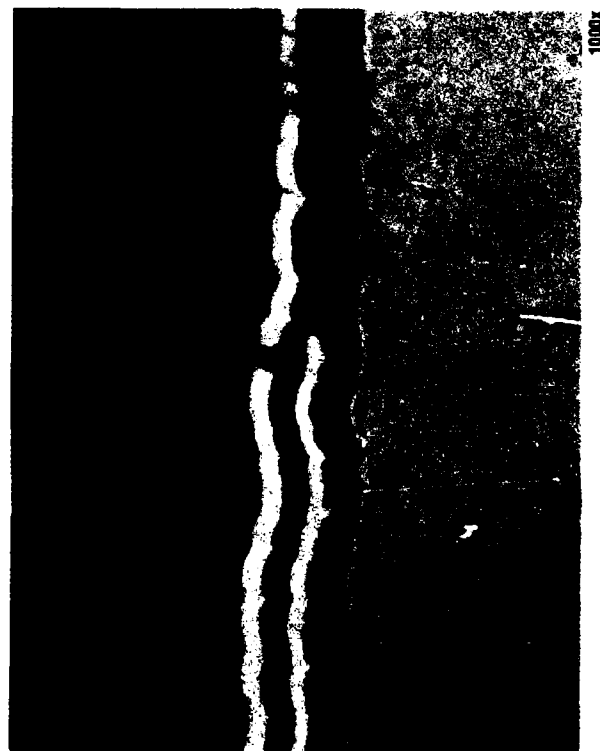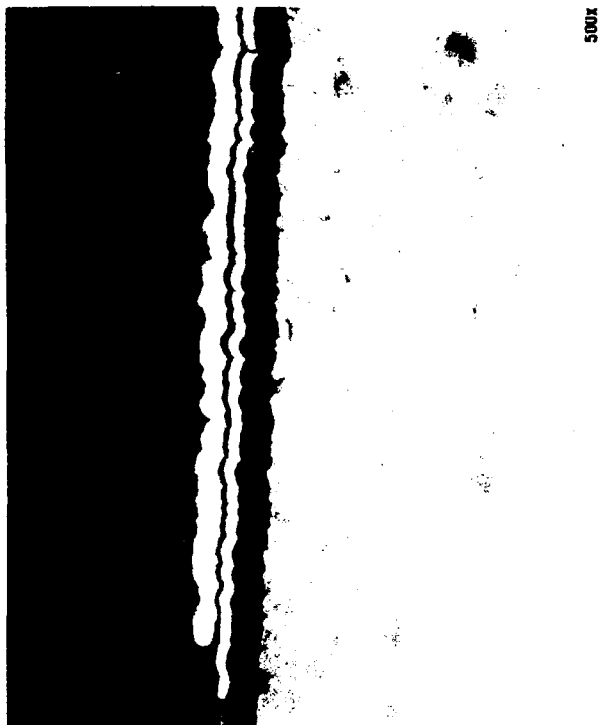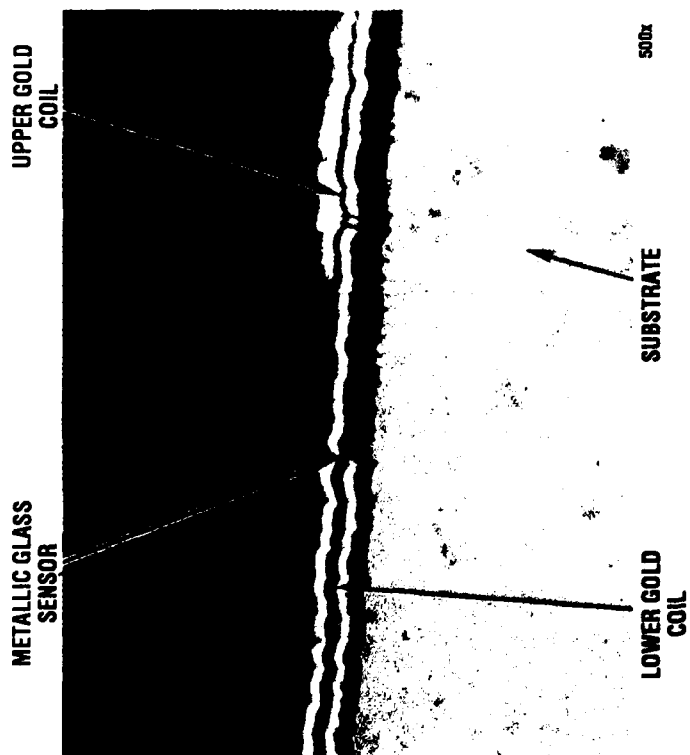
Figure 62. Photomicrographs of Views through the Multi-Layered Thin Film Strain Gage.
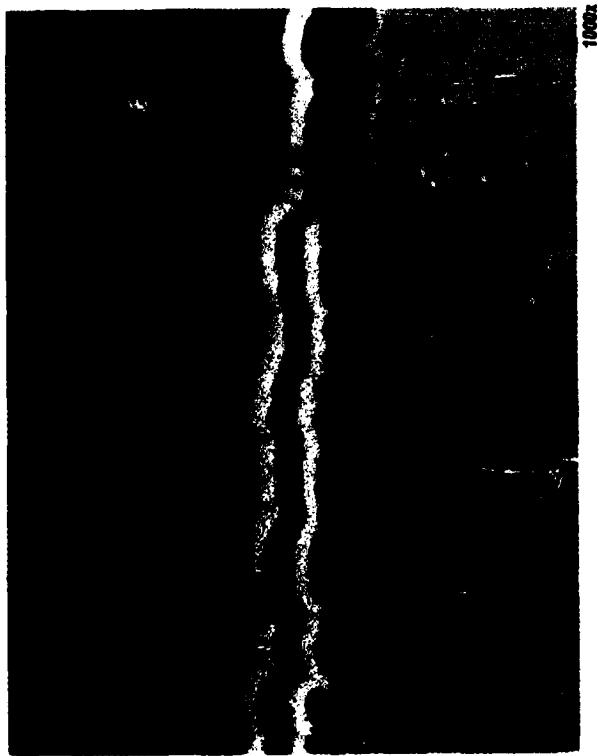
Figure 63. Photomicrographs of Views through the Multi-Layered Thin Film Strain Gage.

96

The edge effect of the sputtered coating, where it transitions over the lower coil elements, was a major source of technique difficulty. The step coverage as well as the insulation barrier for electrical isolation is compromised at that point. Planarization and conformal coverage to allow improved electrical resistance is desired. The metallic glass sensor element is not planar – as it dips below the gold coil bars due to the sputtering techniques.

Simulation experiments to confirm this explanation were done by winding four sets of external coils on one gage as depicted in Figure 64. B-H loops were taken using all possible pairs of coils (both the four sets of external coils and the two thin-film coils). In each case proper loops were obtained when the drive and pickup coils were adjacent as shown in Figure 65. A weak loop was seen driving with A and picking up with D (Figure 66), but no coupling was seen between widely separated coils, whether the thin-film or external coils were used. A final gage configuration would therefore have to entail better magnetic coupling between the two coils.

SEM photomicrographs and an Energy Dispersive Analysis by X-ray (EDAX) were taken to analyze the problem of delamination of the gage due to pull-off by pressure sensitive Kapton tape. Figure 67 reveals the expected elements: Fe, Si from the FeBSi amorphous metal, Al (possibly also Si) from the alumina (and silica) substrate material, and Au conductors. In Figure 68, gage Section B where amorphous metal apparently remains, shows strong Fe and Si EDAX signals. In Figure 68, gage Section C, amorphous metal was removed, and only Au lines remain strong in the EDAX.

It should be recognized that the results of the above described testing of actual gages demonstrate that each of the aspects needed for ultimate gage operation has been demonstrated individually. The failure of the anticipated mode of operation (drive with coil A and

A   B

C   D   E   F

Thin film coils   External Coils

_____   - - - - - - - -
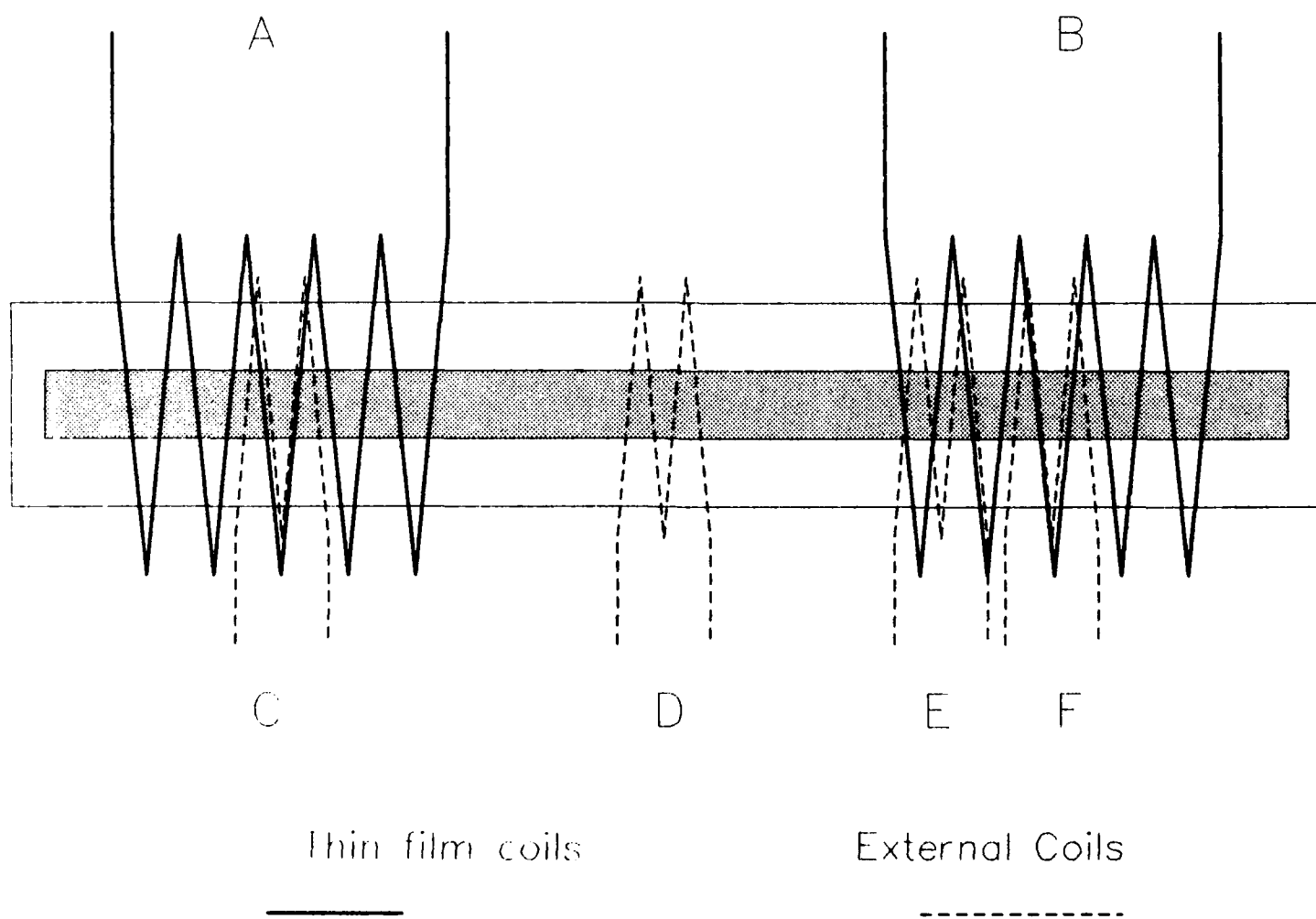
Figure 64. Coil Designations.
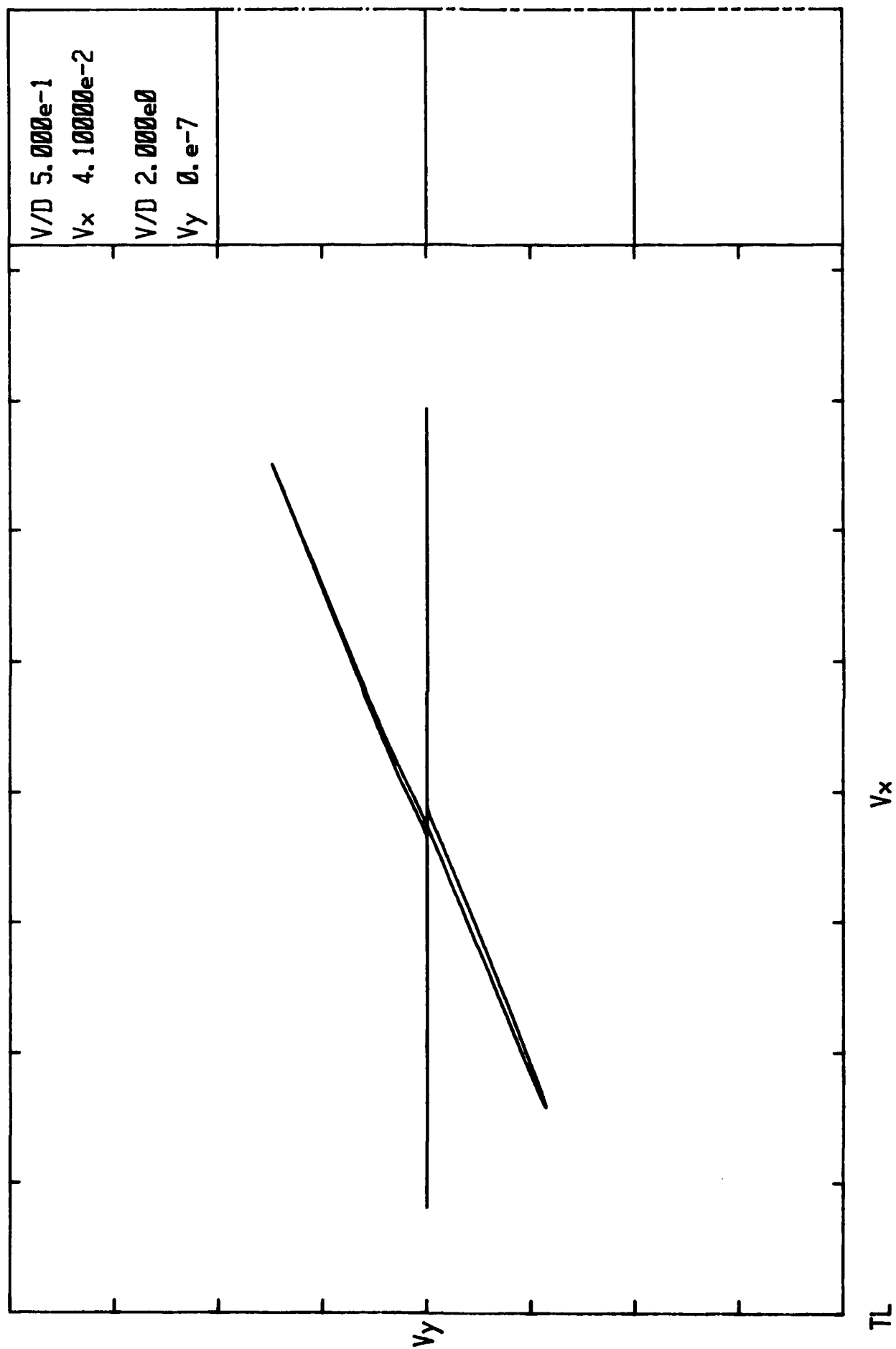
Figure 65. B-H Loop Using Drive Coil E and Pickup F.
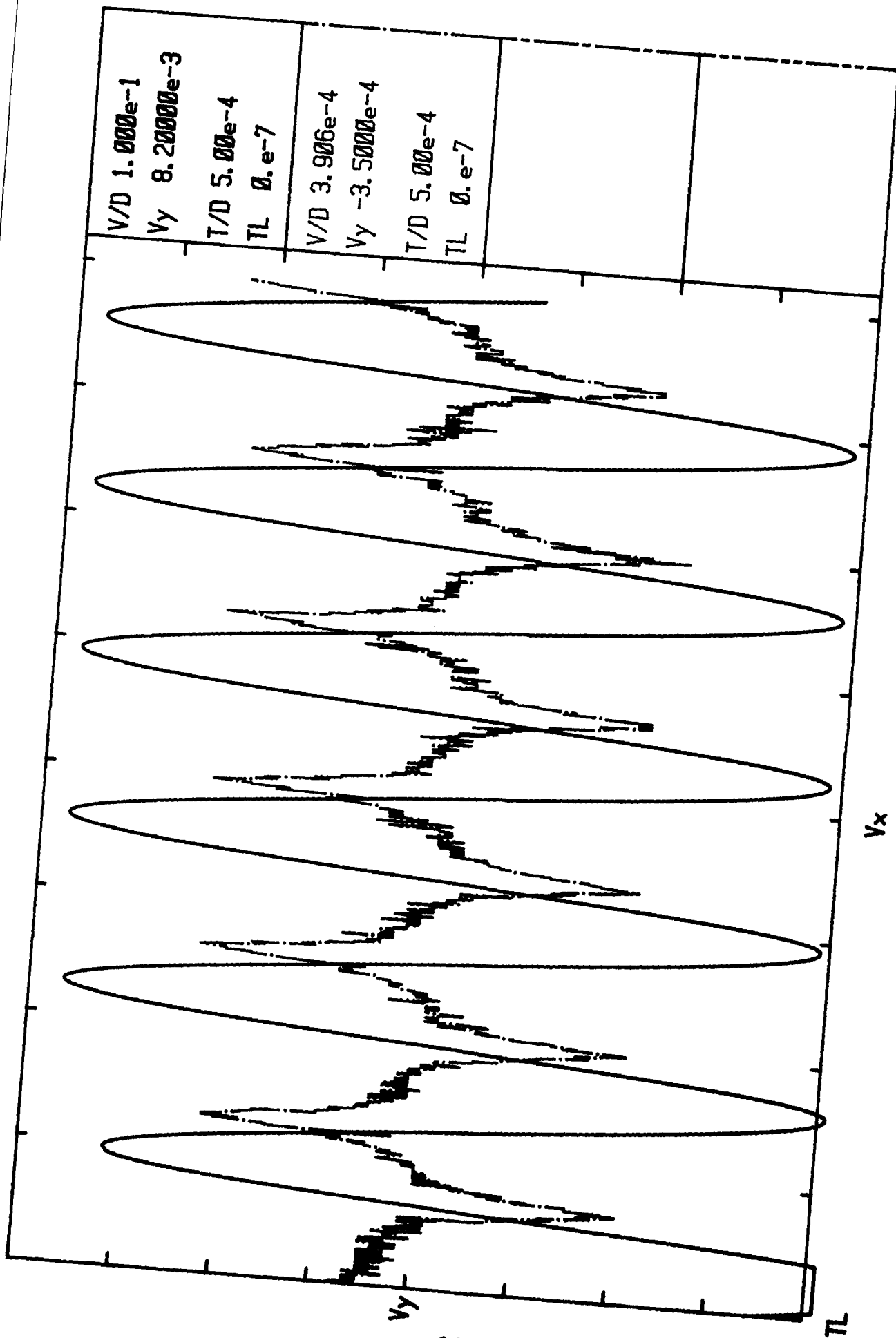
V/D 1.000e-1
Vx 8.0000e-3
V/D 2.500e-2
Vy 0.e-8

Vx

Vy

TL

100
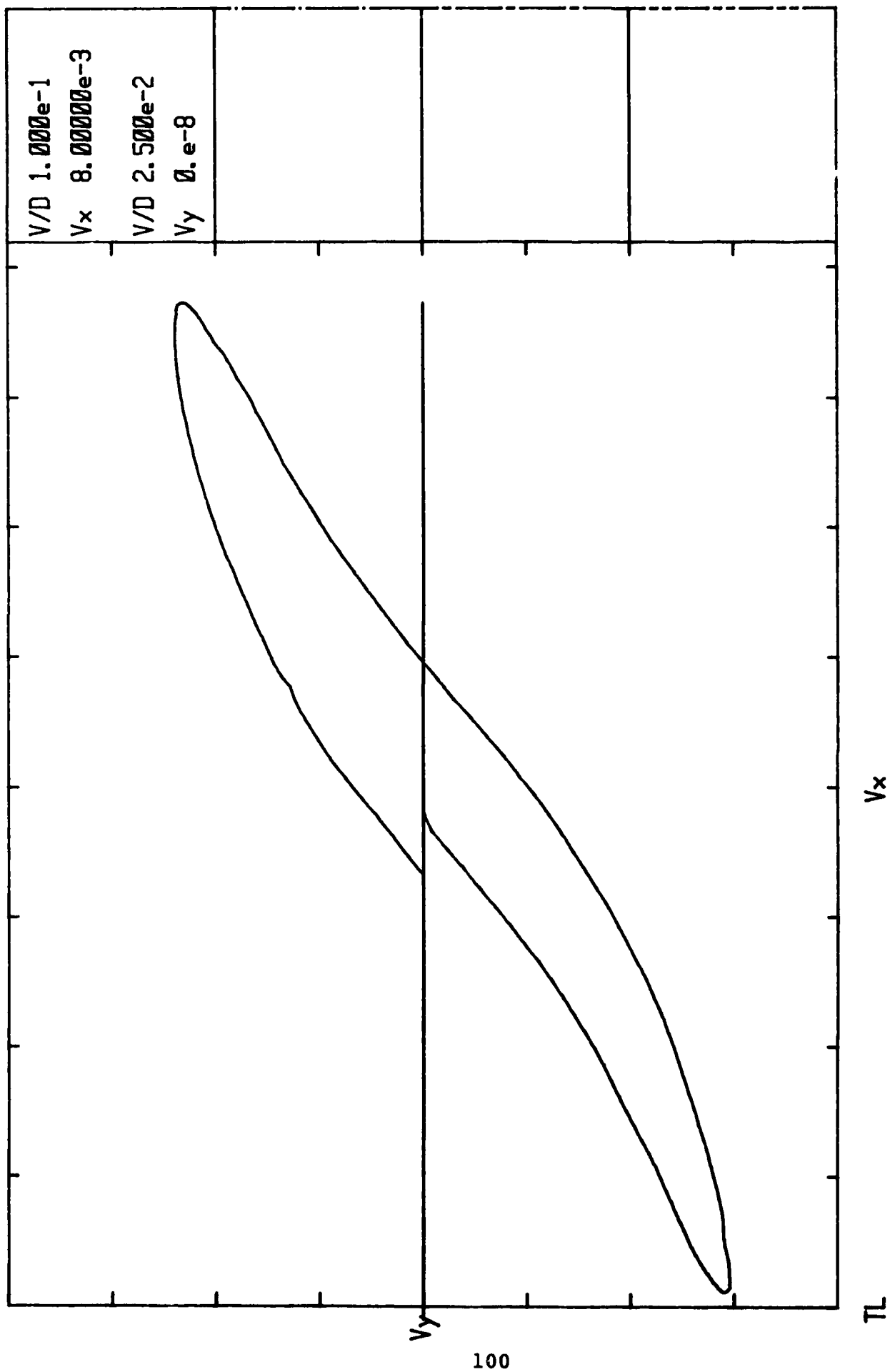
Figure 66. B-H Loop Using Drive Coil A and Pickup Coil D on Alumina Substrate.
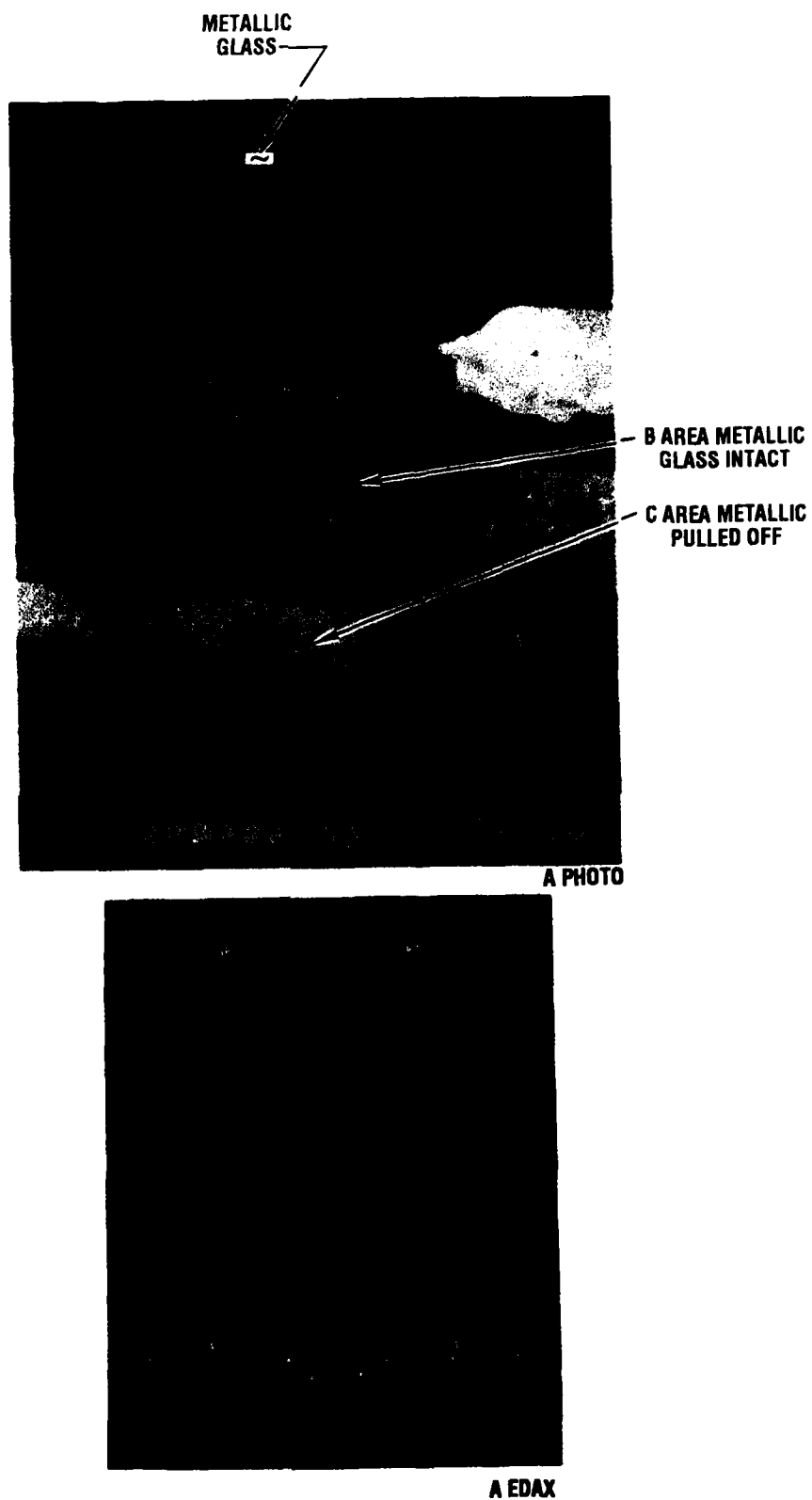
Figure 67.   Photomicrograph and EDAX Analysis of Thin Film
              Gage Section A.

101

B PHOTO

C PHOTO

B EDAX

C EDAX
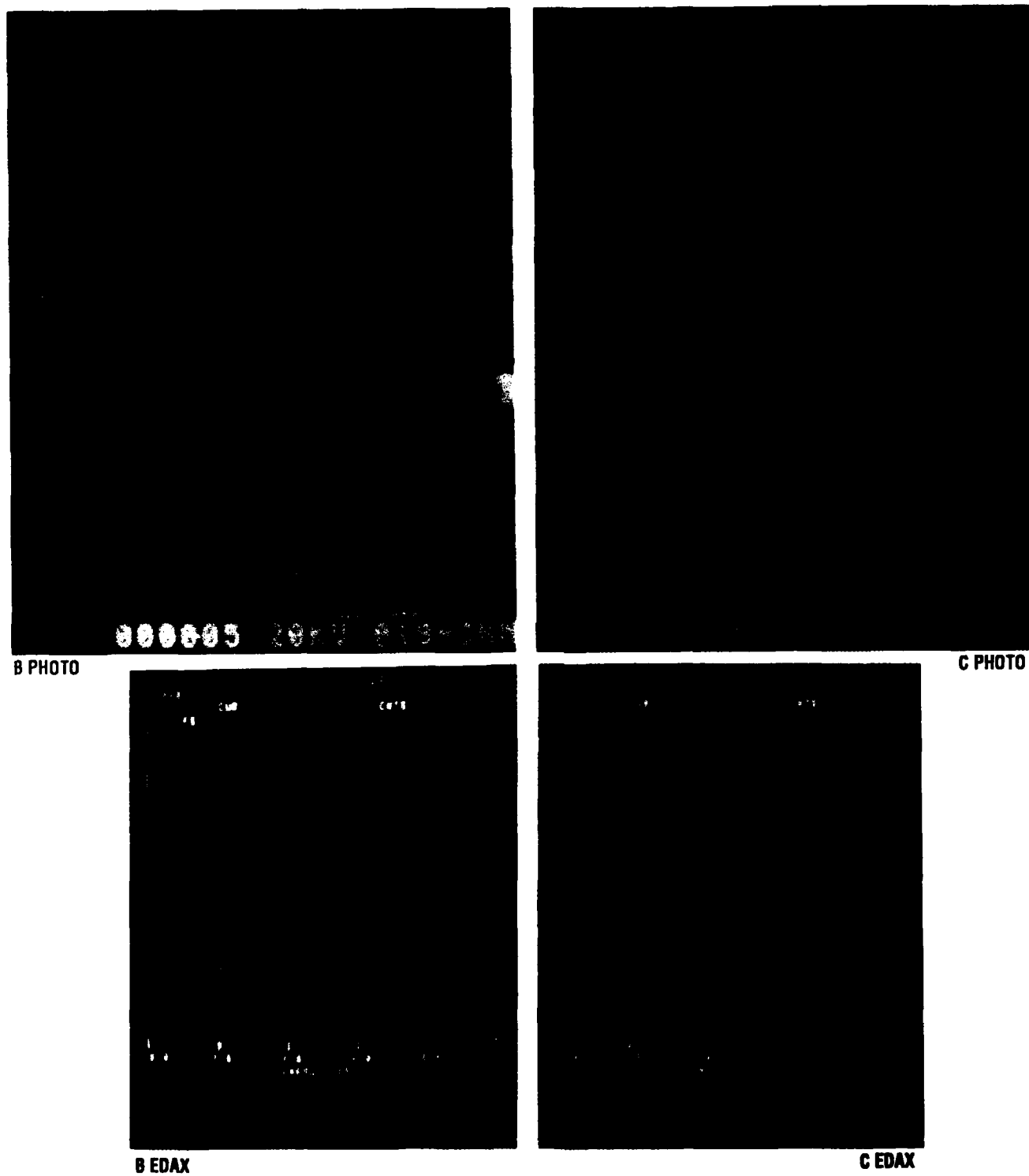
Figure 68.   Photomicrographs and EDAX Analysis of Thin Film
Gage Sections B and C.

pickup with coil B) reflects only a nonoptimized coil design, not a fundamental failure of the magnetic gage concept. Based on the external coil results, the next step forward would be to design improved thin-film coil geometries, such as a bifilar winding (Figure 69) or closely interspersed and alternating drive and pickup coil segments (Figure 70). Either concept, along with a higher ratio of length to square root of cross-section area, would reduce demagnetizing effects and increase coupling. The resulting dB/dt signal should show improved pulse strength, sharpness, and definition in time. In turn, the better dB/dt pulses would improve the precision and accuracy of strain measurements.

Certain practical limitations would be further improved by not restricting the coils to equal numbers of turns and conductor areas in both drive and pickup coils. The drive coil is limited by the need to carry current adequate to achieve sufficiently high H drive field. In contrast, the pickup coil acts as a voltage source with the current flow being limited by the input impedance of the detection circuitry (presumed to be at least many kilohms). Hence the dB/dt signal can be boosted by using pickup coils with many turns which can be of small conductor cross-sectional area.

All indirect techniques for strain measurement rely on the sensitivity of some physical property of a sensor element to mechanical deformation. The magnetic strain gage in the present study represents the marriage of a novel concept (the use of magnetic coercivity as a strain-sensitive property) and advanced materials technology, namely, amorphous metals. These materials, developed in a practical way only in the last 10-15 years, have a unique combination of mechanical and magnetic properties: high mechanical strength and hardness along with extreme magnetic softness (high permeability, low coercive field, and low anisotropy field), moderately high magnetostriction, and very high magnetomechanical coupling. By using state-of-the-art processing it is now possible to obtain these properties in thin films. However, use of this
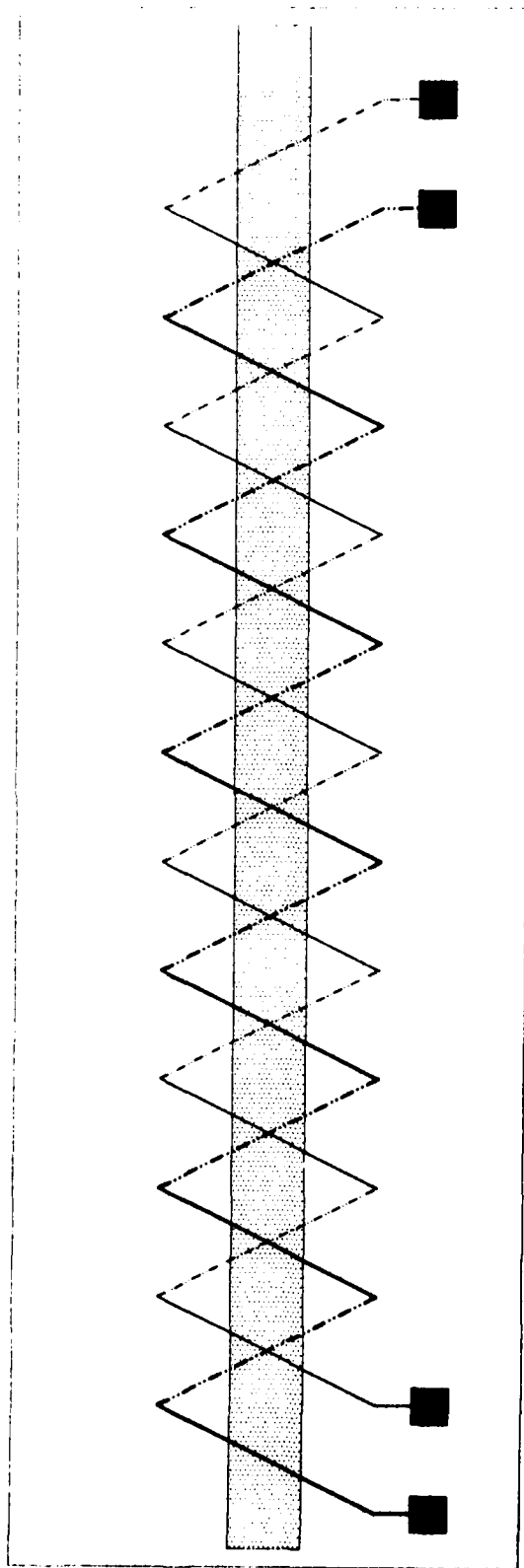
Coils	Layer	
	top	bottom
drive	——	— · — ·
pickup	——	— — —

Amorphous Metal

Figure 69. Suggested Bifilar Drive/Pickup Coil Configuration.
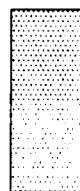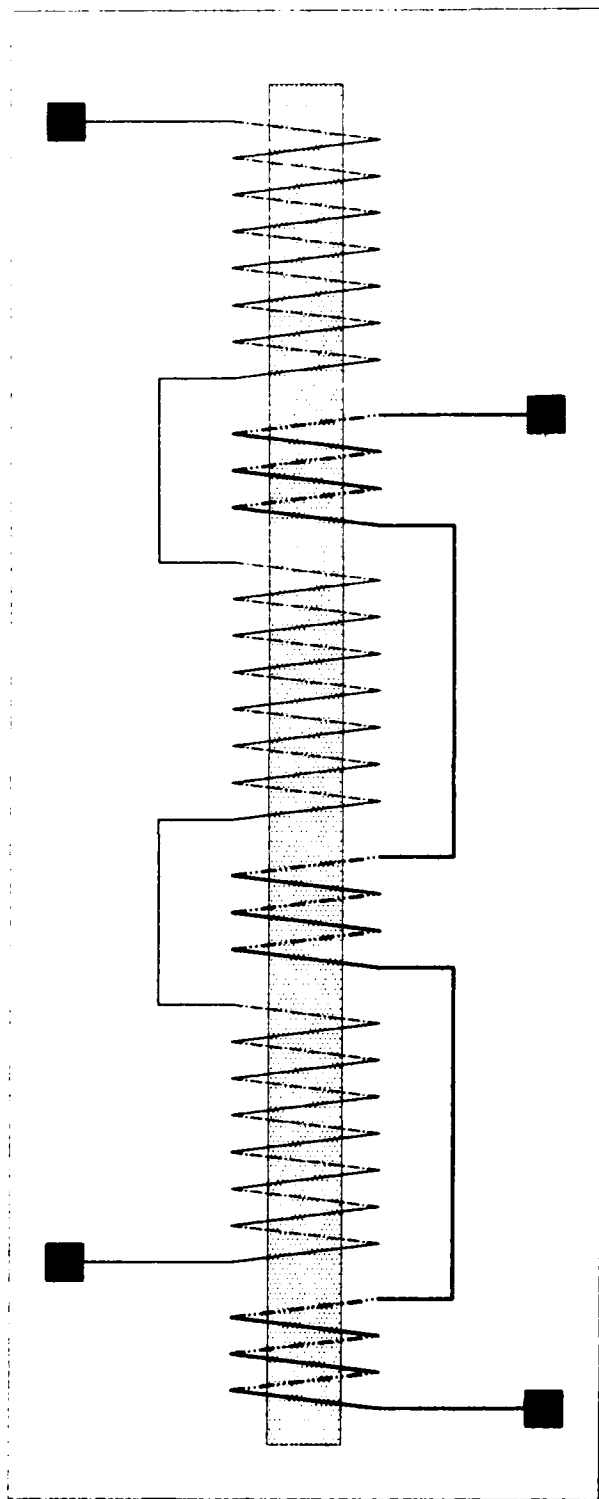
Figure 70. Suggested Interspersed Alternate Drive/Pickup Coil Configuration.

technology for depositing magnetic films (such as for magnetic recording heads) is only gradually becoming routine commercial practice. As the technology develops, it is to be anticipated that further improvements and technology transfer will make application of magnetic strain measurement techniques even more feasible and attractive.

APPENDIX A

AMORPHOUS Fe-B-Si MAGNETIC FILMS BY
REACTIVE SPUTTERING FROM A PURE IRON SOURCE
JOHN L. WALLACE, J. APPL. PHYS. <u>64</u>, 6053 (1988)

Amorphous Fe-B-Si magnetic films by reactive sputtering from
a pure iron source

John L. Wallace

Xi Magnetics Inc., R.D. 8 Box 457A, Coatesville, PA 19320

The author has successfully used reactive sputtering to fabricate amorphous
magnetic thin films with chemical and physical properties similar to those of
Metglas®. The sputtering target was "pure iron" (actually commercially
available mild steel). The amount of each metalloid in the deposited thin
film was controlled by varying the partial pressures of silane and diborane in
the sputtering plasma. Total metalloid concentrations were varied over the
range of 0 - 50 atomic percent. A sample containing 76% Fe: 16.5% B: 3% Si:
3% C was found to be amorphous and to have good soft magnetic properties.
This sample had a well-defined uniaxial anisotropy with an easy axis
coercivity of 4.5 oersteds. The RF permeability (μ') of this sample was
greater than 1000 from 0 to 900 MHz.

PACS numbers: 75.50.Kj, 81.15.Cd

This paper has been accepted for presentation at the 4th Joint MMM-Intermag
Conference, 12 - 15 July 1988, Vancouver, British Columbia, Canada.

XIMAG: HIGH VACUUM AND THIN FILM TECHNOLOGY / III-V AND MAGNETIC MATERIALS

INTRODUCTION

The purpose of this research was to develop a thin film deposition technique capable of depositing amorphous metallic glass layers from a pure iron sputtering target at low cost with real-time control of the alloy composition. Commercially available amorphous magnetic materials prepared by rapid quenching from the melt are restricted in thickness to the range of appproximately 0.5 mils to 5 mils (10 - 100 microns) and cannot be formed directly onto substrates. Many prior workers have used sputtering to deposit small samples of amorphous thin films but the required targets containing large amounts of metalloids tend to be fragile and expensive.

The fact that metal-metalloid sputtering targets are brittle, expensive, and hard to fabricate has been a major impediment to systematic research in this area: it is very difficult to vary the alloy composition in small increments. Some previous workers have attempted to get around this difficulty by co-sputtering. There are two ways to implement co-sputtering and each way has a serious, built-in disadvantage: If one attempts to co-sputter from two widely separated targets onto a rapidly rotating substrate, one inevitably produces an unintended compositional modulation in the vertical direction. If one attempts to co-sputter from two targets located close together, the lateral uniformity on the substrate is poorly controlled. A reactive sputtering technique [1] should avoid all of these problems and still allow controlled variation in metalloid content from one run to the next and also controlled variation as a function of depth to create graded interfaces.

In this effort, we succeeded in depositing layers of amorphous metallic glass with chemical composition similar to Metglas® #2605SC. The films were determined by electron diffraction to be amorphous and they had reasonably good soft magnetic properties. We also deposited multilayer samples having metallic "microlaminations" separated from one another by thin insulating layers; such a structure inhibits eddy currents and thereby enhances the magnetic properties for very high frequencies [2] and very fast risetimes[3][4].

DEPOSITION EQUIPMENT

The deposition and gas handling equipment used in this work is sketched in Fig. 1.

There were three independent variable leak valves for inletting pure argon; pure silane; and a 15% diborane: 85% argon pre-mix. (Pure diborane is not commercially available.) Typically we would do the initial pumpdown of the chamber with the large cryopump while heating the substrate and the surrounding chamber fixtures to > 100°C to drive off water vapor. Then we would valve off the cryopump and begin pumping with the turbo-molecular pump

while the substrates were cooling back down toward room temperature. Typically we were able to achieve partial pressures of water vapor of around 1.5×10^{-6} Torr at the start of the deposition. This was an acceptable background pressure but not really excellent. It is probable that the presence of the background water vapor may have caused the incorporation of some undesirable oxygen into the deposited films and hence lowered their magnetic performance.

All pumping of the reactive gases was done through the turbo-pump while the cryopump was valved off. Any accumulation of reactive gas inside the cryopump would have presented a major safety hazard. Both the turbopump itself and its mechanical backing pump were chemical plasma rated and were lubricated with Fomblin®. The output of the mechanical pump was heavily diluted with dry nitrogen and passed through a "burn box."

Fig. 1 also shows that our substrate platform was equipped with an array of permanent magnets which provided a uniform orienting field in the plane of the growing film to help produce uniaxial anistropy.

RESULTS

Our most interesting single layer sample was sputtered in a plasma containing Ar, B_2H_6 and SiH_4 at approximate partial pressures of 5.8, 1.0, and 2.0 millitorr respectively. The chemical composition of the sample, as determined by Auger spectroscopy was:

boron	16.5 atomic %	oxygen	0.8 atomic %
carbon	3.2 atomic %	silicon	3.0 atomic %
nitrogen	----	iron	76.0 atomic %

This chemical composition is very similar to that of Metglas®#2605SC (Fe81:B13.5:Si3.4:C2).

The complete Auger depth profile is shown in Fig. 2. The resistivity of the sample was approximately 83 micro-ohm centimeters compared to 9.7 which is the published value for pure iron or 130 which is the published [5] value for commercially available Metglas® #2605SC.

Looper photographs in the differential format ($d\Phi/dt$ vs H) are shown in Fig. 3 along with conventional M vs H plots obtained by visually estimating the integral of the $d\Phi/dt$ curves. These curves were both taken in the plane of the film but Fig. 3A was taken along the intended "easy" axis; i.e. along the direction of the orienting field which we had supplied in the plane of the substrate during deposition.

Finally, the VHF permeability spectra of this sample are shown in Fig.

4. These spectra are consistent with a saturation magnetization of 20000 gauss (2 Tesla) and an anisotropy field of 16 oersted (1300 Amp/m). However 16 Oe (while encouraging) is still not a particularly good value and must be lowered even further for most soft magnetic applications.)

We did two runs specifically to determine whether the films were indeed amorphous. Since this determination was done by transmitted electron diffraction, it was necessary for the samples to be ~ 500 Å thick (50 nm) rather than our normal ~ 1000 Å. The reduced thickness made it impractical to do any other measurements on these samples. However we tried to use the same deposition conditions for these runs that we had used on our "best" sample i.e. the one that is discussed in detail in the previous paragraphs. In each case, the lab reported that the electron diffraction pattern revealed no trace of crystallinity. One of the diffraction photographs is reproduced in Figure 5.

The data hint that the composition of the film may be a very non-linear function of the plasma composition. Fig. 6 shows the partial pressure of SiH4 in various plasmas, and the atomic percentages of Si in the resulting alloys. There is great uncertainty in these data especially since we could not measure the partial pressure after the plasma was turned on. Nevertheless, our Fig. 6 is very similar to figures that have been published for other kinds of reactive sputtering. A typical example from the published literature for reactively sputtered TiN can be found in an article by Wittmer entitled "Properties and Microelectronic Applications of Thin Films of Metal Nitrides".[6]

CONCLUSIONS

We have demonstrated that it is possible to produce alloys of iron, boron, and silicon by reactively sputtering an iron target in a plasma containing diborane and/or silane. We have also demonstrated that the amount of boron or silicon incorporated can vary from zero to ~50% depending on the partial pressures of reactive gas in the plasma.

It is not known at this time whether the alloy composition is an approximately linear function of the plasma composition or whether it is highly non-linear (prior published work on other kinds of reactive sputtering--e.g. TiN--has observed extreme non-linearity or even hysteresis). If the alloy composition is a highly non-linear or hysteretic function of plasma composition then real-time computer control of the process might be required to reproducibly deposit alloys with tightly controlled chemical composition. This would not seem to be an insurmountable difficulty however.

The results indicated that the magnetic properties of the film drop off very rapidly when the percentage of metalloids in the film rises above ~ 40%. The samples with metalloid content between ~ 10% and ~ 30% seem to have fairly

good soft magnetic properties.

We have obtained strong circumstantial evidence that the film produced can be amorphous or nearly amorphous when intermediate amounts of metalloids are incorporated. [One would not expect to see amorphous film if the percentage of metalloid was either very low ($\approx 0\%$) or very high (>50%).]

We have demonstrated that these films can be fabricated in a multi-layer format which opens up the possibility of eventually providing pseudo-bulk material combining the best properties of Metglas® (large ΔB) and the best properties of ferrite (excellent wideband frequency response).

ACKNOWLEDGEMENT

REFERENCES

® Metglas is a registered trademark of the Allied Corporation.

® Fomblin is a registered trademark of the Montedison Group.

1. B.Goranchev, K.Reichelt, J.Chevallier, P.Grunberg and W.Vach, Thin
    Solid Films, 100, 257 (1983).

2. R.M.Walser and R.J.Hach, U.S.Patent No. 3 540 047 (10 Nov. 1970).

3. F.B.Humphrey, R.Hasegawa and H.Clow, IEEE Trans. Magn., 2, 557 (1966).

4. J.L.Wallace, Proc. IEEE 6th Pulsed Power Conf., Arlington, VA (1987) p.17.

5. C.H.Smith, IEEE Trans. Magn., 18, 1376 (1982).

6. R.A.Waldron, IEEE Trans. Microwave Theory Tech., MTT10 123 (1964).

7. R.F.Soohoo, J. Appl. Phys., 315, 218S (1960).

8. M.Wittmer, J. Vac. Sci. Technol., 4, 1797 (1985).
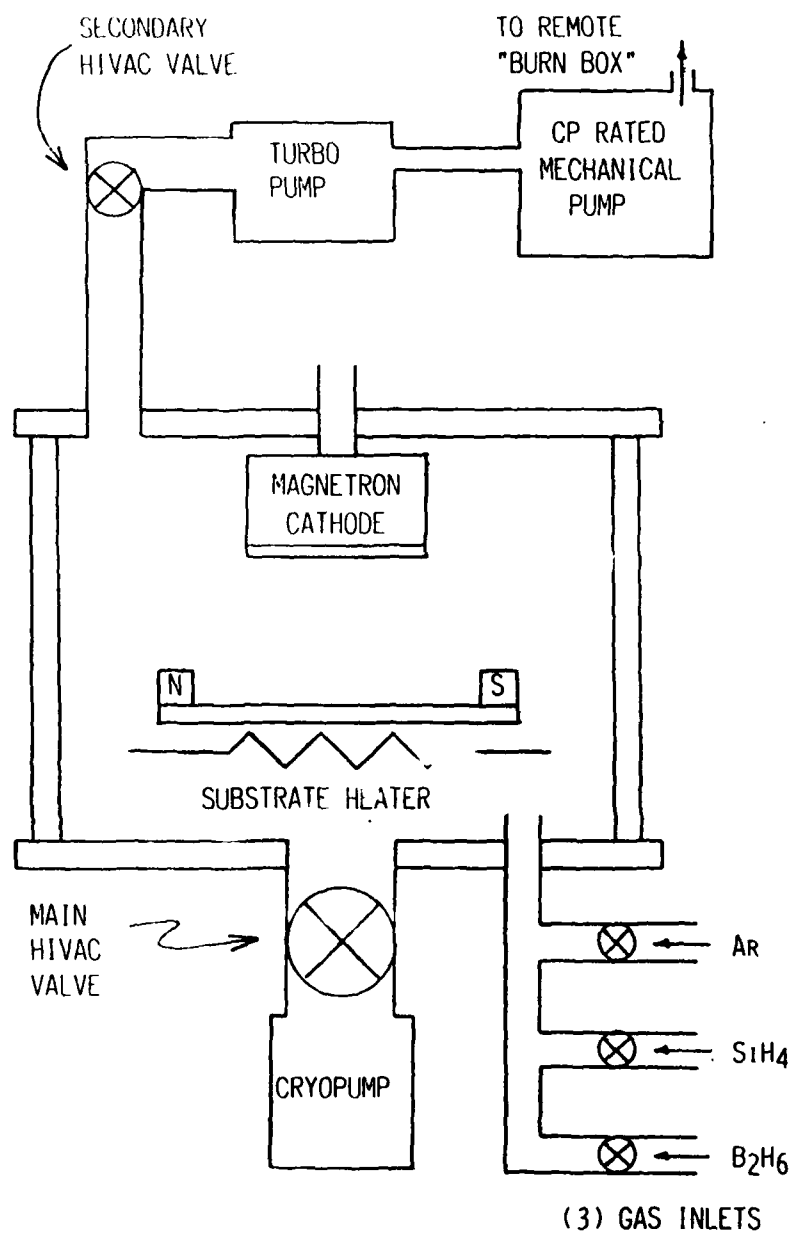
FIG. 1. Block diagram of the deposition equipment.
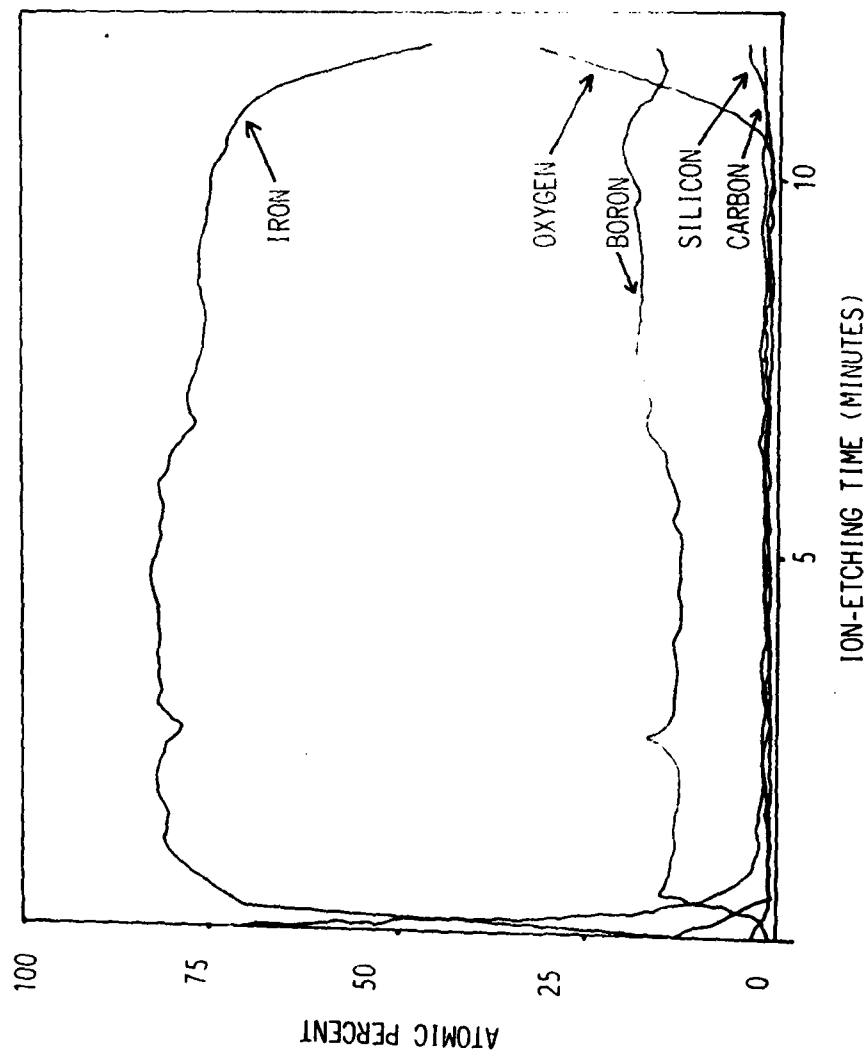
FIG. 2. Auger Depth Profile for sample #25 Nov-3. The estimated ion-etching rate was 100 Å per minute.
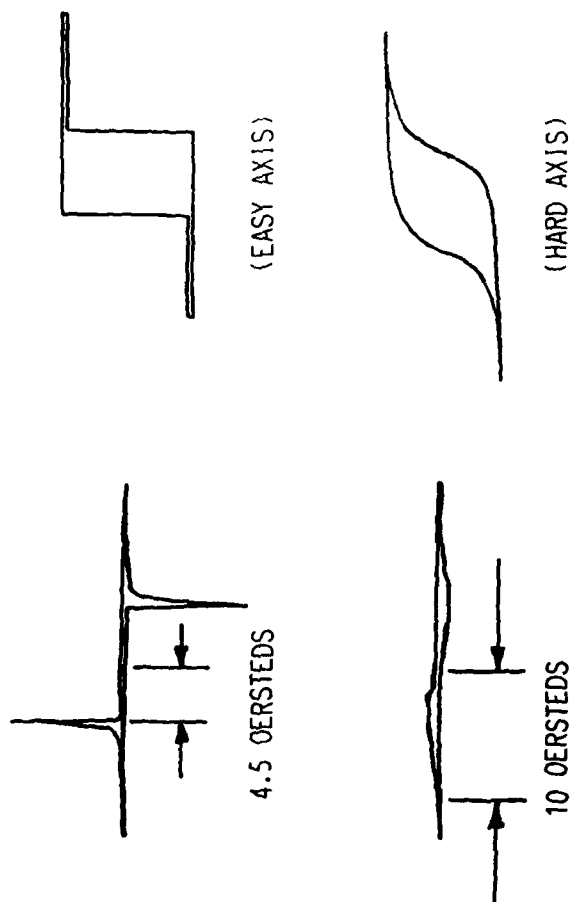
FIG. 3. Looper data for sample # 25 Nov-3 taken at 60 Hz. The looper used in this work was not equipped with an integrating circuit; therefore the left-hand curves are tracings of the actual induced voltage ($-d\phi/dt$) appearing on the oscilloscope screen whereas the right-hand curves are artist's conceptions of the corresponding integrals.
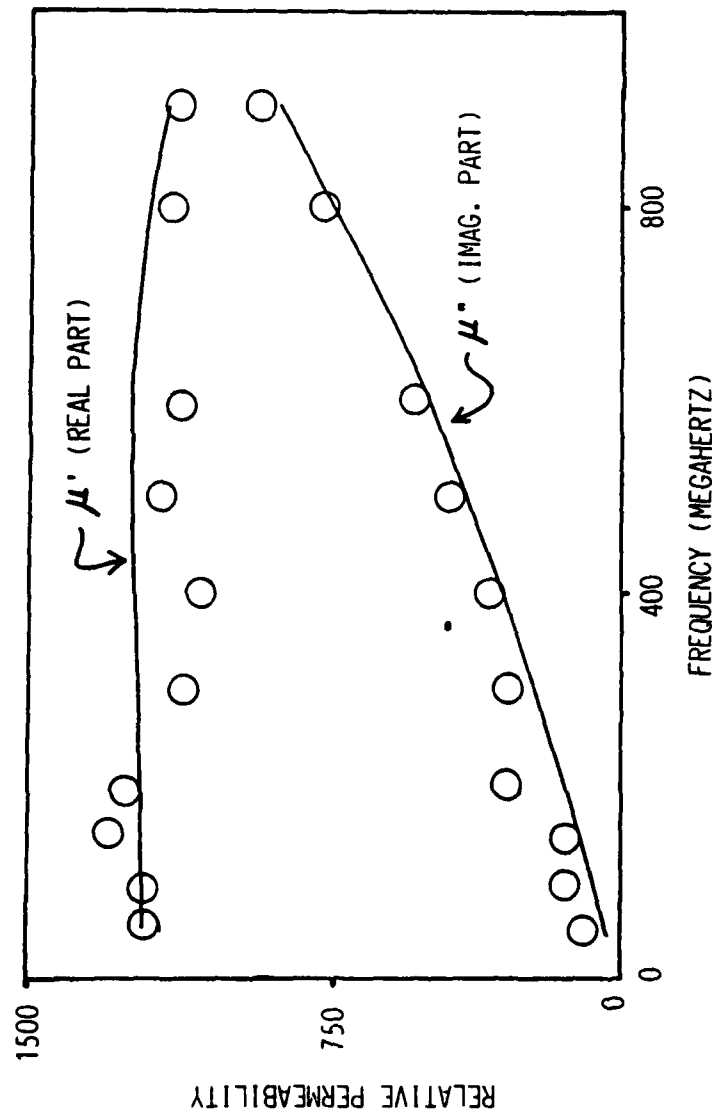
FIG. 4. VHF permeability spectrum of sample #25 Nov-3. The circles are experimental data points obtained by perturbation measurements in a stripline cavity according to the method of Waldron[6]. The solid curves are theoretical values, according to an equation by Soohoo[7], for a single domain thin film of "infinite" area having M_s = 20000 gauss; H_k = 16 oersted; and α (the Gilbert damping parameter) = 0.025.
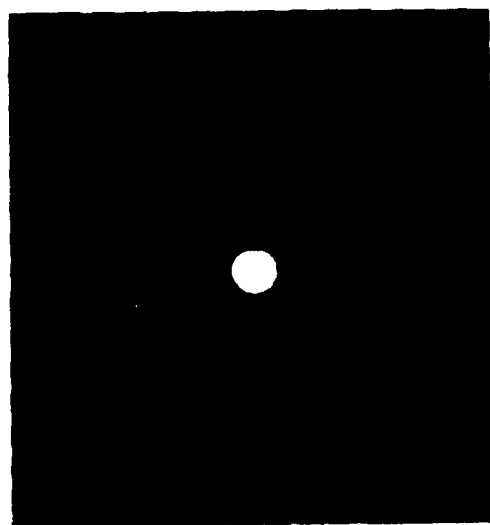
FIG. 5. Transmitted electron diffraction photograph of sample #3 Dec-4.
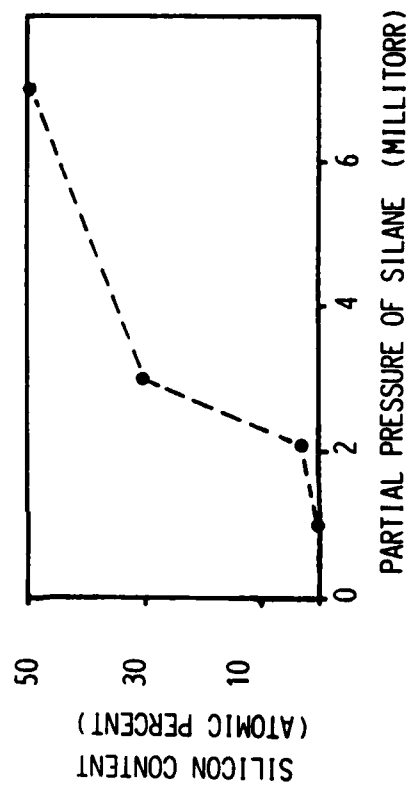
FIG. 6. The amount of silicon incorporated in the deposited film (determined by Auger Electron Spectroscopy) as a function of the partial pressure of silane in the sputtering plasma.

APPENDIX B

COMPRESSIVE STRESS AND
NEGATIVE MAGNETOSTRICTION
DR. GORDON FISH
14 SEPTEMBER 1988

Compressive Stress and Negative Magnetostriction

In a magnetic material, the direction of magnetization (M) when the applied field (H) = 0 is called the "easy axis of magnetization". It is "easy" in the sense that the response (B or M) to the driving force (H) is large. The orthogonal direction is the "hard axis". One can make a simple analogy between the magnetics and ordinary mechanical response of materials, with anisotropic moduli. An elastically "easy" or soft material has low modulus, a hard material has high modulus.

In a magnetic material with no applied field H and under no stress (either applied, cast-in, induced by cold working, etc.), the magnetization vector M will be directed along a particular crystallographic direction called the easy axis. In hexagonal Co, the c-axis is the easy axis. [In α-Fe, the situation is a bit more complicated: the crystal structure is body centered cubic, and any of the (100) cube axes can be the easy direction.] In metallic glass, other magnetic effects are at work, but there is still an easy axis. Within each magnetic domain, the magnetic moments of each of the atoms are aligned in parallel. The domains are each aligned parallel or antiparallel to the easy direction. The overall magnetization of the sample is just the vector sum of the moments of the individual atoms, or the sum of the moments of each domain, depending on your viewpoint.

When tension is applied to a material with positive magnetostriction λ_s, the tensile axis becomes an easy axis; compression makes the compression axis a hard axis. B-H loops in which H is applied along the easy and hard axes magnetization are shown in the attached figure.

The measurement we are doing is to apply a sine or triangular wave current to the drive coil, making H be sine (triangular) in time. The secondary pickup coil senses voltage $V = -NA\ dB/dt$ from Faraday's law (N is number of pickup turns and A is cross-sectional area, both constants). Using the chain rule, $dB/dt = (dB/dH) \times (dH/dt)$. dB/dH is just the instantaneous slope of the B-H loop (called permeability) in the parametric representation, so the voltage pickup shows sharp peaks if the B-H loop has sharp sides (easy axis). The hard-axis loop has flat sides, so the peaks are spread out. Assuming the peak H is enough to drive B to its + and - saturation values for both easy and hard axis loops, the <u>area</u> under each dB/dt peak must be constant, as is obvious by simple integration:

$$\int_0^{T/2} V\ dt = -NA \int_0^{T/2} (dB/dt)\ dt$$

$$= -NA \int_0^{T/2} dB$$

$$= -NA\ [B(t=T/2) - B(t=0)]$$

$$= -NA\ [+B_{sat} - (-B_{sat})]$$

$$= -2\ N\ A\ B_{sat}.$$

T is the period of the sine or triangular wave and B_{sat} is a constant, characteristic of a given magentic material. If the area under the peak is constant, then the height and width must be inversely proportional (more or less, assuming peak doesn't change its underlying shape.)

21-7574

2

B-2

A more rigorous explanation is the following: In quantitative terms, the net direction of magnetization is determined by minimizing an energy balance equation

$$E = K \cos^2 \Theta - M \cdot H,$$

where the first term is the anisotropy energy term with Θ the angle between M and the anisotropy direction and the second term is just the energy of a magnetic dipole of moment M in a field H. $-(M \cdot H)$ is the energy corresponding to the torque on a compass needle, for example. If there are multiple sources of anisotropy, each has a term like the first. In our case, K is dominated by stress anisotropy, so $K = K_a = -(3/2)\lambda_s\sigma$ and Θ is the angle between M and the stress axis. When $\lambda_s > 0$, and $H = 0$, the minimum is clearly for Θ to be 0 (or 180), so the magnetization vector M aligns with the tensile (+) stress direction. For a compressive ($\sigma < 0$) stress, the anisotropy term goes negative, so the magnetization wants to turn so $\Theta = 90^0$ or M is perpendicular to the stress axis. If the material selected has $\lambda_s < 0$, the roles of tension and compression reverse.

As background, a paper by J. D. Livingston [phys. stat. solidi A70, 591 (1982)] treats the problem in more detail. In reading it, you should remember that he is principally concerned with the case in which the applied stress in the metallic glass is small enough so that $K_a = -(3/2)\lambda_s\sigma$ is small compared to the uniaxial induced anisotropy energy density K_u. K_u is produced by annealing the sample in a magnetic field. This sets an easy axis in the annealing field direction, producing an energy term $K_u \cos^2 \Phi$. Φ is measured between M and the annealing field direction. Livingston treats the case where the Φ direction is transverse and Θ is longitudinal. The values of K_u achievable in practice are small enough that K_a dominates K_u at even modest strains, typically tens of microstrains. We are thus working in a totally different regime from Livingston. If the K's are comparable, my equation above has to be modified as Livingston has done to include both the K_a stress axis and the K_u direction. The final direction of M when $H\neq0$ is determined by a competition between the two K's and the $M \cdot H$ term. In the analogy to an elastic system, the K's are each restoring forces making the system elastically anisotropic.
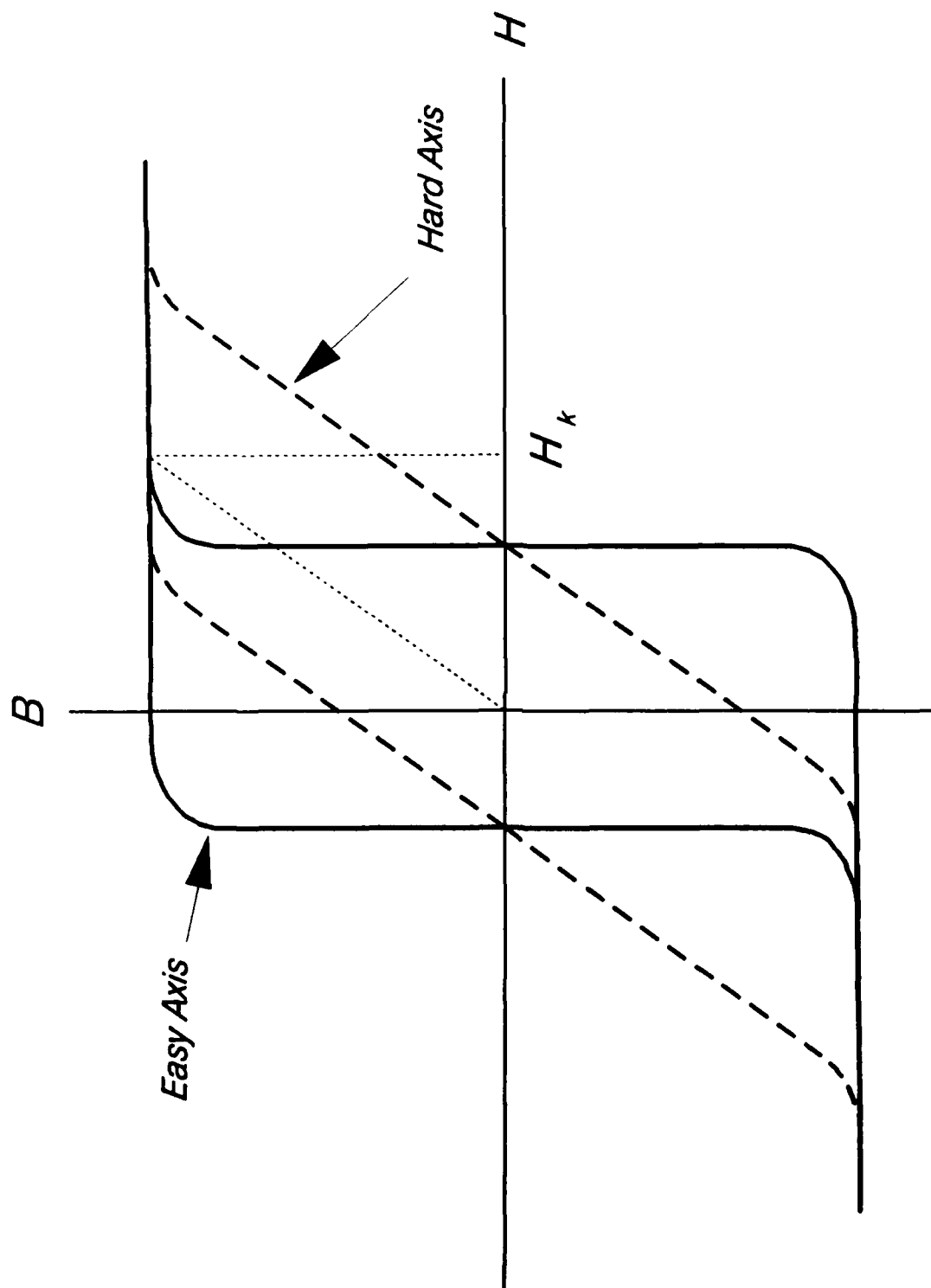
Metallurgy Laboratory, General Electric Corporate Research and Development, Schenectady[1])

Magnetomechanical Properties of Amorphous Metals

By

J. D. Livingston

Amorphous metals have magnetomechanical properties superior to those of crystalline magneto-strictive materials, and are therefore being considered for a variety of transducer and sensor applications. A simplified model is presented of magnetomechanical coupling in amorphous metal ribbons, showing the relation between magnetomechanical behavior and fundamental material parameters. Although high values of magnetization and magnetostriction are important, it is primarily the low values of magnetic anisotropy achievable that give amorphous metals their outstanding magnetomechanical coupling. The magnitude and homogeneity of this anisotropy is controllable through choice of alloy composition and annealing conditions.

Amorphe Metalle haben bessere magnetomechanische Eigenschaften als kristalline Werkstoffe, und werden deshalb für Anwendungen als Energieumwandler und Kraftübertrager betrachtet. Ein vereinfachtes Modell der magnetomechanischen Kopplung in amorphen metallischen Bändern wird gegeben, das die Beziehung zwischen magnetomechanischem Verhalten und grundlegenden Parametern des Werkstoffs erklärt. Obwohl hohe Werte der Magnetisierung und Magnetostrik-tion wichtig sind, stammen die hervorragenden magnetomechanischen Kopplungseigenschaften in amorphen Metallen hauptsächlich von den niedrigen Werten der magnetischen Anisotropie. Die Werte und die Homogenität der Anisotropie werden durch die Legierungszusammensetzung und die Anlaßbedingungen kontrolliert.

1. Introduction

Amorphous metals have been shown to have magnetomechanical properties superior to those of any previous magnetic materials [1 to 5]. As a result, they are being con-sidered for a variety of transducer and sensor applications. As a guide to understanding, optimizing, and applying these properties, we present here a simplified model of magnetomechanical coupling in amorphous metal ribbons.

In amorphous metals, the major sources of magnetic anisotropy are structural anisotropies induced by annealing under magnetic field (and/or applied stress) and magnetostrictive anisotropies produced by the interaction between magnetostrictive strain and applied or residual stresses. Magnetomechanical properties are determined by the competition between these two sources of anisotropy.

2. Model

We consider an amorphous metal ribbon annealed in a large magnetic field parallel to the ribbon width to produce a widthwise magnetic easy axis. We assume a first-order uniaxial anisotropy, with an energy contribution of $K_u \cos^2 \theta$ per unit volume, where $K_u > 0$ and θ is the angle between the magnetization (assumed to remain in the ribbon plane) and the ribbon length. With zero applied field and zero applied stress, the resulting domain structure will be as shown in Fig. 1a. A longitudinal

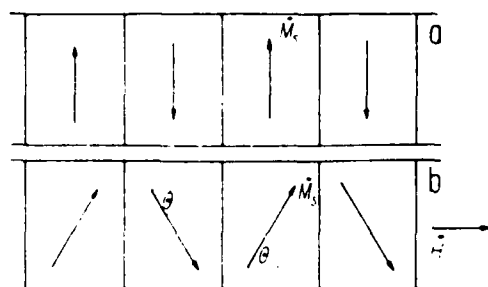[1]) P.O.B. 8, Schenectady, New York 12301, USA.

Fig. 1. a) Zero-field domain structure of transverse-annealed amorphous ribbon. b) Domain structure of transverse-annealed ribbon in longitudinal magnetic field $H < H_A$

magnetic field H will rotate the magnetization from the width towards the length direction (Fig. 1 b) and make a contribution to the energy density of $-M_s H \cos\theta$ where M_s is the domain magnetization per unit volume. Finding the angle θ for minimum energy yields for the longitudinal component of magnetization

$$M = M_s \cos\theta = M_s \frac{H}{H_A} \qquad (H \leqq H_A),$$ (1)

where $H_A = 2K_u/M_s$ is the anisotropy field. The susceptiblity is constant for $H < H_A$ and equal to

$$\chi \equiv \frac{dM}{dH} = \frac{M_s}{H_A} = \frac{M_s^2}{2K_u}.$$ (2)

The spontaneous magnetostrictive strain in each domain is λ_s in the direction of magnetization and $-\lambda_s/2$ in orthogonal directions. Thus, as the magnetization rotates from the width to the length direction, the longitudinal strain ε changes from $-\lambda_s/2$ to $+\lambda_s$, a change of $3\lambda_s/2$. As a function of θ, and, through equation (1), as a function of H, the longitudinal strain is given by

$$\varepsilon = \frac{3\lambda_s}{2}\left(\cos^2\theta - \frac{1}{3}\right) = \frac{3\lambda_s}{2}\left(\frac{H^2}{H_A^2} - \frac{1}{3}\right).$$ (3)

Hence

$$d \equiv \frac{d\varepsilon}{dH} = \frac{3\lambda_s H}{H_A^2}.$$ (4)

This measure of magnetomechanical coupling reaches a maximum at $H = H_A$,

$$d_{max} = \frac{3\lambda_s}{H_A} = \frac{3\lambda_s M_s}{2K_u}.$$ (5)

We now consider the application of a longitudinal stress σ, which produces an anisotropic contribution to the energy density of $-\frac{3}{2}\lambda_s\sigma\cos^2\theta$ [6]. Thus the net anisotropy energy will now be $(K_u - \frac{3}{2}\lambda_s\sigma)\cos^2\theta$. For $\lambda_s\sigma > 0$, i.e. tensile stress on a positive-magnetostriction material or compressive stress on a negative-magneto-striction material, the stress has the effect of lowering the net anisotropy from K_u to $(K_u - \frac{3}{2}\lambda\sigma)$. The magnetic easy axis will remain in the width direction as long as $\sigma < \sigma_0 = 2K_u/3\lambda_s$, but will abruptly switch to the length direction for $\sigma > \sigma_c$. We will consider only the former case.

Magnetization behavior will be as before with H_A replaced by a reduced anisotropy field

$$H_{A\sigma} \equiv \frac{2K_u - 3\lambda_s\sigma}{M_s} \qquad (\sigma \leqq \sigma_c).$$ (6)

Thus

$$M = M_s \frac{H}{H_{A\sigma}} \qquad (H \leqq H_{A\sigma}),$$

(7)

$$\chi_\sigma \equiv \left(\frac{\partial M}{\partial H}\right)_\sigma = \frac{M_s}{H_{A\sigma}},$$

(8)

$$d \equiv \left(\frac{\partial M}{\partial \sigma}\right)_H = \frac{3\lambda_s H}{H_{A\sigma}^2}.$$

(9)

This dependence of M on H and σ is shown graphically in Fig. 2a and b.

The magnetostrictive contribution to longitudinal strain ε will be given by (3) with H_A replaced by $H_{A\sigma}$. There will in addition be a Hooke's law term σ/E_M, where E_M is the Young's modulus at constant magnetization (for example, at saturation). Thus

$$\varepsilon = \frac{\sigma}{E_M} + \frac{3\lambda_s}{2}\left(\frac{H^2}{H_{A\sigma}^2} - \frac{1}{3}\right),$$

(10)

$$d \equiv \left(\frac{\partial \varepsilon}{\partial H}\right)_\sigma = \frac{3\lambda_s H}{H_{A\sigma}^2},$$

(11)
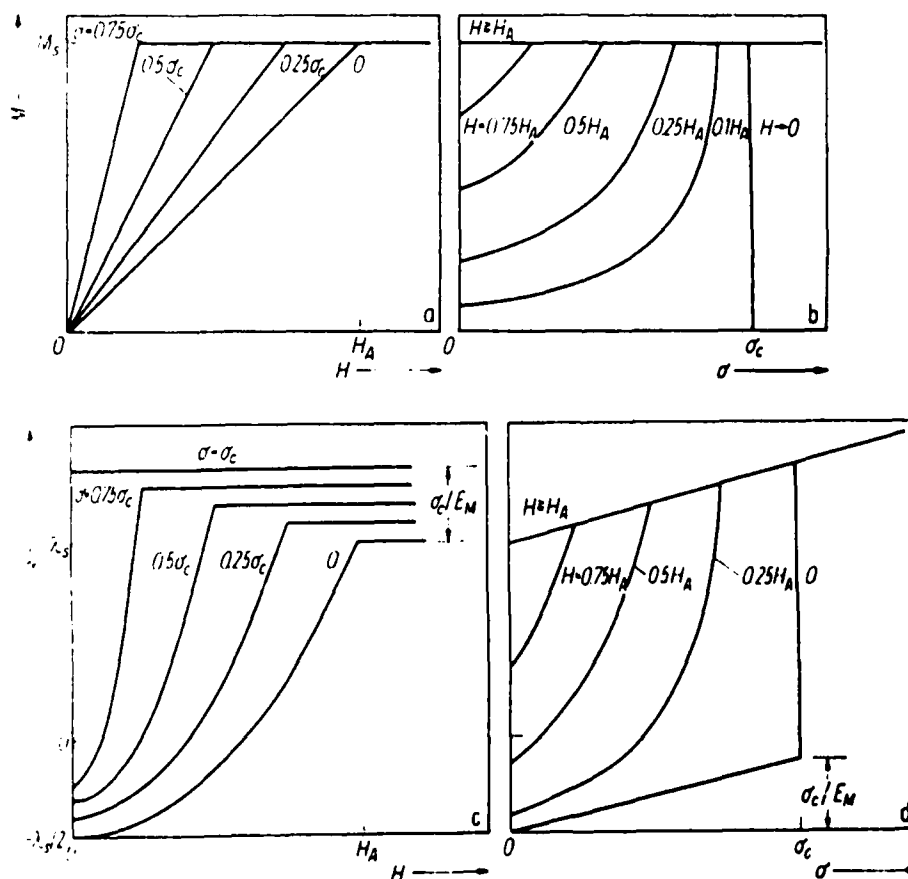
Fig. 2. Results of idealized model. a) Variation of longitudinal magnetization M with longitudinal field H at various values of longitudinal stress σ. b) Variation of M with σ at various values of H. c) Variation of longitudinal strain ε with H at various values of σ. d) Variation of ε with σ for various values of H. In real materials, inhomogeneities in anisotropy and other parameters will lead to rounded, instead of sharp, transitions

$$\frac{1}{E_H} \equiv \left(\frac{\partial \varepsilon}{\partial \sigma}\right)_H = \frac{1}{E_M} + \frac{9\lambda_s^2 H^2}{M_s H_{A\sigma}^3}. \tag{12}$$

This dependence of ε on H and σ is shown graphically in Fig. 2c and d.

A parameter of direct importance in transducer and sensor applications is $d = (\partial \varepsilon / \partial H)_\sigma = (\partial M / \partial \sigma)_H$, the so-called piezomagnetic strain constant. (These two partial derivatives are equal through Maxwell's relations.) This quantity reaches a maximum value at $H = H_{A\sigma}$ of

$$d_{max} = \frac{3\lambda_s}{H_{A\sigma}} = \frac{3\lambda_s M_s}{2K_u - 3\lambda_s \sigma}. \tag{13}$$

Another important parameter for comparing materials is the magnetomechanical coupling factor k, which is related to the fractional energy transfer between magnetic and mechanical energy, and thus is a basic index of energy conversion capability [7, 8]. It can be related [7] to the parameters already derived, and equals

$$k = d\left(\frac{E_H}{\chi_\sigma}\right)^{1/2} = \left[1 + \frac{M_s H_{A\sigma}^3}{9\lambda_s^2 E_M H^2}\right]^{-1/2} \le 1 \tag{14}$$

which reaches, at $H = H_{A\sigma}$, a maximum value of

$$k_{max} = \left[1 + \frac{2K_u - 3\lambda_s \sigma}{9\lambda_s^2 E_M}\right]^{-1/2} \le 1. \tag{15}$$

For applications based on changes in elastic modulus, the parameter of interest is the fractional difference between the elastic modulus at constant magnetization and the modulus at constant field. From (12),

$$\frac{\Delta E}{E_H} \equiv \frac{E_M - E_H}{E_H} = \frac{9\lambda_s^2 E_M H^2}{M_s H_{A\sigma}^3} \tag{16}$$

reaching a maximum at $H = H_{A\sigma}$ of

$$\left(\frac{\Delta H}{E_H}\right)_{max} = \frac{9\lambda_s^2 E_M}{2K_u - 3\lambda_s \sigma}. \tag{17}$$

3. Discussion

It is clear from (13), (15), and (17) why some Fe-rich amorphous ribbons have superior magnetomechanical properties. For an unstressed sample, d_{max} depends on $\lambda_s M_s / K_u$, and k_{max} and $(\Delta E/E_H)_{max}$ depend on $\lambda_s^2 E_M / K_u$. Fe-rich amorphous alloys can have substantial magnetostriction constants $(\lambda_s = (25 \text{ to } 50) \times 10^{-6})$ and, more importantly, can have very low anisotropies. For example, Allied 2605SC ($Fe_{81}B_{13.5}Si_{3.5}C_2$) has been annealed to produce $K_u = 38 \text{ J/m}^3$, $H_A = 70 \text{ A/m}$ (0.9 Oe), and $\sigma_c = 0.7 \text{ MPa}$ (100 psi) [5]. *It is these low values of K_u, H_A, and σ_c that permit rotation of the magnetization and accompanying magnetostrictive strain with low applied fields or stresses, yielding outstanding magnetomechanical properties.*

For 2605SC a coupling constant k of 0.98 and a $\Delta E/E_H$ exceeding ten have been estimated [5]. Most crystalline magnetostrictive materials have k-values of 0.3 or lower and $\Delta E/E_H$ less than unity. Even the rare-earth–iron compounds with giant magnetostriction constants, which are currently being considered for sonar applications, have only $k \approx 0.7$ (competitive with piezoceramic materials such as lead titanate zirconate) [8, 9].

The equations also show that the application of a longitudinal stress σ can further reduce the effective anisotropy and increase the magnetomechanical coupling. The maximum values given by (13), (15), and (17), however, are only achieved at a precise balance of field, stress, and anisotropy given by $H = H_{A\sigma}$. Further, in many applications it may not be desirable to further increase magnetomechanical coupling. Allied 2605SC may already be too sensitive for some applications.

This simplified model has assumed that $K_u, \lambda_s, M_s, E_M, H$, and σ are all completely homogeneous throughout the sample. In reality, there are likely to be inhomogeneities in all these quantities (leading, for example, to rounding of the "knee" of the magnetization curve [5]). Surface defects and irregularities will lead to local variations in σ, as will any components of bending or twisting. The non-ellipsoidal shape of the sample leads to variations in H. More importantly, the material parameters will be inhomogeneous, particularly K_u. A major source of variations in K_u will be internal stresses, which will lead to variations in both the amplitude and the direction of the net anisotropy. It is thus necessary that the anneal be sufficient to remove the internal stresses present in the as-cast ribbon without inducing significant crystallization. This may be difficult in alloy compositions with low crystallization temperatures.

Spano et al. [5] have observed in 2605SC the linear decrease of χ_σ^{-1} with σ predicted by (8), but found a minimum χ_σ^{-1} in excess of that expected from the demagnetizing factor alone. This minimum may result from the inhomogeneity in anisotropy, δK_u, which prevents $H_{A\sigma}$ from reaching zero simultaneously at all points in the sample. If this is the source of the observed minimum χ_σ^{-1}, we conclude $\delta K_u \approx 0.27 K_u \approx$ ≈ 10 J/m³. If this δK_u results from internal stresses, their magnitude is $\delta\sigma \approx 0.2$ MPa (30 psi). The presence of internal stresses of this magnitude in an annealed sample is not unreasonable. The δK_u value so estimated can also be used in (13), (15), and (17) to estimate the upper limits of the various magnetomechanical parameters obtainable by stressing.

The properties desired for high magnetomechanical sensitivity are high λ_s, M_s, and E_M, and low (and homogeneous) K_u. All these quantities vary with alloy composition. In particular, the induced anisotropy constant K_u of Fe-base amorphous alloys is increased strongly by the presence of additional transition elements such as Ni or Co [10, 11]. This is probably why the coupling factors of Allied 2605CO ($Fe_{67}Co_{18}B_{14}Si_1$) were inferior to those of 2605SC [1].

The value of K_u is also sensitive to annealing temperature and time, the kinetics of K_u development, and relief of quenched-in stresses both increasing with increasing temperature, but the ultimate value of K_u decreasing as the Curie temperature is approached [10 to 12]. In many alloys, a simple transverse-field anneal may not be able to both remove the internal stresses and also achieve minimum K_u. It may be necessary to first anneal in zero or longitudinal field to remove internal stresses and then anneal in transverse field for a short time at the same or a lower temperature to produce a low transverse K_u. Cooling rate may also influence K_u.

In some alloys, there may be changes in K_u during low-temperature aging. This would clearly be undesirable, and lack of severe aging effects should be another criterion for material selection. There may also be problems of reproducibility of K_u and other material parameters from sample to sample. The equations presented suggest that some of these potential problems could be controlled in device applications with the use of applied stresses to adjust or tune the effective anisotropy ($K_u - \frac{3}{2}\lambda_s\sigma$) of the sample.

We have considered the simple case of uniform H and/or σ directed exactly perpendicular to the induced anisotropy K_u. This yields the maximum magnetomechanical

coupling.[2]) The treatment can easily be extended to different relative orien'.ations of H, σ, and K_u, but the equations become more complex. Bending or twisting stresses can be considered, and here the non-uniform σ also decreases the overall magneto-mechanical coupling. Nevertheless, geometries producing bending or twisting will be advantageous in some device applications. In some applications, choice of material and operating conditions will be governed not by maximum magnetomechanical sensitivity, but by maximum ranges of linear response [13].

The magnetization process in the domain geometry assumed is pure rotation (Fig. 1 b), with no contribution from domain-wall motion. Thus eddy-current losses should approximate those calculated from classical theory, i.e. there should be no "anomalous" losses. Because of the thinness of the ribbons and the high resistivity of the amorphous alloys, these classical eddy-current losses should be very low, far lower than those of conventional magnetostrictive materials. Another advantage of amorphous materials in magnetomechanical applications is their high mechanical strength.

4. Summary

A simplified model has been used to demonstrate why amorphous metals can exhibit outstanding magnetomechanical properties. Although high values of λ_s, M_s, and E_M are needed, a low value of K_u is of primary importance. The need for a low and homogeneous K_u should guide the selection of alloy composition and annealing conditions for optimum properties.

Acknowledgements

References

[1] C. MODZELEWSKI, H. T. SAVAGE, L. T. KABACOFF, and A. E. CLARK, IEEE Trans. Magnetics 17, 2837 (1981).
[2] M. A. MITCHELL, J. R. CULLEN, R. ABBUNDI, A. E. CLARK, and H. T. SAVAGE, J. appl. Phys. 50, 1627 (1979).
[3] M. BROUHA and J. VAN DER BORST, J. appl. Phys. 50, 7594 (1979).
[4] K. I. ARAI and N. TSUYA, Sci. Rep. Res. Inst. Tôhoku Univ.. Suppl. A28, 247 (1980).
[5] M. L. SPANO, K. B. HATHAWAY, and H. T. SAVAGE, J. appl. Phys. 53, March 1982.
[6] J. D. LIVINGSTON, phys. stat. sol. (a) 56, 637 ('979).
[7] C. M. VAN DER BURGT, Philips Res. Rep. 8, 91 (1953).
[8] C. H. SHERMAN, IEEE Trans. Sonics Ultrasonics 22, 281 (1975).
[9] R. W. TIMME and S. W. MEEKS, J. Physique 40, Colloq. C5, 280 (1979).
[10] F. E. LUBORSKY and J. L. WALTER, IEEE Trans. Magnetics 13, 953 (1977).
[11] H. FUJIMORI, H. MORITA, Y. OBI, and S. OHTA, in: Amorphous Magnetism, Vol. 2. Ed. R. A. LEVY and R. HASEGAWA, Plenum Press, New York 1977 (p. 393).
[12] W. CHAMBRON and A. CHAMBEROD, Solid State Commun. 35, 61 (1980).
[13] I. J. GARSHELIS, IEEE IECI Conf. Proc. 76 CH1 117-1 IECI, 99 (1976).

---

[2]) The results would have been similar if the magnetic easy axis had been normal to the ribbon plane rather than widthwise. However, such an easy axis requires surface closure domains with in-plane magnetization [6], and magnetomechanical effects would be somewhat reduced unless there was also in-plane anisotropy to assure a widthwise magnetization direction for these closure domains.